NAVAL AIR DEVELOPMENT CENTER

WARMINSTER, PA. 18974

REPORT NO. NADC-72071-VT 5 Sept 1972

EVALUATION OF THE -S/N- FATIGUE LIFE GAGE UNDER CONSTANT AND VARIABLE AMPLITUDE LOADING

Final Report

AIRTASK NO. FXX.412.001
IED ST #3

Approved for public release; distribution unlimited.

From: Commander, Naval Air Development Center
To: Distribution List

Subj: NAVAIRDEVCEN Report NADC-72071-VT, "Evaluation of the -S/N-Fatigue Life Gage Under Constant and Variable Amplitude Loading", 5 Sep 1972; errata to

1. It is requested that the following changes be made to the subject report:

a. Figures A-4 and A-5 on Page B-8 should be on Page A-12.

b. Figure B-1 on Page A-12 should be on Page B-8.

DEPARTMENT OF THE NAVY
NAVAL AIR DEVELOPMENT CENTER
WARMINSTER, PA. 18974

AIR VEHICLE TECHNOLOGY DEPARTMENT

REPORT NO. NADC-72071-VT

5 Sept 1972

EVALUATION OF THE -S/N- FATIGUE LIFE GAGE UNDER CONSTANT AND VARIABLE AMPLITUDE LOADING

Final Report

AIRTASK NO. FXX.412.001
IED ST #3

An experimental program was conducted to evaluate the -S/N- Fatigue Life Gage and a number of gage installations was evaluated for constant and variable amplitude loading.

The test results demonstrated that while there was a qualitative relation between gage resistance change and specimen life expended, a usable quantitative correlation was not attainable. Test results also proved that the fraction of specimen life to initial detectable crack was a better indicator of the time for retirement of a structure than was the fatigue life gage, although no estimate of the damage incurred can be obtained prior to crack detection.

Reported by: M. S. Rosenfeld
M. S. ROSENFELD
Staff Scientist

S. Scheindlinger
S. SCHEINDLINGER
Aerospace Engineer

Approved by: C. G. Weeber
C. G. WEEBER
Supt., Structures Div

SUMMARY

An experimental program was conducted to evaluate the -S/N- Fatigue Life Gage for constant amplitude and variable amplitude loading. Gage installations inside of, and immediately tangent to filled and unfilled holes in a plate were evaluated for both types of loading. Gages installed on strain multipliers were installed in the nominal stress field near the edges of the plates and were evaluated only for variable amplitude loading.

The constant amplitude tests were performed for maximum nominal net section stresses of approximately 30 and 20 or 22 ksi for R =0, -1, and -½. Variable amplitude tests were performed for a nominal net section stress of 30 ksi for positive loads spectra A and B and for the complete spectrum A of MIL-A-8866.

The test results demonstrated a qualitative relation between gage resistance change and specimen life expended. However a usable quantitative correlation was not attainable. In fact the fraction of specimen life to initial detectable crack proved to be a better indicator of when to retire a structure than was the fatigue life gage although no estimate of the damage incurred can be obtained prior to crack detection.

TABLE OF CONTENTS

LIST OF TABLES

LIST OF FIGURES

INTRODUCTION

The current trend toward development of higher performance aircraft representing greater financial investment per vehicle has generated a strong need for development of a reliable fatigue life indicator to determine the extent of airframe damage experienced and to establish safe economical retirement lives for individual aircraft.

In the past, the safe life for airframes was established in flight hours on the basis of laboratory fatigue tests. This method is quite arbitrary because it is erroneously assumed that all aircraft of a particular model experience exactly the same usage. The current method relies on obtaining the history of normal c.g. acceleration for individual aircraft, which when used with laboratory fatigue data and a cumulative damage analysis, permits more accurate estimates of the fatigue damage incurred and life remaining for individual aircraft. This method is also subject to large errors because the effects of aircraft gross weight variations, weight distribution, altitude, airspeed, etc., which affect the fatigue damage estimates, are neglected or average corrections are assumed. Currently, strain recorders and counters are being developed to obtain the nominal strain histories in the critical areas and thus eliminate most of the errors inherent in the use of c.g. acceleration histories. Both acceleration and strain counting methods of obtaining stress (or strain) histories are electromechanical and/or electronic systems, have the typical systems reliability problems, and rely on cumulative damage theories of questionable accuracy for estimating the life remaining.

To bypass these problems and inaccuracies, many investigators have attempted to detect changes in the structure or material that would be indicators of fatigue damage. Direct measurement of fatigue damage has been attempted by X-ray diffraction, ultrasonics, eddy currents, etc.; however, these methods can be successful only under ideal laboratory conditions and at best leave something to be desired. Attempts to use crack detection wires and conductive paints for the detection of initial cracking in structures have produced extremely unreliable data even in the laboratory.

At the Second SESA International Congress on Experimental Mechanics, a sensor designed for the purpose of measuring cumulative fatigue damage was announced. It is in the form of a foil type strain gage with a full epoxy encapsulation as shown in Figure 1. The unique design feature of this gage is that it changes electrical resistance permanently as a continuous function of its fatigue

experience. Since its introduction, there have been a number of investigations performed to determine the sensor characteristics. The conclusions reached from the work are:

1. The sensor threshold sensitivity is too high.

2. Resistance change at structure failure is variable and very seldom approaches the resistance change measured for material failure.

From the work performed to date, many investigators are skeptical of the possibility for developing this gage into a practical fatigue damage indicator. It is felt that this skepticism may be premature because all the investigations emphasized the sensor characteristics, and the practical considerations of the sensor installation, such as gage size, gage location, material stress state (elastic and/or plastic), environmental effects, gage protection, etc., which must be investigated before drawing conclusions regarding the practicability of this method of fatigue damage indication, have been ignored.

Consequently this in-house exploratory development program was established to investigate the practical consideration noted above and to recommend gage installation methods for fleet use if the gage should appear to be practical.

The initial phase of the investigation, reference (a), was an analytical study of the effect of gage size and location in the high-gradient strain field around the hole in an infinite plate. Two gage installations were investigated; the first with the gage placed inside the hole and the second with the gage placed immediately tangent to the hole.

The results of the study demonstrated the superiority of the gage installation inside the hole; however, for this investigation both tangent and inside the hole installations would be investigated.

The original objectives of the experimental program were:

1. To investigate and develop methods for installing fatigue life gages at a notch root in the critical region of a structure to provide a means for measuring fatigue damage incurred by the structure in service and

2. to develop methods for determining the life remaining from the gage resistance measurements.

About half-way through the test program, strain multipliers similar to the one shown in Figure 2 were procured and the units were installed on a number of the specimens to investigate their behavior during variable-amplitude tests.

GAGE DESCRIPTION AND USE

The -S/N- Fatigue Life Gage is similar to a foil strain gage and is manufactured by the same basic processes. The gage consists of a specially treated constantan foil grid encapsulated in a glass fiber-epoxy laminate. When bonded to a structural member, the gage accumulates a permanent change in electrical resistance with cyclic strain in a manner ostensibly similar to the accumulation of fatigue damage in the member. Figure 1 shows the gage sizes and configurations available from one manufacturer.

Since the resistance change in the gage is permanent and irreversible under normal conditions, permanent electronic instrumentation is not required. A measure of the fatigue damage incurred can be monitored by simply measuring the gage resistance with a Wheatstone bridge or a strain indicator. The initial gage resistance is usually 100 ohms, and the resistance change corresponding to the initiation of fatigue cracks is normally 5 to 8 ohms according to the gage manufacturer. This resistance change depends upon the material to which the gage is bonded and the strain gradient with respect to gage size. Special 20 ohm gages with a gage length of 0.030 inches have been developed in lieu of 100 ohm gages for this size because of the many problems involved in the production of these small gages. These special 20 ohm gages were used in this program; the same percent change in resistance occurs for both type gages.

The gage manufacturer claims that the cumulative resistance change in the gage is a highly repeatable function of the cyclic strain history to which the gage has been subjected and limited independent verification bears this out. Once the gage accumulates a small but significant resistance change, the remaining life of the part can theoretically be estimated with the usual statistical reliability inherent in fatigue. This assumes that the future service experience will be similar to that already experienced.

The above discussion describes the gage and its theoretical usage in an area of significant strain that would produce the desired resistance change. However, we also know that the threshold of sensitivity of the gage is too high for many applications hence considerable work has gone into the development of strain multipliers to increase the effective sensitivity. All the proposed multipliers, except one, have the following disadvantages:

1. Large size
2. High multiplier to structure bond strength required.
3. Considerable stiffening effect on structure.

4. Possibility of buckling under compressive strain.

5. Possibility of multiplier failure under high strains.

One exception to these disadvantages is the slotted multiplier proposed by Thomas in reference (b) and shown in Figure 2. Multipliers having factors of 2.5 and 3.0 were procured from the Boeing Company and were installed on the variable - amplitude specimens with ½ in. dia. holes.

DESCRIPTION OF SPECIMENS

The superiority of an inside-the-hole installation for the fatigue life gage was demonstrated in reference (a). However there is considerable reluctance to have open holes in the critical areas of aircraft structures. To demonstrate that the open hole is not necessarily more critical than a hole with a non-interference bolt installed, the photoelastic investigation reported in Appendix A was performed to investigate the effect of the open hole size and spacing in a line of holes. A second investigation, Appendix B, was performed to determine the relation between bolt-hole clearance and nominal strain to see if the open hole would be more critical than a hole with a bolt installed. The results show that a nominal strain of 2100-2500 micro-inches/inch is required to deform the hole laterally by 0.001 in. Since bolt clearance usually exceeds 0.001 in., then for all practical purposes a reamed hole with a non-interference bolt installed should have the same stress concentration factor as an open hole.

The final design of the test specimen is shown in Figures 3 to 7. Specimens were fabricated with nominal ¼ in. dia. and ½ in. dia. holes to assess the effect of the gage/hole size relation calculated in reference (a) and to develop techniques for installing gages in both large and small holes. Bolts were selectively installed in the holes so that the clearance for each bolt installation was approximately 0.001 in. Interference fit bolts (0.002 in. interference for ¼ in. and 0.003 in. interference for ½ in. dia. bolts) were installed in the end holes after failure of ½ in. hole specimen No. 1 through the end hole. This was done to force the failure to occur through the other holes in the test section rather than through the end holes.

It was originally planned to test both -05 and -07 gages (g. l. = 0.060 in. and 0.030 in., respectively) with initial gage resistance of 100 ohms. However, the gage manufacturer discontinued making the -07 gages because the results obtained with this gage were extremely inconsistent due to the extreme thinness required to produce the initial resistance of 100 ohms. The gage manufacturer developed a thicker gage with a gage length of 0.030 in. and initial resistance of 20 ohms to replace the -07 gage; the new gage designation is -07-20 and this gage was used for the investigation.

Subsequent to the constant-amplitude tests, fatigue life gages mounted on Hawker-Siddely slotted strain multipliers were procured for evaluation during the variable-amplitude tests. These multipliers are similar to those described in reference (b); the sequence of manufacture is shown in Figure 2. Multipliers with factors of 2.5 and 3.0 were obtained because they would bracket the stress concentration factor for the open hole installation and the test results should be directly comparable to the results for the gages installed inside the open holes. The multipliers were installed at the edges of the ½ in. dia. hole specimens as shown in Figure 8.

TEST EQUIPMENT

Test Machine

The tests were performed in an M-T-S tape controlled, digitally programmable 100,000 pound capacity fatigue test machine shown in Figure 9. The machine control contains the following units:

1. Model 425.41 D.C. Transducer Conditioner to provide "expanded-range" when the machine is used below rated capacity.

2. Model 401 Servac with Model 401.52 Command Input Module.

3. Model 426.01 Limit Detector which stops the machine if either upper or lower load limits exceed the desired values.

4. Model 410.21 Cyclic Function Generator for providing the cyclic waveshape and frequency control for constant amplitude tests.

5. Model 424.01 Digital Programmer for system programming during variable amplitude tests.

6. Model 416.01 Amplitude Measurement Panel with Hewlitt-Packard Model 132A Dual Beam Oscilloscope for monitoring the applied loads.

Gage Readout

Normally a simple Wheatstone bridge is used to determine the resistance change; for the standard 100 ohm gages this resistance change is also the percent change in resistance. Since both 100 ohm and 20 ohm gages were used, a special Wheatstone bridge unit was fabricated to read the resistance change directly in percent for either the 100 ohm or 20 ohm gages. The inputs to the bridge were arranged for three-wire connection. The actual test setup shown in Figure 9 used two wires from the gage to the rotary selector switch and then three wires from the switch to the bridge connections.

TEST METHODS

Constant-Amplitude Tests

The test specimen was installed in the test machine after aligning the test machine grips using a dummy specimen. For tests with negative load ratios, the specimen was encased in a Teflon-lined anti-buckling guide. A ½ in. dia. hole specimen installed in the test machine with the anti-buckling guide is shown in Figure 10.

The original test program was established for net section stress levels of 35 and 20 ksi. at frequencies of 2 and 5 cps., respectively. However after the ¼ in. dia. hole specimen tested at 20 ksi. and R = 0 failed in the machine grip, the lower stress level for the ¼ in. dia. hole specimens was increased to 22 ksi. Tests were performed for R = 0, -½, and -1 using a sine wave function. Initial and periodic readings of the percent change in gage resistance were obtained with a reference load of 500 pounds applied to each specimen.

Variable-Amplitude Tests

Because of the similarity of results of the constant amplitude tests for the ¼ in. dia. and ½ in. dia. specimens, these tests were limited to the ½ in. dia. hole specimens only. The test setup was identical to that used for the constant-amplitude tests except that the test machine was controlled by the digital programmer instead of the cyclic function generator. Tests were performed for the positive loads only spectra A and B and the positive and negative loads spectrum A and MIL-A-8866. The spectra were applied in 50 hr. blocks using the sequence shown in Tables I and II; 1000 hr. tapes were used and the sequence was repeated every 1000 hrs. The limit load stress was 30 ksi for all tests. Initial and periodic readings of the percent change in gage resistance were obtained with a reference load of 500 pounds applied to each specimen.

RESULTS

Constant-Amplitude Tests

The test conditions, lives to failure and failure locations are summarized in Table III. The test data showing percent resistance change vs. cycles applied and vs. percent specimen life to failure are contained in Appendix C. For the fatigue life gages to be usable as fatigue damage detectors and life estimation devices, a specific percent resistance change should indicate the same amount of damage experienced, within reasonable tolerance, regardless of stress history. Examination of the data contained in Figures C-27 to C-44 show

this not to be the case.

One of the objectives of this test series was to demonstrate that an open hole in a line of holes containing non-interference fit bolts is not more critical than the hole with the bolt installed. Ten of the thirteen failures occurred through holes in the specimen; five occurred through open holes and four occurred at a hole with a bolt installed. One failure occurred through the end hole and is not considered to be a valid failure because interference fit fasteners were installed in the end holes for all subsequent tests.

Variable Amplitude Tests

The test spectra, lives to initial crack and final failure, and failure locations are summarized in Table IV. All tests were performed for a limit load net stress level of 30 ksi. The lives to initial crack were determined after failure by determining the crack propagation lives from the beach marks on the fracture surfaces and counting back to estimate crack initiation. The test data showing percent resistance change vs. number of 50 hour blocks applied and vs. percent specimen life to failure are contained in Appendix D. As for the constant amplitude data, these data do not substantiate that a specific resistance change corresponds with a given amount of fatigue damage.

Initially it was planned to investigate both spectra A and B for two different stress levels and for the two loading cases of positive loads only and positive plus negative loads. However the program was changed because of the very few negative loads in spectrum B and because it was deemed more advisable to investigate a larger number of nominally identical specimens for the same loading condition. Five specimens, 2A through 6A, were tested for the complete spectrum A. The data from only four tests are contained in Table IV because specimen 3A failed prematurely due to malfunction of the test machine control system.

The data from specimens 2A, 4A, 5A, and 6A were replotted in Figures D-19 to D-29 to show the variations of resistance change with time (in 50 hr. blocks) for each gage location for the four nominally identical specimens subjected to the same stress history. Plotted in this manner the data for gage installation numbers 1, 8, and 9 appear to be fairly consistent; however, when the comparison is made based on percent specimen life as in Figures D-30 and D-35 the dispersion appears to be too great for a usable life indicator. Furthermore 50% of the gage No. 1 installations and 25% of the gage Nos. 8 and 9 installations failed before indicating a resistance change of 6%.

The performance of the strain multipliers shown in Figures D-28, D-29, and D-36 is considered unacceptable because of their limited lives

(75% failed before indicating a resistance change of 6%) and because of the extreme inconsistency in results as shown in Figure D-36.

Table IV contains a column listing the fraction of life to initial detectable crack. The average life fraction to initial cracking is 0.74 with a variation of -.12 and +.08 for the four nominally identical tests. This indicates that initial crack detection is a better indicator of when to retire a structure than is the fatigue life gage although no estimate of the damage incurred can be obtained prior to initial crack detection.

CONCLUDING REMARKS

The development of a passive fatigue damage indicator requiring no in-flight instrumentation has been the aim of the aircraft industry for the past 20 years. The annealed foil fatigue sensor has given promise of accomplishing this aim. However, as yet, this promise is still unfulfilled.

In this program, the basic sensor installed at a typical stress concentration (a fastener hole) and the basic sensor installed on a strain multiplier located in an area remote from the concentration were evaluated for the nominal stress histories likely to be encountered by fighter and attack aircraft. The results indicated that the sensor does experience a resistance change that can be related to nominal stress history. In this respect, the data agree with the results of tests performed using strain multipliers installed at a large number of locations over the C-5A fatigue test airplane (reference (c)). However, the test data reported herein demonstrate that the results are not consistent for a group of nominally identical structural members experiencing the identical nominal stress history. Consequently it must be concluded that it is not possible to correlate a given percent resistance change with the actual fraction of life expended for each specimen using the currently available sensors.

Because of the importance of aircraft structure fatigue life prediction it is felt that work to develop a passive fatigue damage sensor of this type should continue. Reference (d) reports the work accomplished towards development of a bondable resistive gage fabricated of vacuum deposited metallic material rather than of Constantan foil. One of the gage manufacturers, Micro-Measurements, has developed an "improved" strain multiplier based upon a completely different multiplier design than the Hawker-Siddeley type evaluated in this program.

REFERENCES

(a) Rosenfeld, M. S.; The Effect of Gage Size and Location on the Response of -S/N- Fatigue Life Gages, Naval Air Development Center Report No. NADC-ST-6908, 15 December 1969.

(b) Thomas, E. D. R.,; Development of a Strain Multiplier for Fatigue - Sensor Applications, Experimental Mechanics, Vol. 10, No. 8, August 1970, also Proceedings of the Society for Experimental Stress Analysis, Vol. XXVII, No. 2, 1970, pp 346-352.

(c) Horne, Robert S. and Freyre, Oscar L.; Annealed Foil Fatigue Sensor Development, Air Force Flight Dynamics Laboratory Report AFFDL-TR-71-127, March 1972.

(d) Horne, Robert S.; Improvement of a Structural Fatigue Sensor, Air Force Flight Dynamics Laboratory Report No. AFFDL-TR-70-141, April 1971.

TABLE I - TEST LOAD SEQUENCE
MIL-A-8866 SPECTRUM A
50 HR. BLOCKS

% LIMIT STRESS	BLOCK NO. 1	2	3	4	5	6	7	8	9	10	11	12	13	14	15	16	17	18	19	20
35	850	←																	→	850
45	475	←																	→	475
55	325	←																	→	325
65	225	←																	→	225
75	125	←																	→	125
85	75	←																	→	75
95	15	←																	→	15
105	8	7	8	7	8	7	8	7	8	7	8	7	8	7	8	7	8	7	8	7
115	2	2	2	2	2	2	2	2	2	2	2	2	2	2	2	2	2	2	2	2
125	-	1	1	1	1	-	1	1	1	1	-	1	1	1	1	-	1	1	1	1
-110	-	-	-	1	-	-	-	-	-	1	-	-	-	-	-	1	-	-	-	-
-100	-	-	1	-	-	-	1	-	-	-	1	-	-	-	1	-	-	-	1	-
- 90	-	1	-	1	-	1	-	1	-	1	-	1	-	1	-	1	-	1	-	1
- 80	-	1	1	1	-	1	1	1	-	1	1	1	-	1	1	1	-	1	1	1
- 70	1	1	1	1	1	1	1	1	1	1	1	1	1	1	1	1	1	1	1	1
- 60	2	1	1	1	2	1	1	1	2	1	1	1	2	1	1	1	2	1	1	2
- 50	1	2	1	2	1	2	1	2	1	2	1	2	1	2	1	2	1	2	1	1
- 40	2	2	2	1	2	2	2	1	2	2	2	1	2	2	2	1	2	2	2	3
- 30	3	←																	→	5
- 20	5	←																	→	10
- 10	10	←																	→	25
0	25	←																		

TABLE II - TEST LOAD SEQUENCE
MIL-A-8866 SPECTRUM B
50 HR. BLOCKS

% LIMIT STRESS	BLOCK NO. 1	2	3	4	5	6	7	8	9	10	11	12	13	14	15	16	17	18	19	20
35	1250	←	←	←	←	←	←	←	←	←	←	←	←	←	←	←	←	←	→	1250
45	500	←	←	←	←	←	←	←	←	←	←	←	←	←	←	←	←	←	→	500
55	175	←	←	←	←	←	←	←	←	←	←	←	←	←	←	←	←	←	→	175
65	50	←	←	←	←	←	←	←	←	←	←	←	←	←	←	←	←	←	→	50
75	25	←	←	←	←	←	←	←	←	←	←	←	←	←	←	←	←	←	→	25
85	10	←	←	←	←	←	←	←	←	←	←	←	←	←	←	←	←	←	→	10
95	3	4	4	4	3	4	4	4	3	4	4	4	3	4	4	4	3	4	4	4
105	1	1	1	2	1	1	1	2	1	1	1	2	1	1	1	2	1	1	1	2
115	-	1	-	1	-	1	-	1	-	1	-	1	-	1	-	1	-	1	-	1
125	-	-	-	-	-	1	-	-	-	-	-	1	-	-	-	-	-	1	-	-
-30	1(1)	-	-	-	-	-	-	-	-	-	-	-	-	-	-	-	-	-	-	-
-20	-	-	-	-	-	-	-	-	1	-	-	-	-	-	-	-	-	-	-	-
-10	-	-	-	-	1	-	-	-	-	-	-	-	-	-	1	-	-	-	-	-
0	-	-	-	1	-	-	-	1	-	-	-	1	-	-	-	1	-	-	-	1

NOTE: 1. One cycle in block 41 and at 80 block intervals thereafter.

TABLE III - CONSTANT AMPLITUDE TEST DATA

HOLE DIA.	SPECIMEN NO.	Smax (ksi) (1)	R	N_f	FAILURE LOCATION (2)
	1	34.06	0	15,787	7
	2	20.00	0	137,763	grip
¼"	2a	22.00	0	83,901	6
	3	35.00	-0.5	5,178	2
	4	22.00	-0,5	84,707	7
	5	35.00	-1	1,767	10
	6	22.00	-1	48,749	grip
	1	35.19	0	5,769	1
	2	20.57	0	97,476	9
½"	3	35.00	-0.5	5,623	10
	4	20.00	-0.5	64,554	5
	5	35.00	-1	1,341	2
	6	20.00	-1	35,757	grip

NOTES: 1. Net section stress
2. See Figure 5 for location; grip denotes failure in upper grip.

TABLE IV - VARIABLE AMPLITUDE TEST DATA

Specimen No.	Test (1) Spectrum	(2) N_{b_f}	(3) ΔN_{b_c}	(4) N_{b_c}	$\frac{N_{b_c}}{N_{b_f}}$	Failure Location (5)
1A	A	507	80	427	.84	2
2A	Ac	92	35	57	.62	10
4A	Ac	220	48	172	.78	10
5A	Ac	213	38	175	.82	2
6A	Ac	139	33	106	.76	2
2B	B	500 nf	--	---	---	--

NOTE: 1. A Spectrum A positive loads only
Ac Spectrum A positive and negative loads
B Spectrum B positive loads only

2. No. of 50 hour blocks to failure

3. Crack propagation life determined using 30X optical microscope

4. No. of 50 hour blocks to initial crack = $N_{b_f} - \Delta N_{b_c}$

5. See Figure 5 for location

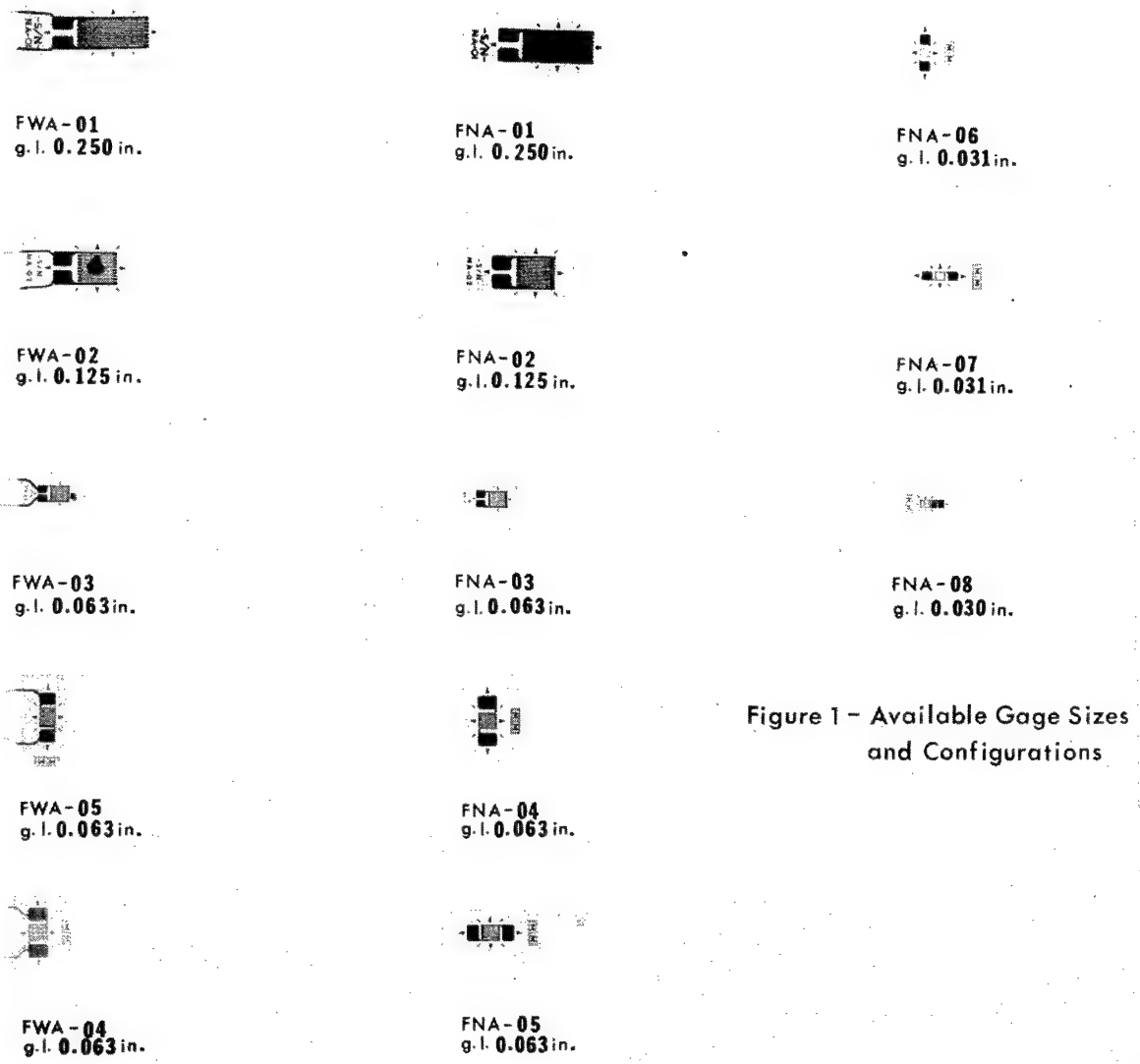

Figure 1 – Available Gage Sizes and Configurations

Figure 1. Available Gage Sizes and Configurations

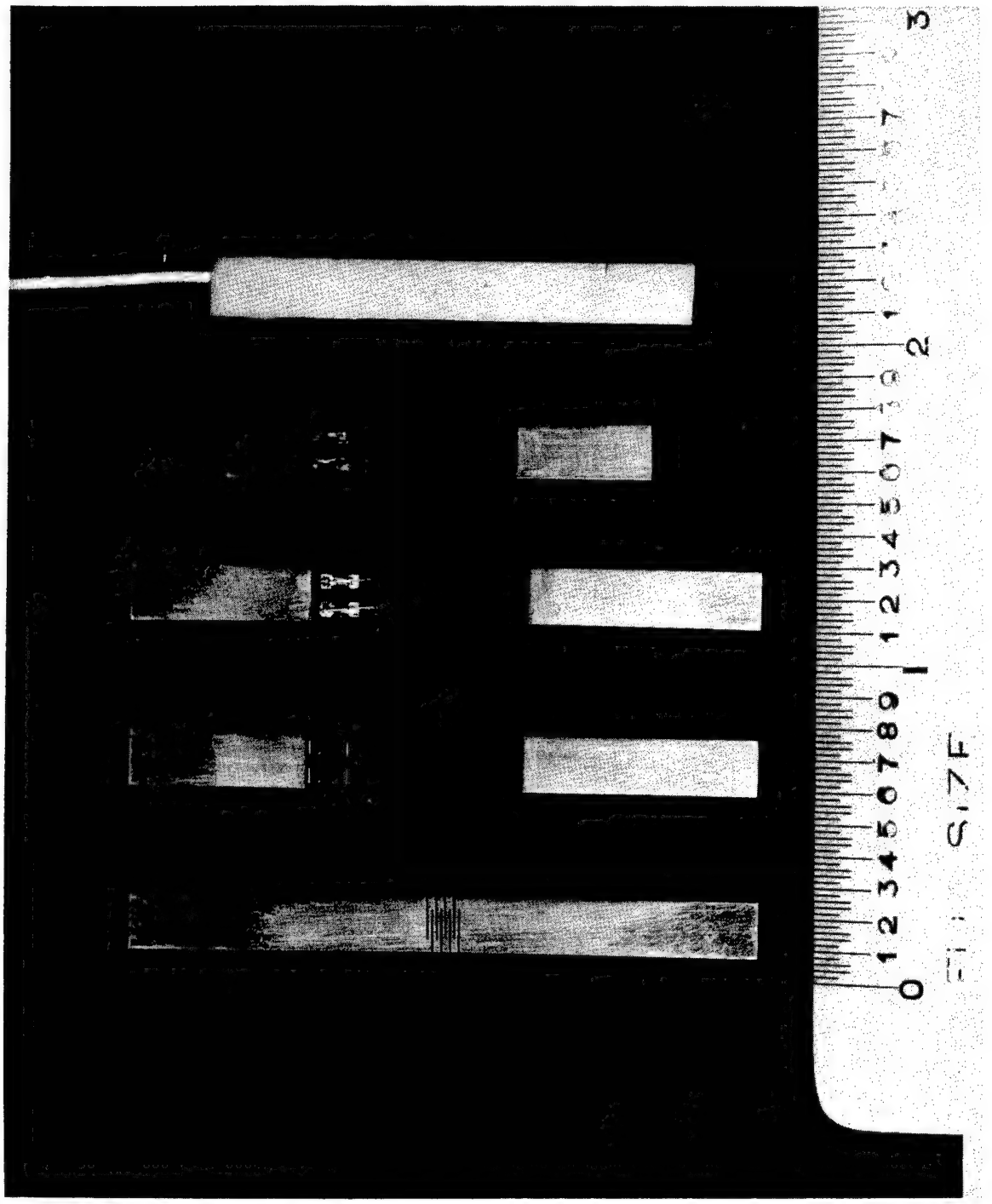

Figure 2. Slotted Strain Multiplier Showing Steps in Manufacture

	L	$\frac{L}{2}$	ℓ	$\frac{\ell}{2}$	a	$\frac{a}{2}$	d
-1	24	12	6.75	3.375	0.750	0.375	$\frac{.2480}{.2470}$
-2	30	15	13.50	6.750	1.500	0.750	$\frac{.4990}{.4980}$

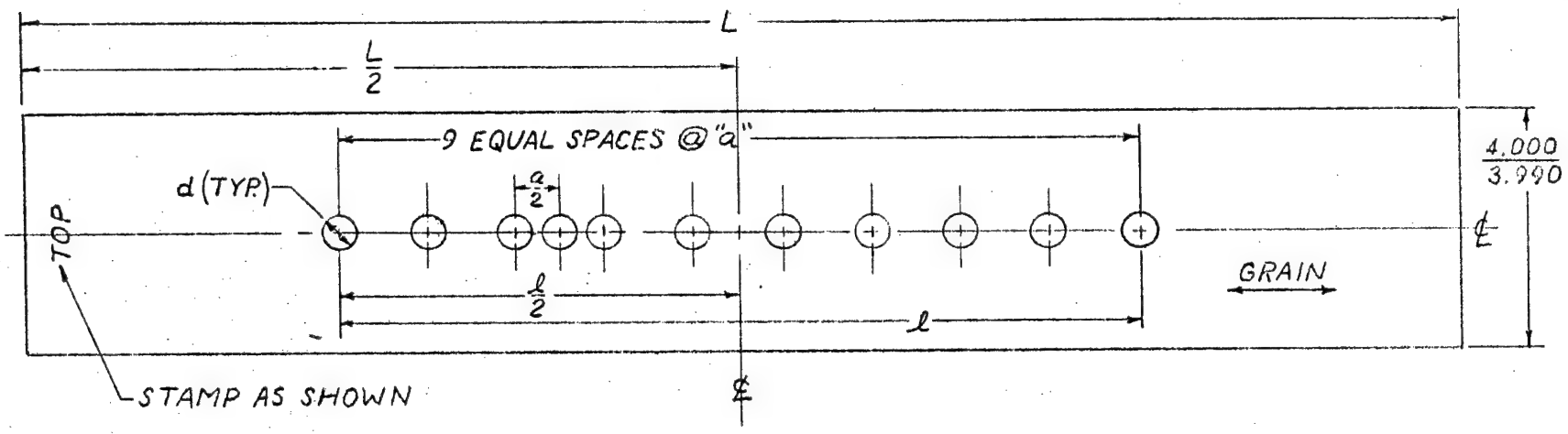

Figure 3. Basic Test Specimen

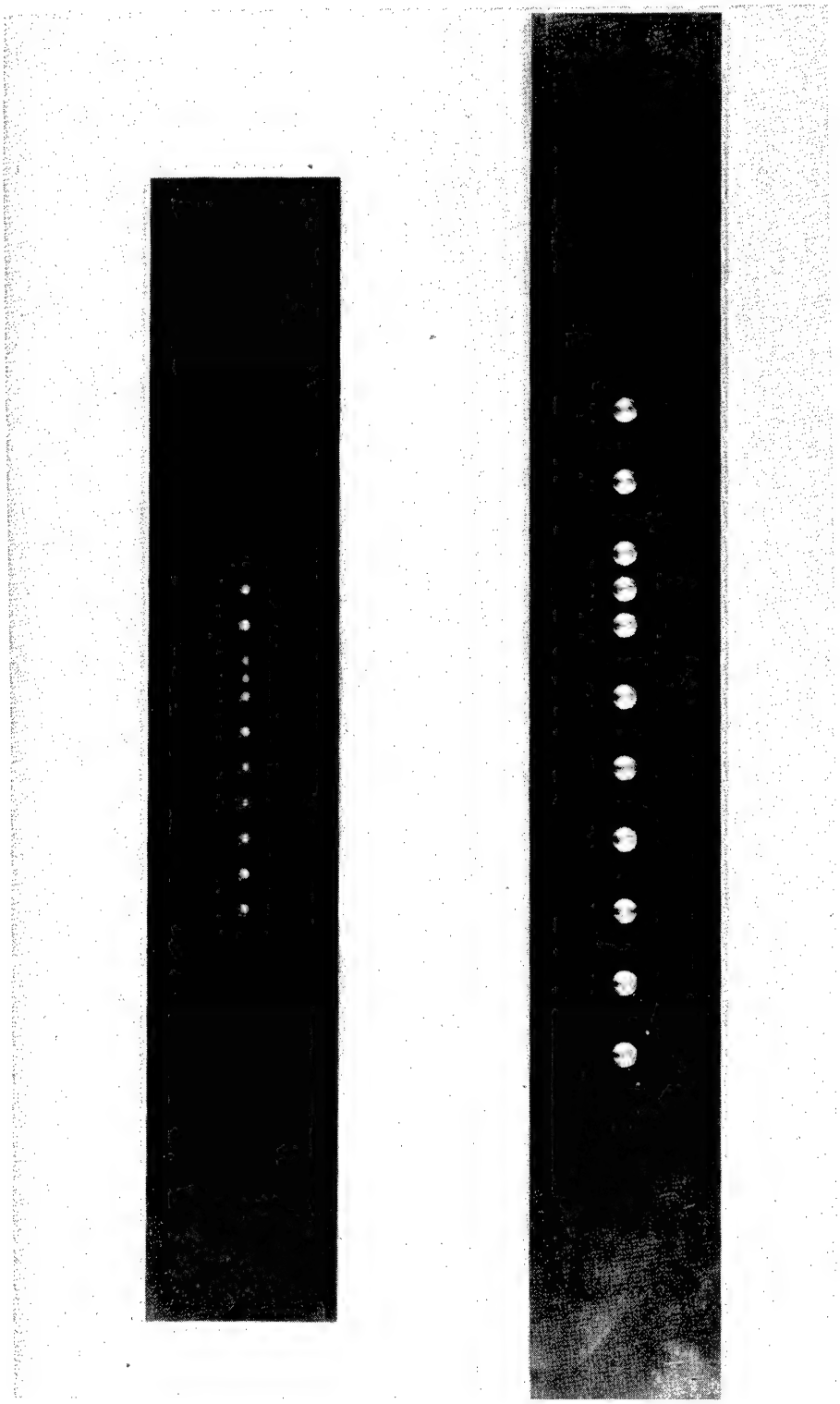

Figure 4. Test Specimens Prior to Gage Installation

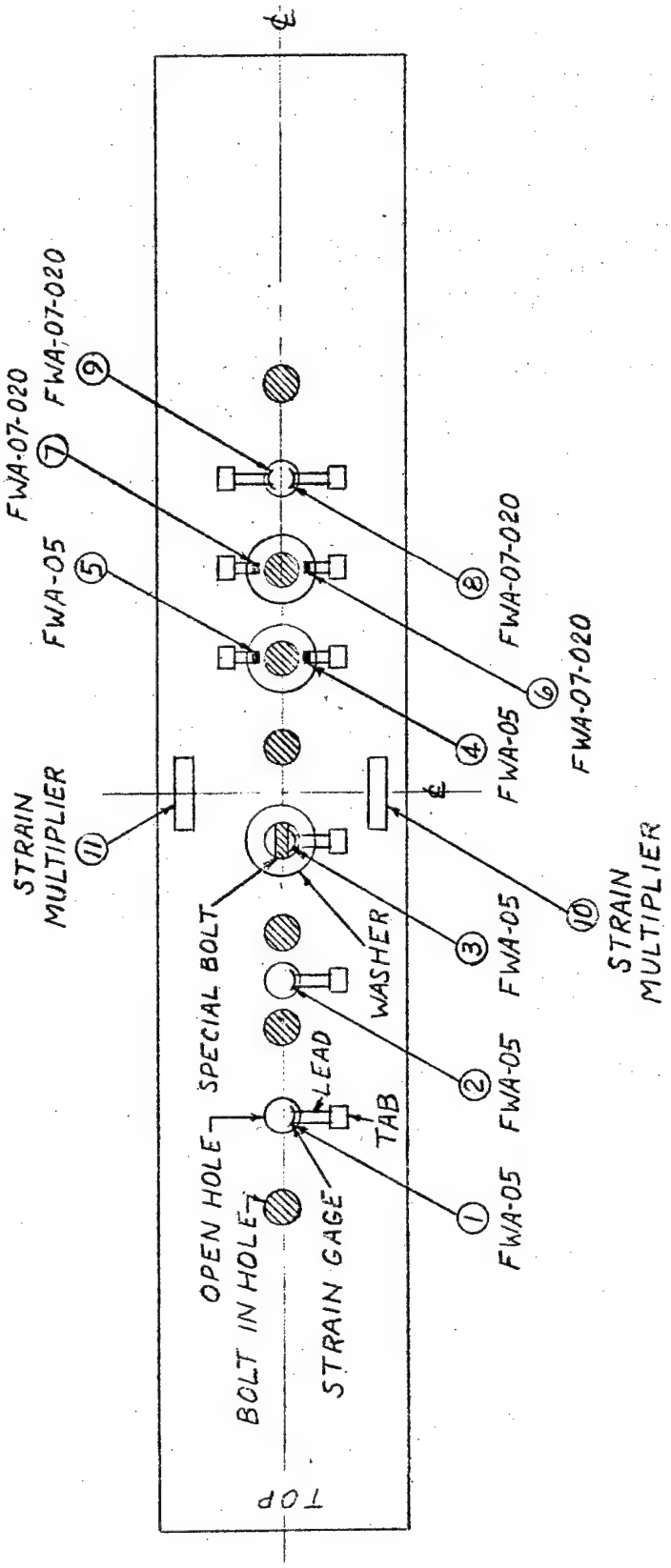

Figure 5. Gage Installation

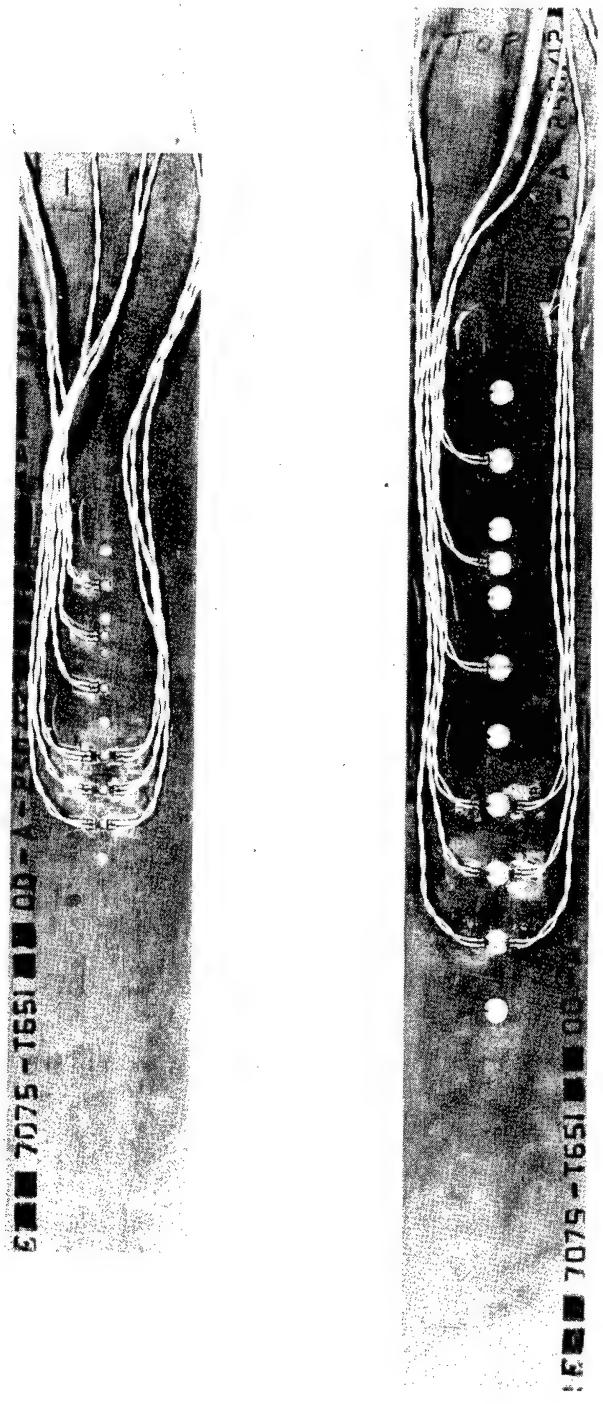

Figure 6. Test Specimens with Gages Installed

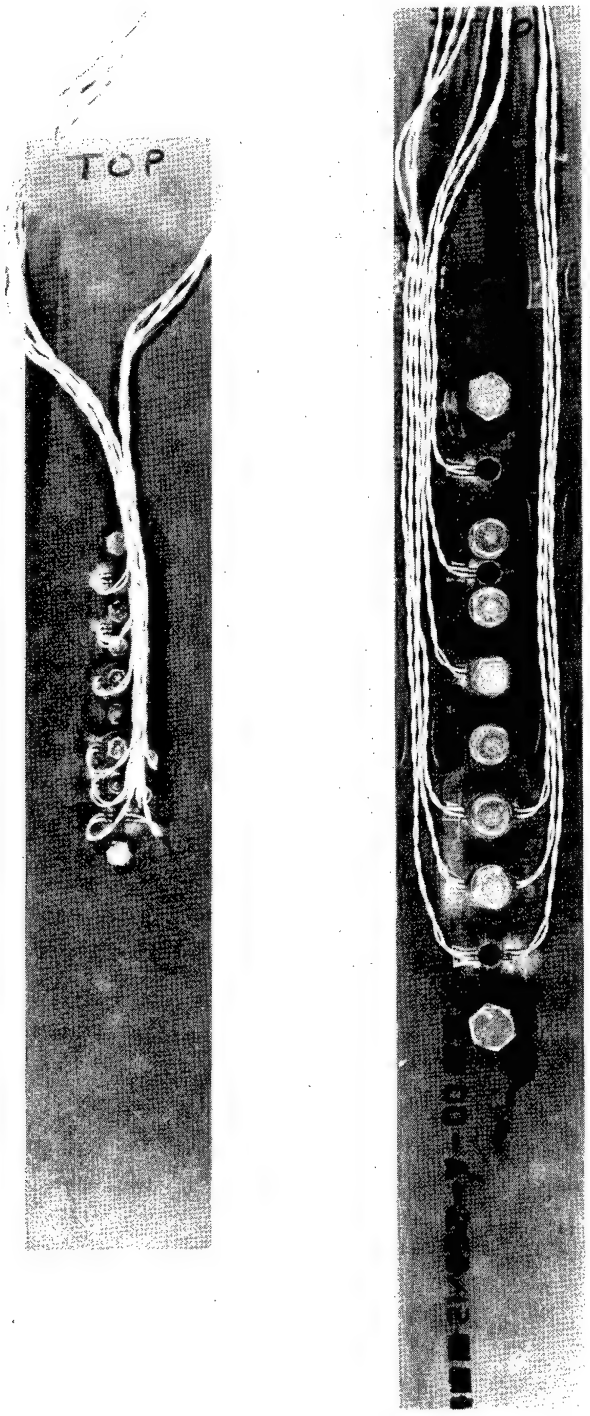

Figure 7. Completed Test Specimens

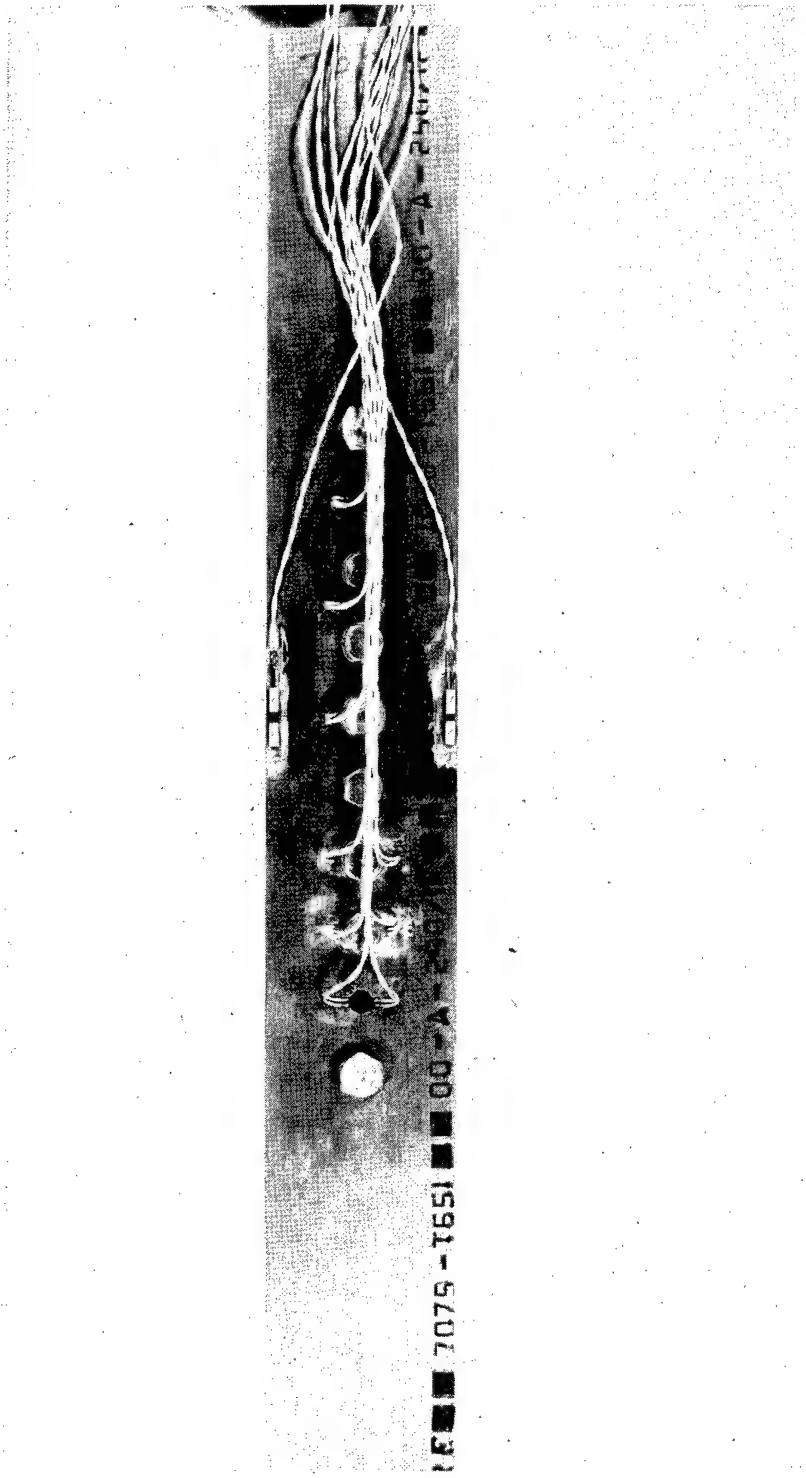

Figure 8. Completed Test Specimen with Strain Multipliers Installed

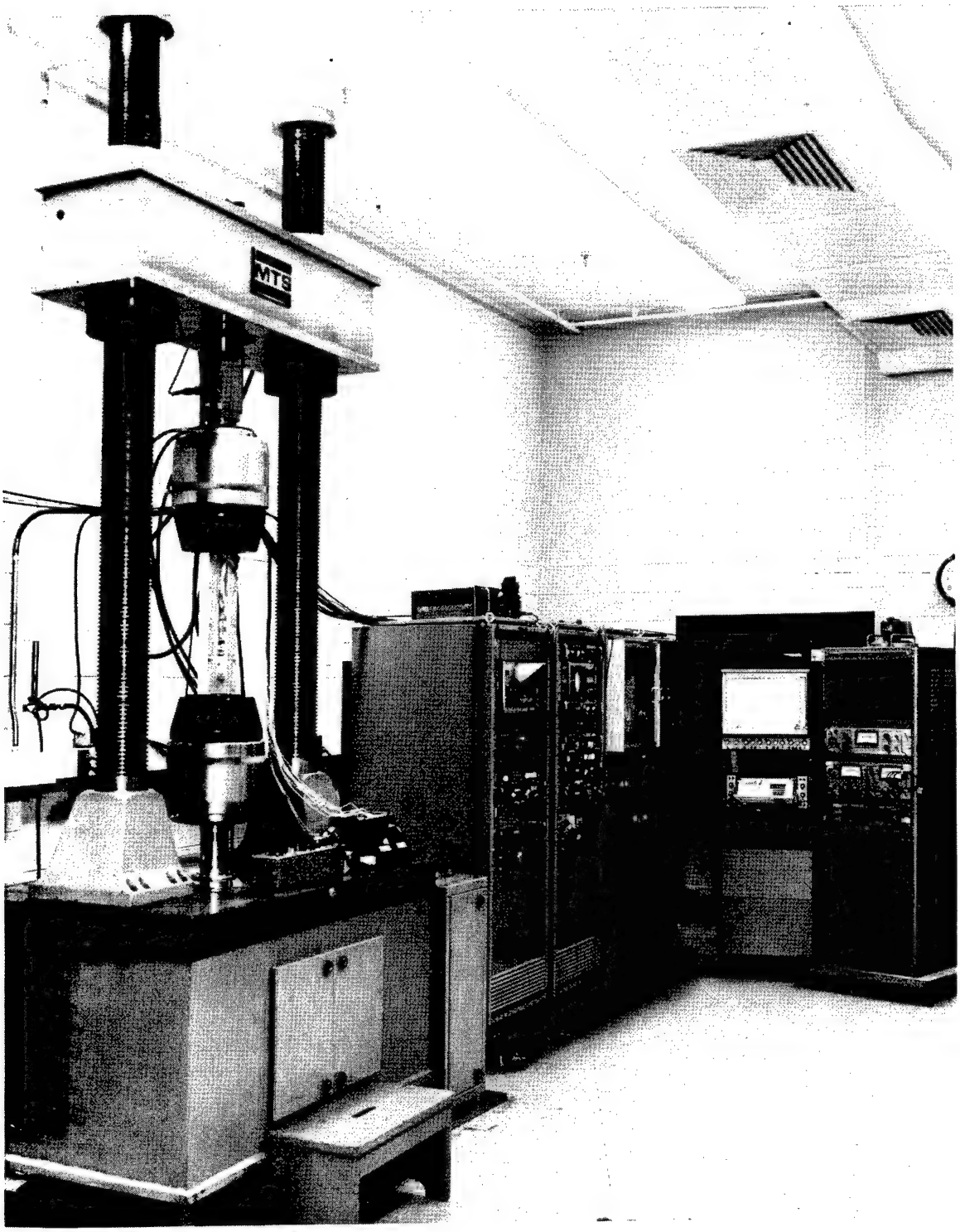

Figure 9. Overall View of Test Setup and Equipment

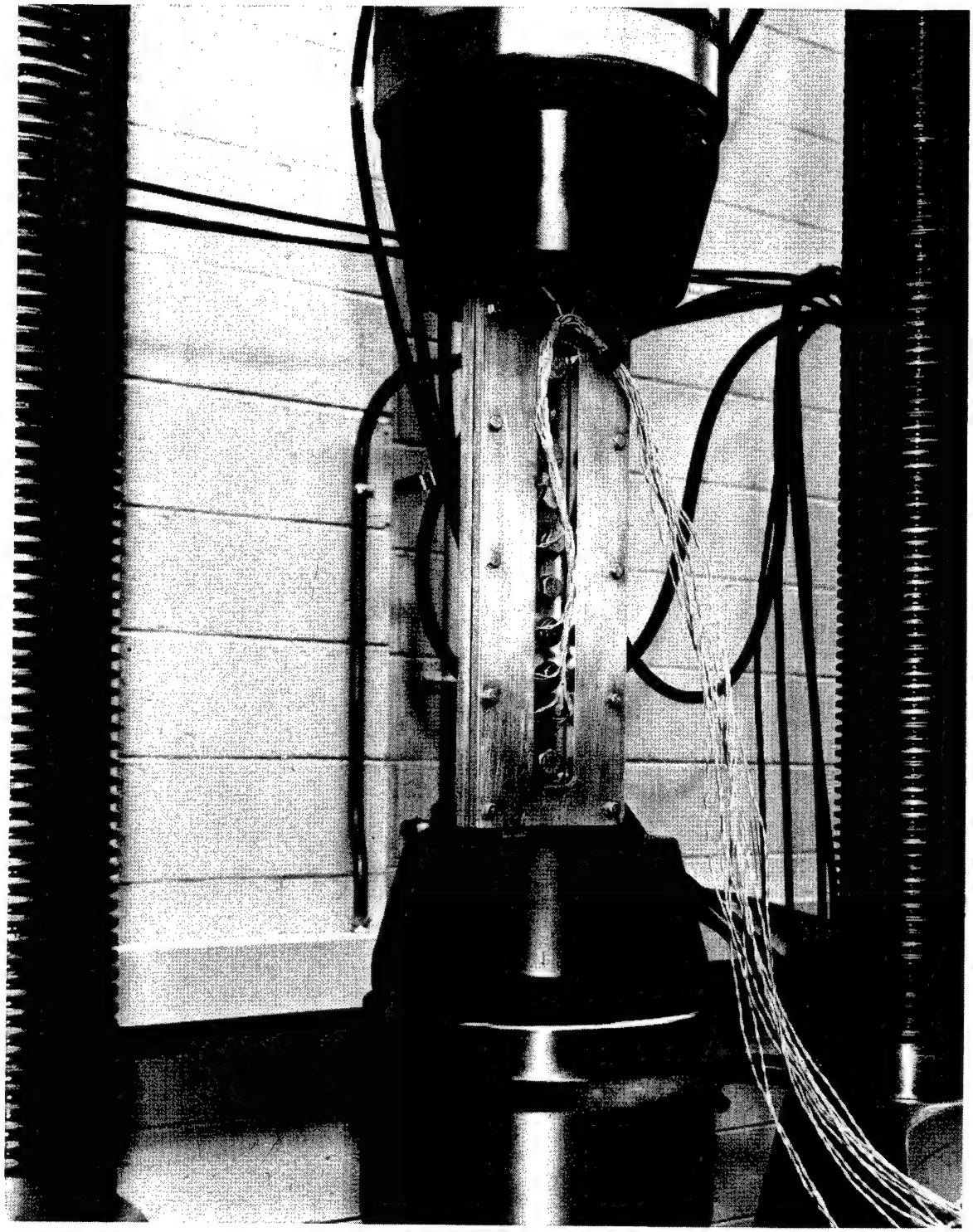

Figure 10. Specimen Installed in Test Machine with Anti-Buckling Guide

APPENDIX A

INFLUENCE OF ADDITIONAL HOLES IN PERFORATED TENSILE PLATES--A PHOTOELASTIC STRESS ANALYSIS

by Daniel Post

PHOTOLASTIC, INC.
67 Lincoln Highway
Malvern, Pennsylvania

Contract No. N00156-70-C-1524
November 20, 1969

INFLUENCE OF ADDITIONAL HOLES IN PERFORATED TENSILE PLATES--A PHOTOELASTIC STRESS ANALYSIS

OBJECT

This investigation was conducted to determine the location and intensity of stress concentrations in tensile plates with multiple perforations. Tensile plates with perforations simulating fastener holes were studied and the influence of additional holes on stress concentrations was analyzed. Cases of holes along the axial centerline of the plate and holes offset from the centerline were investigated, both with ¼ inch and ½ inch dia. holes, as specified in Contract No. N00156-70-C-1524 of November 20, 1969.

TEST CONDITIONS, SPECIMENS AND PROCEDURE

The perforated tensile plates used in this investigation are illustrated in Figure A-1a. Four photoelastic models and an additional calibration bar were produced with dimensions given in the figure. One pair of plates had perforations along the vertical centerline, while another pair had perforations along a line off-set from the center, as shown by the dashed circles.

The loading arrangement is also illustrated in Figure A-1a. Loads were applied through a system of metal links connected by lubricated dowel pins. Pins engaging the specimen were ½ inch dia. and pins between links were ¼ inch dia. Loads were applied by a screw actuated straining frame.

Twenty test conditions were studied. Ten test conditions are illustrated in Figure A-1b and the remaining ten were identical, except the perforations were along a line offset by W/4 from the specimen centerline, where W is plate width. The six test conditions shown at the left of Figure A-1b were performed with one specimen. After the photoelastic pattern was photographed in each test, additional holes were drilled for the next test condition. The four conditions indicated at the right of Figure A-1b were investigated with another tensile plate, and similarly, the ten test conditions with offset holes utilized two more specimens.

The four plates and calibration bar were all cut from a single sheet of PSM-1 photoelastic plastic, 0.123 inch thick. The external machining was done by a high speed router which followed a previously machined aluminum template. A large stream of cold water was directed onto the router tool to act as coolant and to wash away chips.

Holes were located and drilled in a milling machine equipped with a drilling head. A base plate was clamped to the milling machine table and dowel pins inserted in the base plate were used to locate the specimen. A rim was attached to the base plate so as to form a large basin, which was subsequently filled with water to ½ inch depth. Accordingly, the drilling was done under water to facilitate cooling during the cutting action. Newly sharpened drills were employed.

The material calibration test was conducted to determine stress-optical sensitivity. The calibration specimen was connected in series with a commercial load cell. Crossed plane polarizers with axes 45° to the direction of load were installed on each side of the calibration bar; illumination was by diffuse fluorescent light and observation was from a fixed point through a narrow band interference type filter for wavelength 546 millimicrons. Loads were applied to the calibration bar in succession to produce integral values of photoelastic fringe order (N = 1,2,3---) and corresponding load cell readings were recorded.

The calibration specimen was made to produce small bending stresses superimposed upon the tensile stresses. This was done by locating loading points 0.01W from the specimen centerline, where W is specimen width. Accordingly, the photoelastic fringes appear as longitudinal dark bands, and the load is adjusted until the dark band is well centered with respect to the centerline marked on the specimen. This departure from common practice affords substantially improved accuracy in establishing integral fringe orders.

Results of the calibration showed a linear stress vs. fringe order relationship through the tenth fringe order, with a calibration constant of C = 38.3 psi per fringe per inch thickness. Slight decrease of both load and fringe order with time was observed, but when the load was readjusted to its original value, fringe order returned to its original value.

Photoelastic patterns around the holes were observed in a lens-type transmission polariscope, with mercury vapor light source, interference filter (wavelength 546 millimicrons) and 4" x 5" camera. Light-field circular polarization was used to obtain optimum boundary clarity.

The calibration specimen was loaded in series with the 5" wide tensile plates, as shown in Figure A-1a. A small load was applied, the specimen was aligned and the camera was focused. The load was then increased until the 10.0 fringe was centered in the calibration specimen and a photographic exposure of the pattern around the holes was made. This procedure was repeated for each test case.

After the calibration specimen was used in series with the test specimens for nine test conditions, a repeat calibration experiment was conducted. Results showed a deviation of less than ½% from the original calibration, and this deviation was ascribed to experimental

error. Accordingly, the calibration specimen produced repeatable performance as a load transducer.

With the 2½ inch wide tensile plates, a calibration specimen was made as an integral part of each test specimen. Again, the 10.0 fringe was used as an indicator of load in the test specimen.

RESULTS

Stress concentration factor, K, is defined as peak stress at the boundary of a hole, δ_s, divided by the average stress across a non-perforated section of the plate, δ_a. Since

$$\delta_a = \frac{P}{W_s t_s} \quad ; \quad \delta_c = \frac{P}{W_c t_c} \quad ;$$

$$\delta_s = \frac{CN_s}{t_s} \quad ; \quad \delta_c = \frac{CN_c}{t_c} \quad ;$$

where

- δ is stress
- P is applied load
- W is plate width
- t is plate thickness
- C is stress-optical constant
- N is photoelastic fringe order
- s is subscript denoting perforated specimen
- c is subscript denoting calibration member

The stress concentration factor is

$$K = \frac{\delta_s}{\delta_a} = \left(\frac{W_s}{W_c N_c} \right) N_s$$

For each specimen the term is parentheses was constant -- since N_c was always 10 -- and the stress concentration factor was directly proportional to the peak photoelastic fringe order at the boundary of the hole.

Typical photoelastic patterns are shown in Figures A-2 and A-3. Photographic negatives for each of the 20 test conditions were viewed under magnification for determination of fringe order. Peak fringe orders at each hole were estimated to 0.1 fringes.

Stress concentration factors were computed from this data by Eq. 1 and compiled in Tables A-I and A-II. Table A-I given stress concentration factors for the largest stress occurring at the boundary of the additional hole, or at the boundary of the central fastener holes.

Table A-II given stress concentration factors for specific locations depicted at the bottom of the table. In both cases, stress magnitudes at corresponding points may be calculated by multiplying the stress concentration factor by 868 psi.

Figure A-4 illustrates the stress distribution along the hole boundaries. Data was taken from the specimen shown at the upper left in Figure A-3. Figure A-4a represents boundary stresses for the added hole in this case of 3-D spacing. Data for Figure A-4b was taken from the lowermost hole in the same photoelastic pattern, which represents stresses in the fastener hole prior to introduction of the additional hole.

Figure A-5 illustrates the distribution of longitudinal stress along the horizontal centerline of a hole. Data was taken from the added hole in the 6-D spacing series, with holes along the specimen centerline. Frocht's Slope-Equilibrium method (1) was used for this analysis, and the zero degree isoclinic fringes required for the analysis was photographed during the course of the experiments.

DISCUSSION

The maximum experimental error in stress concentraction determinations is assessed as +2%. This includes errors in N_C, N_S and specimen dimensions, and non-linearity of model material performance.

Test conditions for $\frac{1}{4}$ inch and $\frac{1}{2}$ inch holes were identical, except for the model scale factor. Consequently, the resultant stress concentration factors should be identical. Specifically, in Tables A-I and A-II, the concentrations shown in the first and third columns (Fastener Holes Only) should be equal, and values in the second and fifth columns should be equal. These corresponding experimentally determined values are indeed equal within the small deviation attributed to experimental error. Further corroboration of this identity is shown in Figure A-3, in which corresponding paris of photoelastic patterns are seen to be virtually identical.

Several generalizations can be drawn from the results compiled in Tables A-I and A-II:

(1) Peak stresses at off-set holes are only 2% to 6% higher than peak stresses in corresponding centrally located holes. This result can be rationalized by analogy to the case of a hole in an infinite plate, wherein location of the hole is inconsequential. In the present case, the ratio of plate width to hole diameter (vix. 10) was sufficiently larger and the holes sufficiently far from the edge of the plate, to approach the analogous condition. One could further reason that the position of any row of holes would have only minor effect

(1) Frocht, M.M., Photoelasticity, Vol. 1, Chapter 7, John Wiley & Sons, Inc., New York (1941).

on stresses, as long as the row is located within the central half of the plate width.

(2) Peak stresses at additional holes are lower than peak stresses that had existed in adjacent fastener holes before the additional hole was introduced.

(3) Presence of the additional holes decreases peak stresses in adjacent fastener holes. Stresses at holes located far from the additional hole remain unaffected.

(4) Stress concentrations become smaller as hole spacing decreases. This remains true even for the end holes in a row of holes.

(5) For off-set holes, the two peak stresses at each hole differ by about 3½% for 3-D spacing and 2% for 6-D spacing, with the larger value occurring further from the centerline of the plate.

Figures A-4 and A-5 show that the gradient of tangential stresses is very low near the stress maxima, while the gradient of radial stresses is severe . Therefore, strain measuring devices of finite gage length should be located on the cylindrical surface of the hole rather than on the face of the plate adjacent to the hole.

For completeness, gradients in the third direction--parallel to the axis of the hole--should be considered. When plate thickness is not small compared to hole diameter, the peak tangential stress varies slightly with distance from the midplane of the plate. The photoelastic results presented herein give the average value of stress through the plate thickness. The analytic solution (2) for the case of a hole in a thick infinite plate in uniaxial tension provides valuable insight into the question. For that case, Sternberg and Sadowsky show that the peak tangential stress at the midplane is greater than the average value of peak tangential stress by an amount that never exceeds 3% of the average value, regardless of thickness-to-diameter ratio. When thickness-to-diameter ratio is larger, the deviation again reduces to zero at the midplane. Therefore, if uniaxial strain measuring devices are installed on the boundary of the hole near the midplane of the plate, only very small deviations from the present plane stress analysis will be encountered, and these deviations can be assessed and the stresses corrected by application of the Sternberg-Sadowsky solution.

(2) Sternberg, E. and Sadowsky, M.A., "Three-dimensional Solution of the Stress Concentrations Around a Circular Hole in a Plate of Arbitrary Thickness," Jl. Applied Mechanics, 16(1), 27 (March 1949).

TABLE A-I

	CENTRAL HOLE(S) STRESS CONCENTRATION FACTOR $K = \frac{\text{maximum stress at central hole}}{\text{average stress without holes}}$				
	6-D SPACING				
	¼" Dia. Holes		½" Dia. Holes		
	Fastener Holes Only	Additional ¼" hole	Fastener Holes Only	Additional ¼" hole	Additional ½" hole
Load Along Fastener ℄	2.86	2.60	2.88	2.51	2.59
Load Off-set from Fastener ℄	2.93	2.66	2.92	2.54	2.71
	3-D SPACING				
Load Along Fastener ℄	2.53	2.06	2.51	1.54	2.01
Load Off-Set from Fastener ℄	2.63	2.26	2.68	1.67	2.24

Note: To obtain stress at corresponding point, multiply stress concentration factor by 868 psi.

TABLE II

	STRESS CONCENTRATION FACTOR AT SPECIFIED LOCATIONS				
	6-D SPACING				
	¼" Dia. Holes		½" Dia. Holes		
	Fastener Holes Only	Additional ¼" Hole	Fastener Holes Only	Additional ¼" Hole	Additional ½" Hole
Load along Fastener ℄	$K_a = 2.86$	$K_b = 2.60$ $K_a = 2.63$	$K_a = 2.88$	$K_b = 2.51$ $K_a = 2.84$	$K_b = 2.59$ $K_a = 2.68$
Load Off-set from Fastener ℄	$K_c = 2.93$ $K_d = 2.90$	$K_e = 2.66$ $K_f = 2.63$ $K_c = 2.83$ $K_d = 2.80$	$K_c = 2.92$ $K_d = 2.88$	$K_e = 2.54$ $K_f = 2.51$ $K_c = 2.92$ $K_d = 2.88$	$K_e = 2.71$ $K_f = 2.64$ $K_c = 2.84$ $K_d = 2.81$
	3-D SPACING				
Load along Fastener ℄	$K_g = 2.53$ $K_j = 2.61$	$K_h = 2.06$ $K_g = 2.26$ $K_i = 2.52$ $K_j = 2.61$	$K_g = 2.51$	$K_h = 1.54$ $K_g = 2.47$ $K_i = 2.51$	$K_h = 2.01$ $K_g = 2.28$ $K_i = 2.51$
Load Off-set from Fastener ℄	$K_k = 2.63$ $K_l = 2.60$ $K_q = 2.86$ $K_r = 2.76$	$K_m = 2.26$ $K_n = 2.19$ $K_k = 2.39$ $K_l = 2.32$ $K_o = 2.63$ $K_p = 2.56$ $K_q = 2.86$ $K_r = 2.76$	$K_k = 2.68$ $K_l = 2.61$	$K_m = 1.67$ $K_n = 1.60$ $K_k = 2.61$ $K_l = 2.58$ $K_o = 2.68$ $K_p = 2.61$	$K_m = 2.24$ $K_n = 2.18$ $K_k = 2.41$ $K_l = 2.34$ $K_o = 2.64$ $K_p = 2.58$

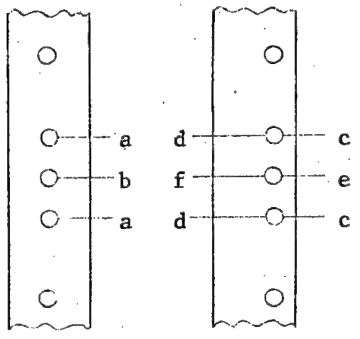

6-D Spacing

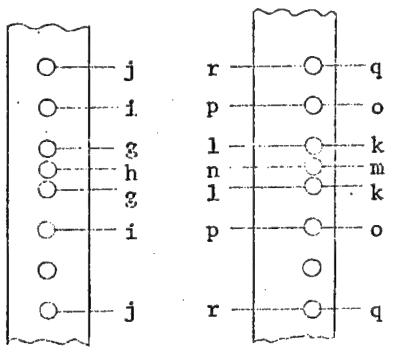

3-D Spacing

FIG. A-1

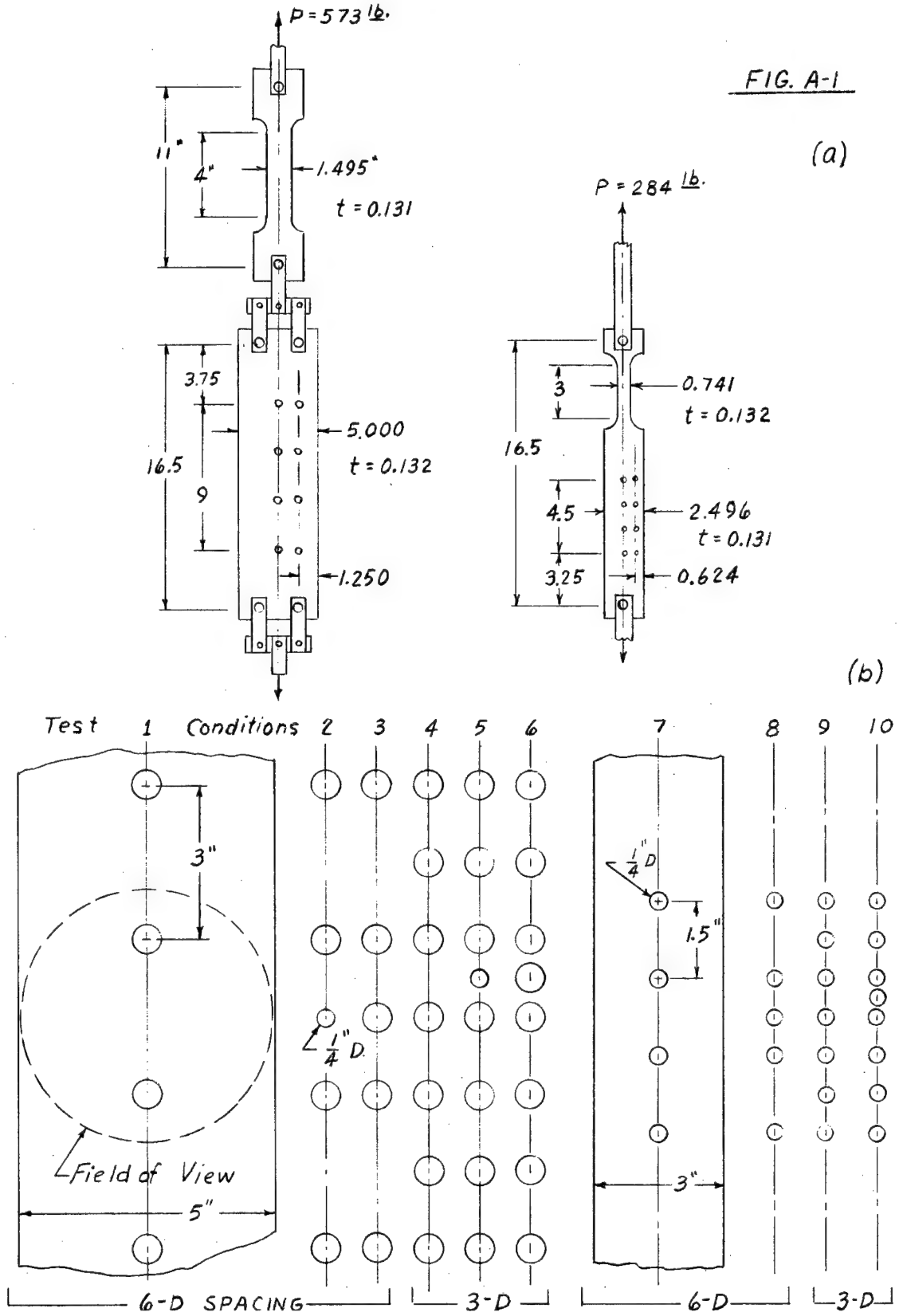
(a)
P = 573 lb.
11"
4"
1.495"
t = 0.131
3.75
16.5
9
5.000
t = 0.132
1.250
P = 284 lb.
3
0.741
t = 0.132
16.5
4.5
2.496
t = 0.131
3.25
0.624
(b)
Test 1 Conditions 2 3 4 5 6 7 8 9 10
3"
Field of View
5"
1/4" D
1/4 D
1.5"
3"
6-D SPACING
3-D
6-D
3-D

Fig. A2 Photoelastic patterns for 6-D spacing of fastener holes. Stress peaks occur at boundary of each hole on horizontal centerline.

Left: ½" fastener holes only
Center: ¼" added hole
Right: ½" added hole

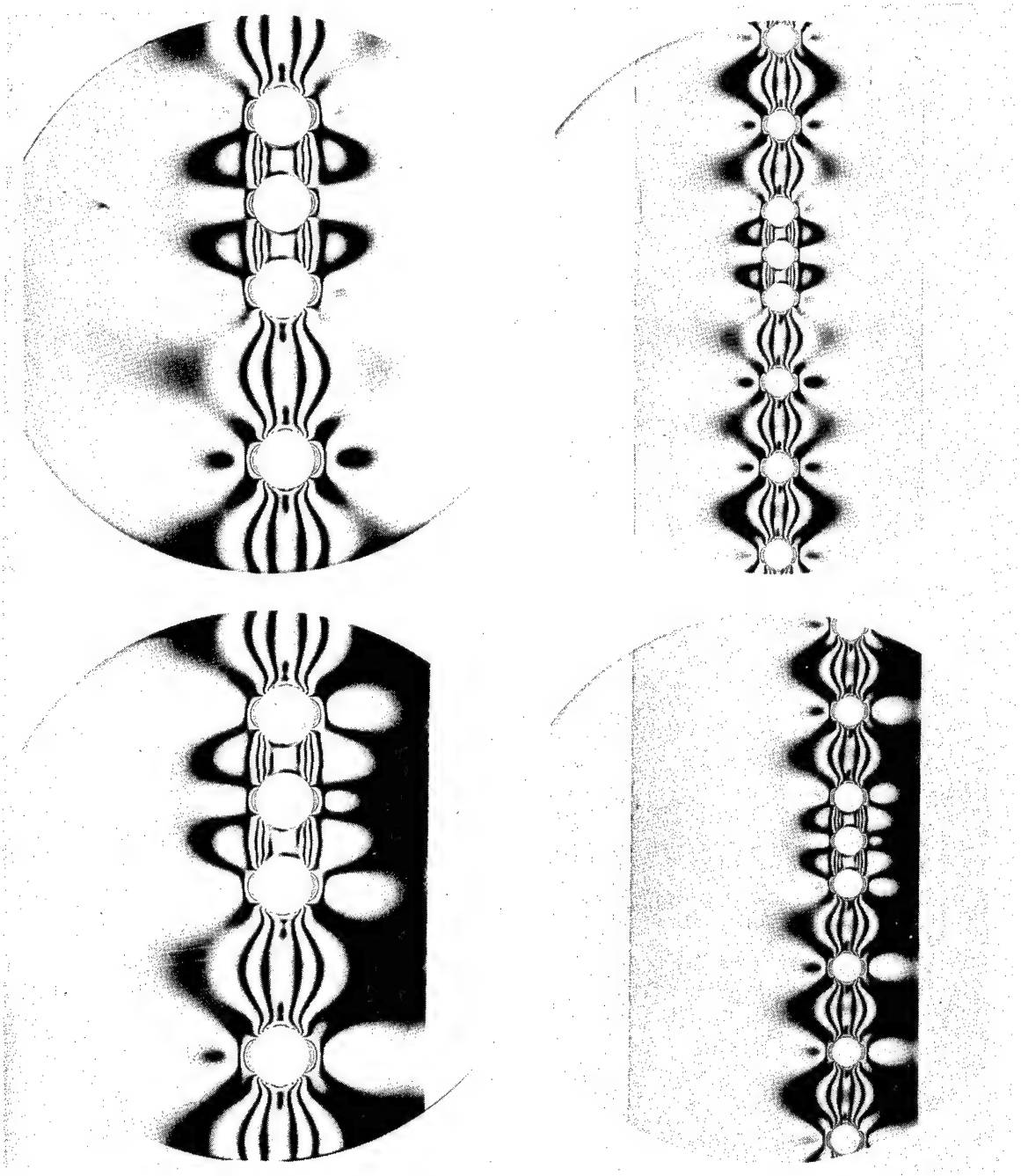

Fig. A 3 Photoelastic patterns for 3-D spacing of fastener holes with added hole of same diameter.

Top: holes along centerline of tensile member; ½" holes on left, ¼" holes on right.
Bottom: holes offset ¼ plate width from centerline; ½" holes on left, ¼" holes on right.

FIG. B-1

(a)

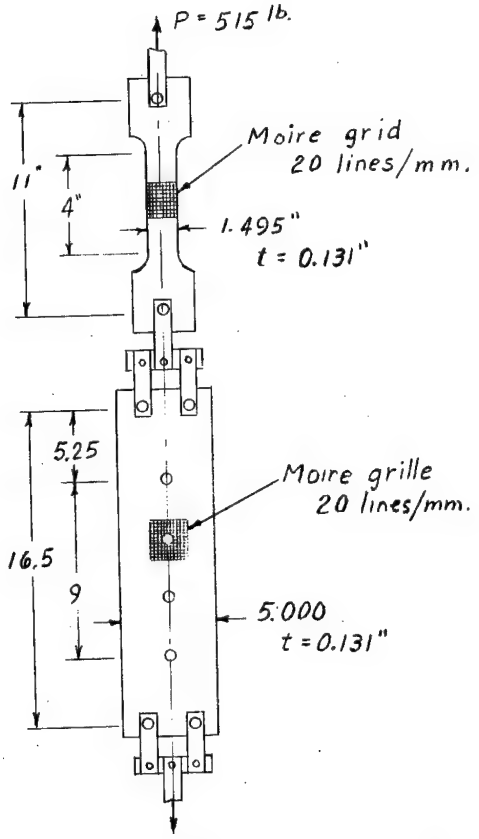
P = 515 lb.
11"
4"
Moire grid
20 lines/mm.
1.495"
t = 0.131"
5.25
16.5
9
Moire grille
20 lines/mm.
5.000
t = 0.131"

(b)

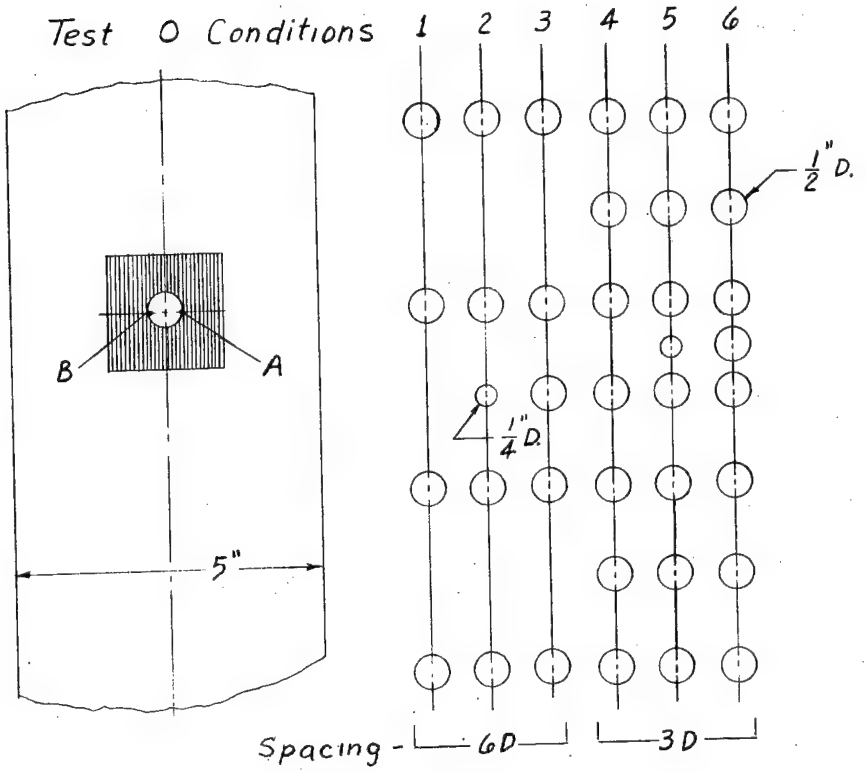
Test O Conditions
1
2
3
4
5
6
B
A
5"
1/2" D.
1/4" D.
Spacing - 6D
3D

APPENDIX B

INFLUENCE OF ADDITIONAL HOLES IN PERFORATED TENSILE PLATES

by Daniel Post

PHOTOLASTIC, INC.
67 Lincoln Highway
Malvern, Pennsylvania

Contract No. N00156-70-C-1524

INFLUENCE OF ADDITIONAL HOLES IN PERFORATED TENSILE PLATES

INTRODUCTION

This investigation is an extension of the study reported November 20, 1969 under Contract No. N00156-70-C-1524, in which stress concentration factors were determined in tensile plates with several perforation configurations. In the present study, the reduction of diameter of holes was measured. Perforation configurations identical to those of the centrally loaded series in the previous analysis were investigated. The issue is important in non-interference fit riveted or bolted structures where the initial diameter of the hole is slightly larger than the fastener diameter; with this information, the nominal stress or strain at which first contact is made between fastener and hole can be calculated.

TEST CONDITIONS, SPECIMENS AND PROCEDURE

The model and test conditions are illustrated in Figure B-1. The model was machined from PSM-1 photolastic plastic, as in the previous study. The calibration member--of the same material--was the part used in the previous study.

The moire method of analysis was used to determine displacements:

(1) displacement of point A with respect to point B on the hole diameter (see Figure B-1b)

(2) longitudinal displacements in calibration member

(3) transverse displacements in calibration member.

The latter measurements were used to determine Young's modulus and Poisson's ratio of the model material.

Moire screens of 20 lines per millimeter were applied to the specimen and calibration member as shown. For this purpose, a photographic emulsion (BX-201, Rockwell Associates, N.Y.C.) was applied and images of master screens were transferred by contact printing in areas shown in Figure B-1.

Subsequently, the specimen and calibration member were loaded in series as illustrated. Load was applied and contact prints of the specimen grille and calibration grid were made on Kodak High Resolution Plates. In this contact printing process, mineral oil was applied to the specimen screen and the photographic plate was clamped against the specimen with a lightweight fixture; illumination by diffused light from the back side of the specimen was used for the photographic exposures. This is the basic data-taking step in the procedure, wherein photographic replicas of the deformed moire screens were obtained.

For each test condition, the load was adjusted such that the 9th order photoelastic fringe was centered in the calibration bar. A photographic replica of the deformed specimen grille was made and then additional holes were drilled in the specimen for the next test condition. A contact print of the grid on the calibration bar was made at the same load. In addition, prints were made with zero load.

These prints of moire screens were analyzed by the method of moire fringe multiplication. In each case, a diffraction grating of 200 lines per millimeter was positioned adjacent to the print and viewed in monochromatic collimated light. Optical filtering in the plane of the decollimating lens yielded clear moire patterns in which each fringe represented a displacement of 1/200 mm.

Parallelism of lines on the print and diffraction grating was adjusted by a micrometer screw. Figure B-2a shows a moire pattern around the hole (for condition 3) when the lines were essentially parallel, while Figure B-2b shows the same combination with slight rotation of the grating. Patterns of the latter type were photographed for all test conditions; they were preferred for measurements since the intersections of fringes with the hole boundary are more clearly defined. These patterns provide permanent records of the displacement fields around the holes.

Data for the various test conditions are compiled in Table B-I. The data for Test Condition 2 were unreasonable and they were rejected, although no reason for the experimental error was uncovered.

CALCULATIONS AND RESULTS

The stress in the calibration member was calculated from previous photoelastic data as follows:

$$\delta_c = \frac{CN}{t} = \frac{38.3(9)}{.131} = 2630 \text{ psi}$$

Stress in the specimen:

$$\delta_s = \frac{\sigma_c w_c}{w_s} = \frac{2635(1.495)}{5.000} = 788 \text{ psi}$$

Strain in the calibration member:

Longitudinal

$$\epsilon_\ell = \frac{\Delta L}{L} = \frac{MP}{L} = \left(\frac{28.5 \quad \frac{1}{(200)\ (25.4)}}{1} \right) = 0.00758$$

Transverse

$$\varepsilon_t = \frac{\Delta L}{L} = \frac{MP}{L} = \frac{-15.3 \left(\frac{1}{5080}\right)}{1} = -0.00301$$

Young's Modulus:

$$E = \frac{\delta_c}{\varepsilon_\ell} = \frac{2630}{0.00758} = 348{,}000 \text{ psi}$$

Poisson's Ratio:

$$\nu = \frac{-\varepsilon_t}{\varepsilon_\ell} = -\frac{-0.00301}{0.00758} = 0.40$$

Nominal Strain in specimen, longitudinal:

$$\varepsilon_\ell = \frac{\delta_s}{E} = \frac{788}{348{,}000} = 0.00226$$

Displacement of point A with respect to B:

For $\varepsilon_\ell = 0.00226$

$$\delta_{A/B} = M_{A/B}^{P} = -6.4 \left(\frac{1}{(200)\ (25.4)}\right) = -0.00126 \text{ in.}$$

For $\varepsilon_\ell = 0.001$

$$\delta_{A/B} = -0.00126 \left(\frac{0.001}{0.00226}\right) = -0.000557 \text{ in.}$$

The decrease of hole diameter is given in Table B-II for various test conditions. The third column lists the change of diameter per 1000 micro-strain, while the fourth column lists the strain required to induce 0.001 in. decrease of hole diameter. In both cases the nominal strain is the longitudinal strain occurring in a uniformly stressed non-perforated portion of the tensile plate.

DISCUSSION

The hole at which measurements were made may be assumed to be a fastener

hole--rivet hole or bolt hole--in a tensile plate. The results show that the decrease of diameter of the fastener hole diminishes as additional holes are introduced in series.

The decrease of hole diameter is controlled by two primary actions:

(1) The flow of tensile forces in material surrounding the hole is not uniformly longitudinal, as it is far from the hole, but rather, it exhibits transverse force components directed toward the longitudinal centerline of the hole.

(2) The Poisson effect causes transverse contraction of the specimen.

Rationalization indicates that the first action predominates, and substantial decrease of diameter would occur even when Poisson's ratio is zero.

The first action explains why the decrease of hole diameter diminishes as additional holes are introduced. As a series of holes become more closely spaced the stress distribution and force flow become more nearly uniaxial and offer less transverse force around the hole.

Poisson's ratio for the model material was 0.4, while the value for structural materials is lower. Consequently, the decrease of hole diameter for structural materials is less than that reported in Table B-II. For a given decrease of diameter, nominal strain in a structural material is larger than that reported. The dependence upon Poisson's ratio is not large, however, and for a material of $\nu = 0.3$, a reasonable estimate puts corresponding values within 10% of those reported.

The foregoing analysis applies to a free insert in the hole. Contact between fastener and hole occurs at an earlier stage when the fastener is pressed against the hole by external forces. In that case, however, contact is made on one side of the hole only, in contrast to the case of contact on two sides caused by deformation of the hole around a free fastener.

TABLE B-I TEST DATA

Test Condition	$M_{A/B}$ full-load	$M_{A/B}$ no-load	$M_{A/B}$ total
0	-5.6	0.8	-6.4
1	-5.2	0.8	-6.0
2	(-5.9)	0.8	
3	-5.1	0.8	-5.9
4	-4.5	0.8	-5.3
5	-4.2	0.8	-5.0
6	-3.8	0.8	-4.6
calibration, longitudinal	40.0*	1.5	38.5
calibration, transverse	-13.85*	1.45	-15.3

$M_{A/B}$ = moiré fringes between points A and B

*For calibration specimen, points A and B were 1.000 in. apart

TABLE B-II DECREASE OF HOLE DIAMETER

Test Condition	$\delta_{A/B}$ measured for nominal strain of ε_ℓ = 0.00226	$\delta_{A/B}$ for nominal strain of ε_ℓ = 0.001 = 1000 μ in/in	ε_ℓ nominal strain for $\delta_{A/B}$ = -0.001 in
0	-0.00126 in.	-0.00056 in.	1800 μ in/in
1	-0.00118	-0.00052	1920
3	-0.00116	-0.00051	1950
4	-0.00104	-0.00046	2170
5	-0.00098	-0.00043	2300
6	-0.00090	-0.00040	2500

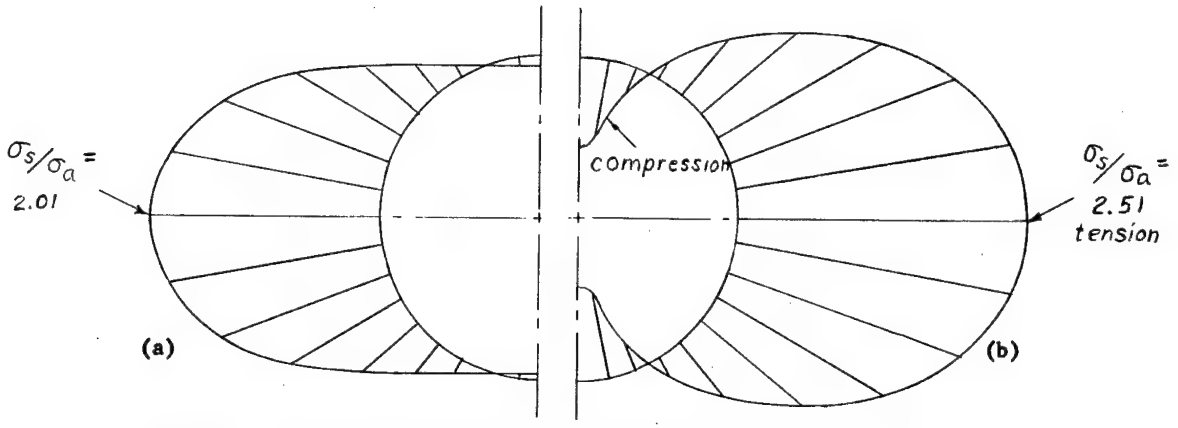

Fig. A-4. Stress distribution around boundary of hole for 3-D spacing, holes along centerline of plate.

(a) added hole
(b) fastener hole

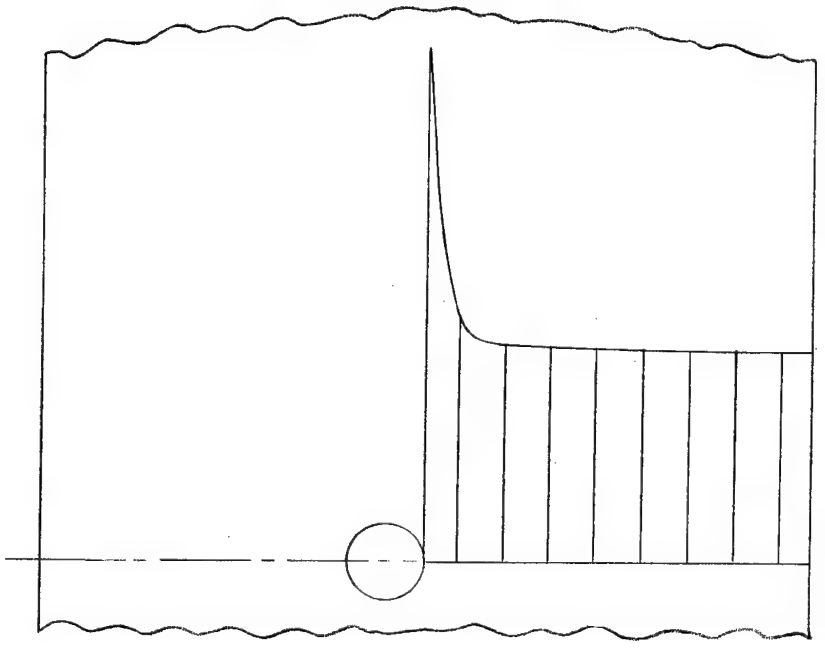

Fig. A-5. Distribution of tensile stress in plate along horizontal centerline of added hole; 6-D spacing, holes along centerline of plate.

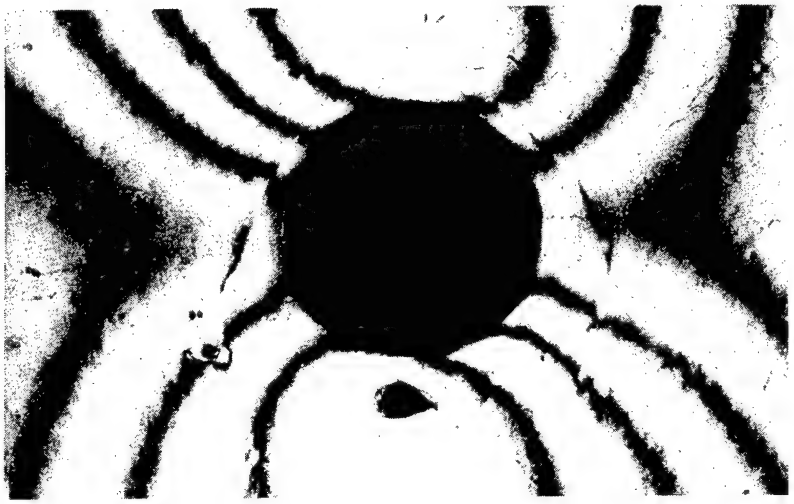

A

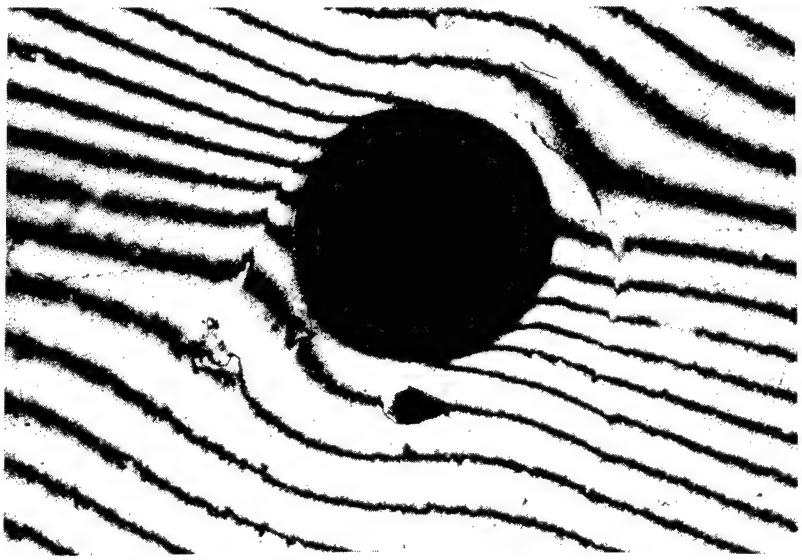

B

Fig. B 2

APPENDIX C

CONSTANT AMPLITUDE TEST DATA

LIST OF FIGURES

LIST OF FIGURES

The constant amplitude test data are plotted in Figure C-1 to C-10 for R = 0, in Figure C-11 to C-18 for R = -½, and in Figure C-19 to C-26 for R = 1. To reduce the data to a more readily comparable basis, the abscissa was normalized by dividing it by the life to failure for each specimen. The normalized data are compared in Figure C-27 to C-32 for R = 0, in Figure C-33 to C-38 for R = -½, and Figure C-39 to C-44 for R = -1.

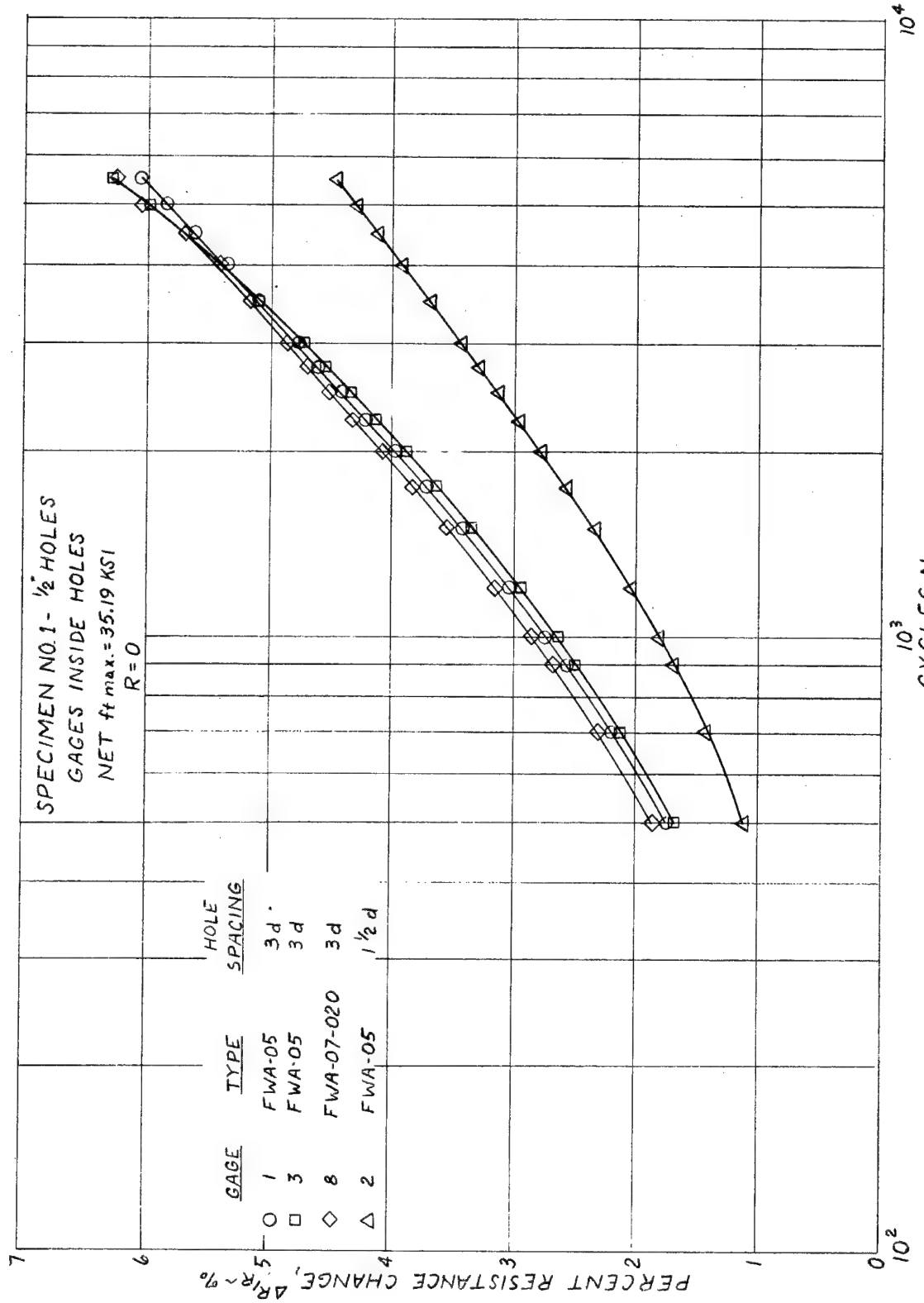

FIG. C-1 GAGE RESPONSE VS. NO. OF CYCLES

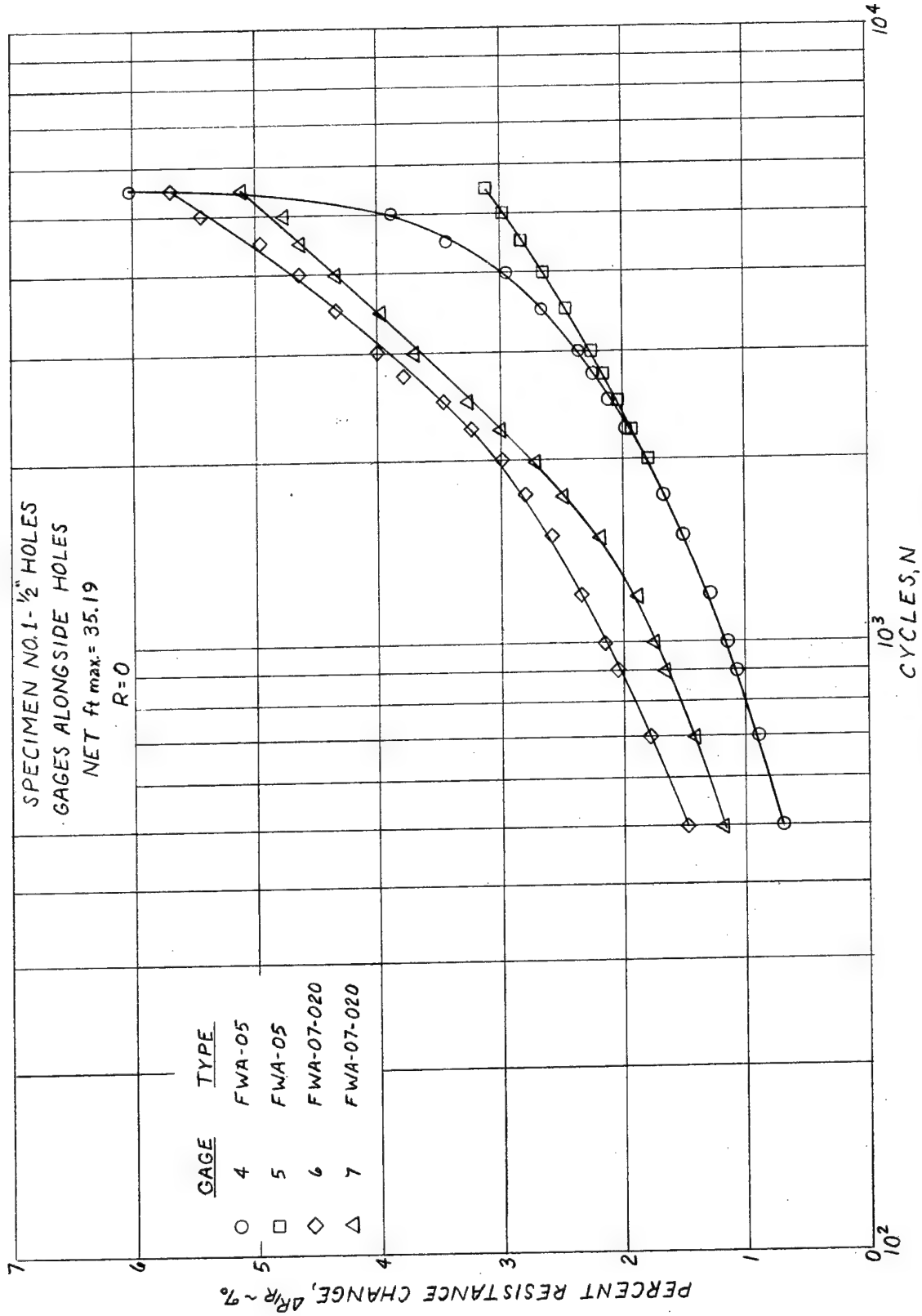

FIG. C-2 GAGE RESPONSE VS. NO. OF CYCLES

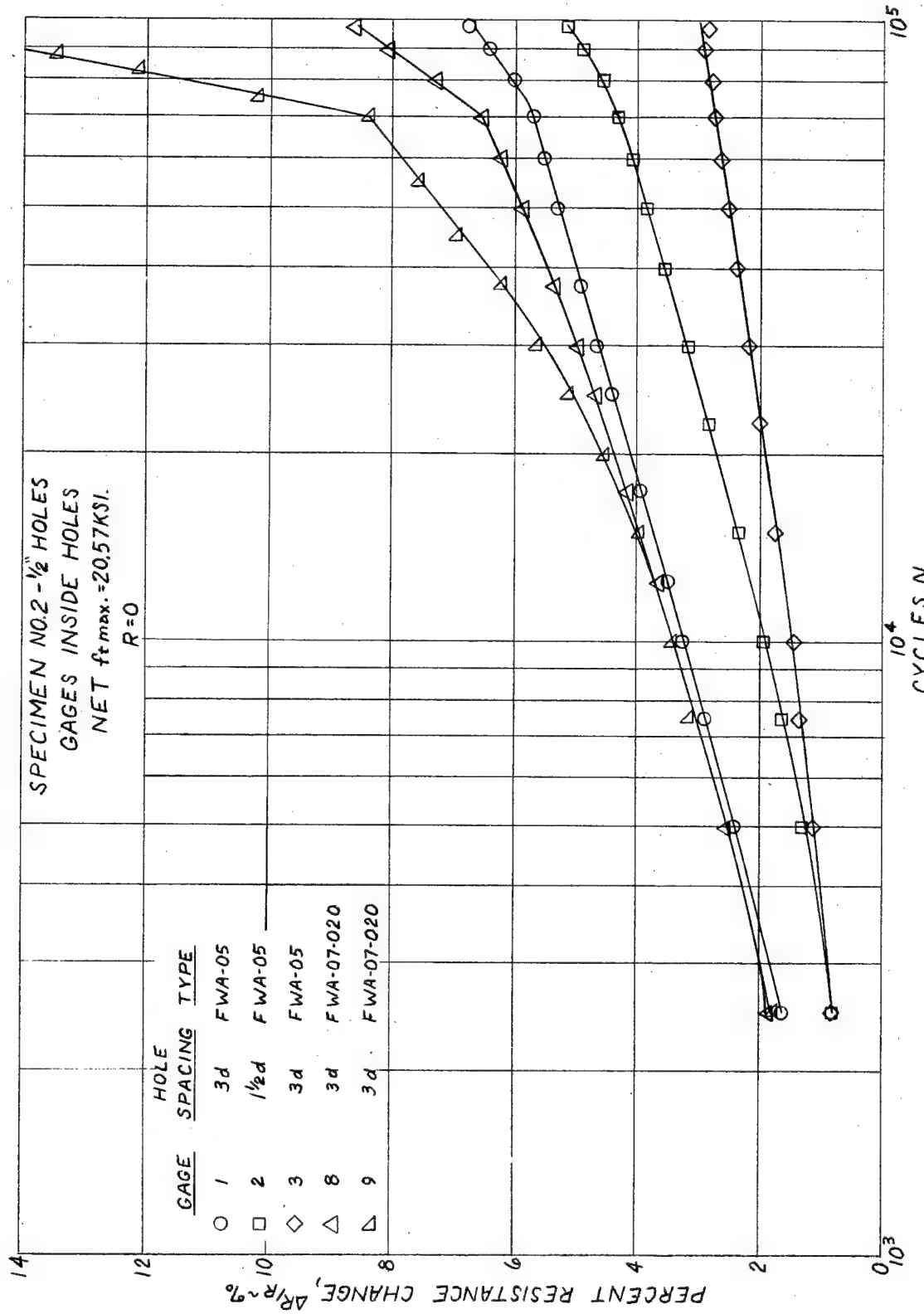

FIG. C-3 GAGE RESPONSE VS. NO. OF CYCLES

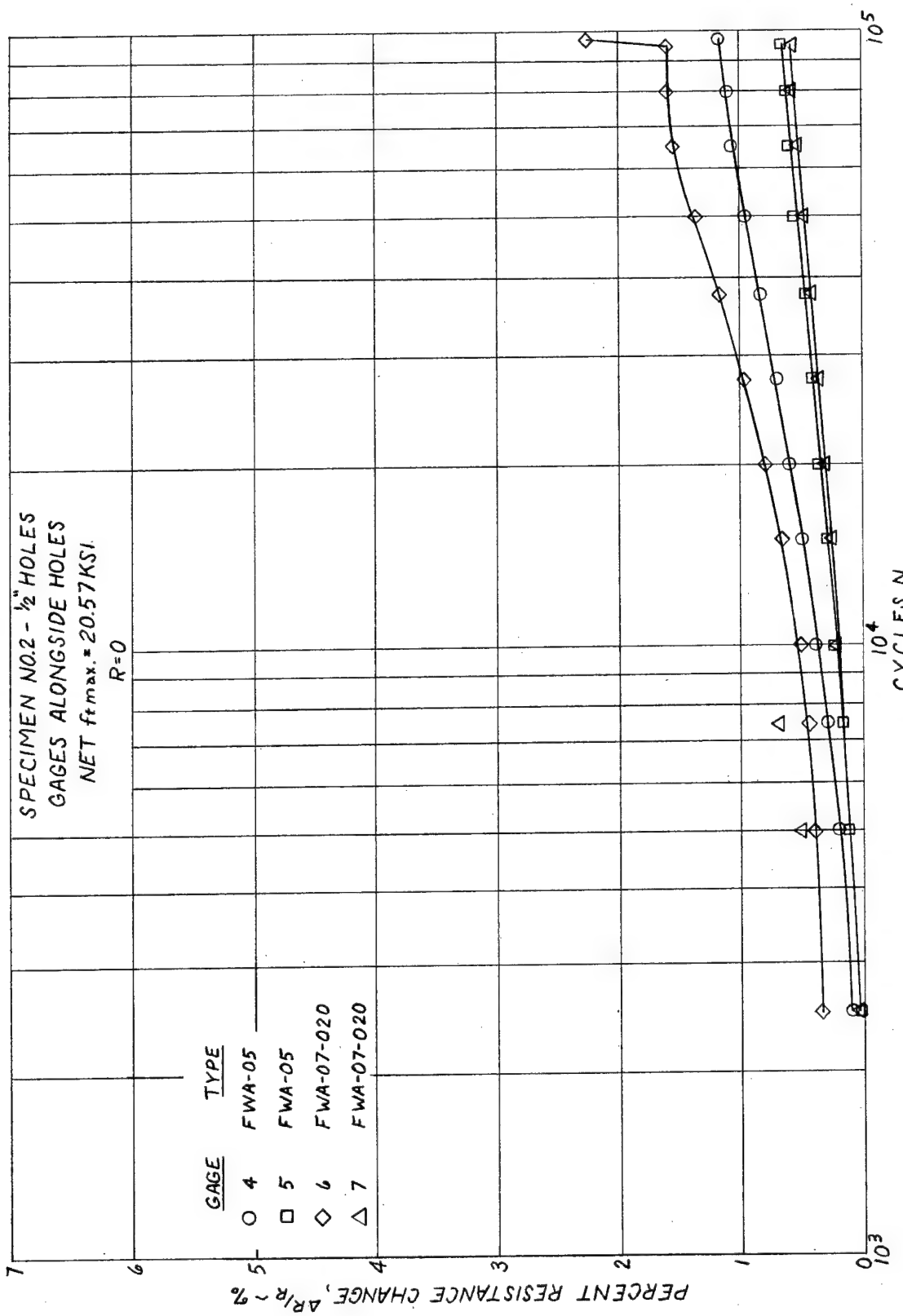

FIG. C-4 GAGE RESPONSE VS. NO. OF CYCLES

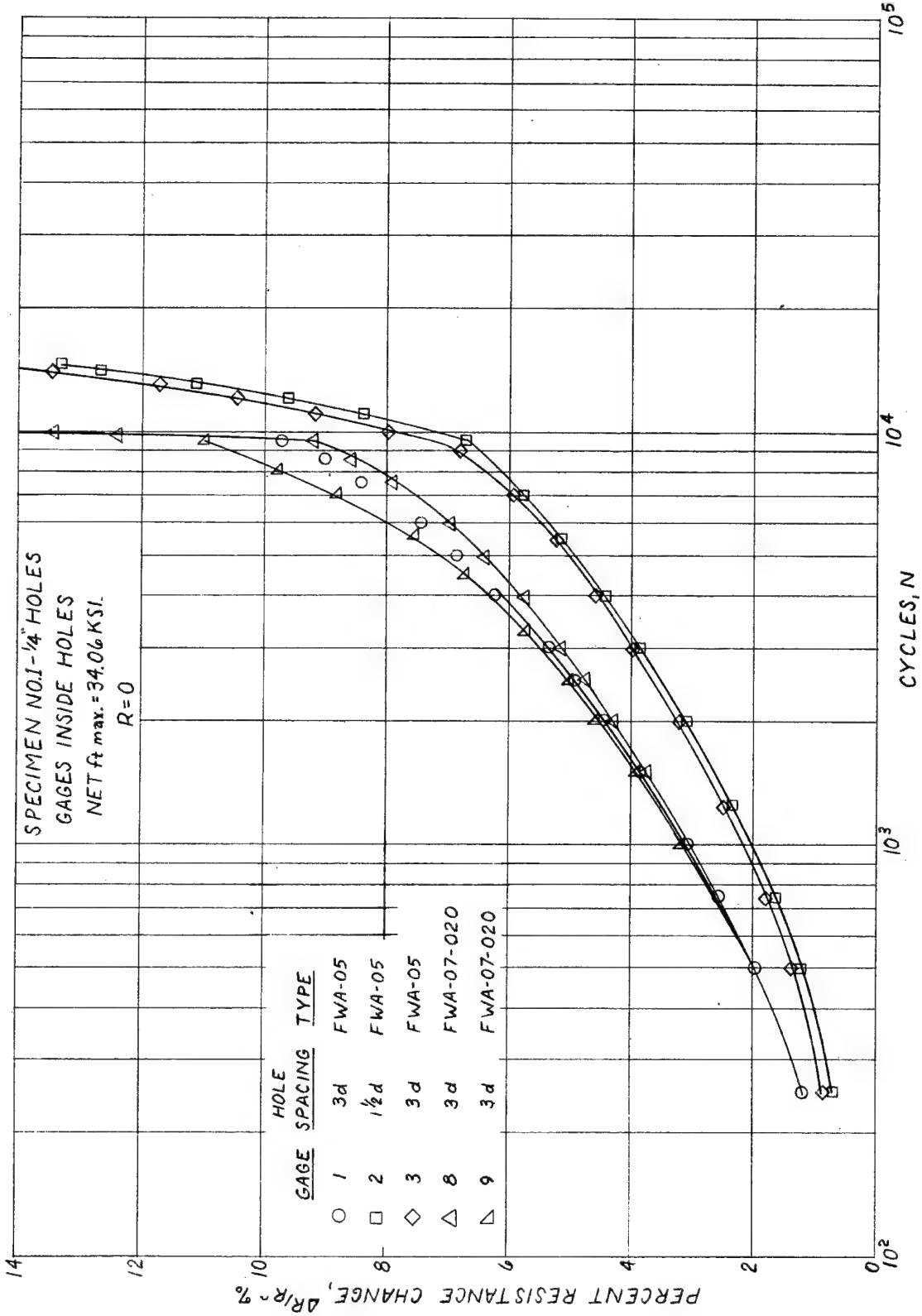

FIG. C-5 GAGE RESPONSE VS. NO. OF CYCLES

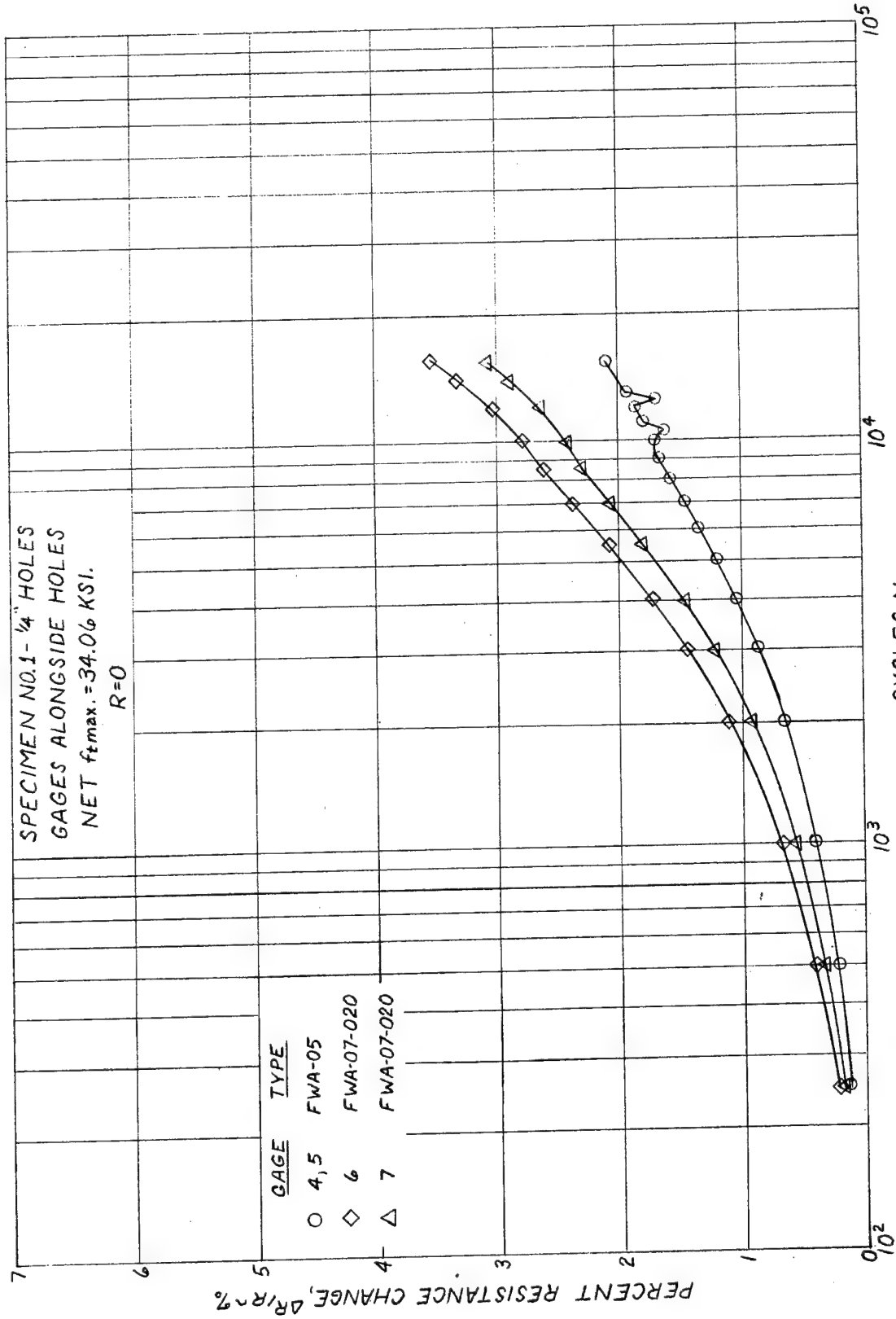

FIG. C-6 GAGE RESPONSE VS. NO. OF CYCLES

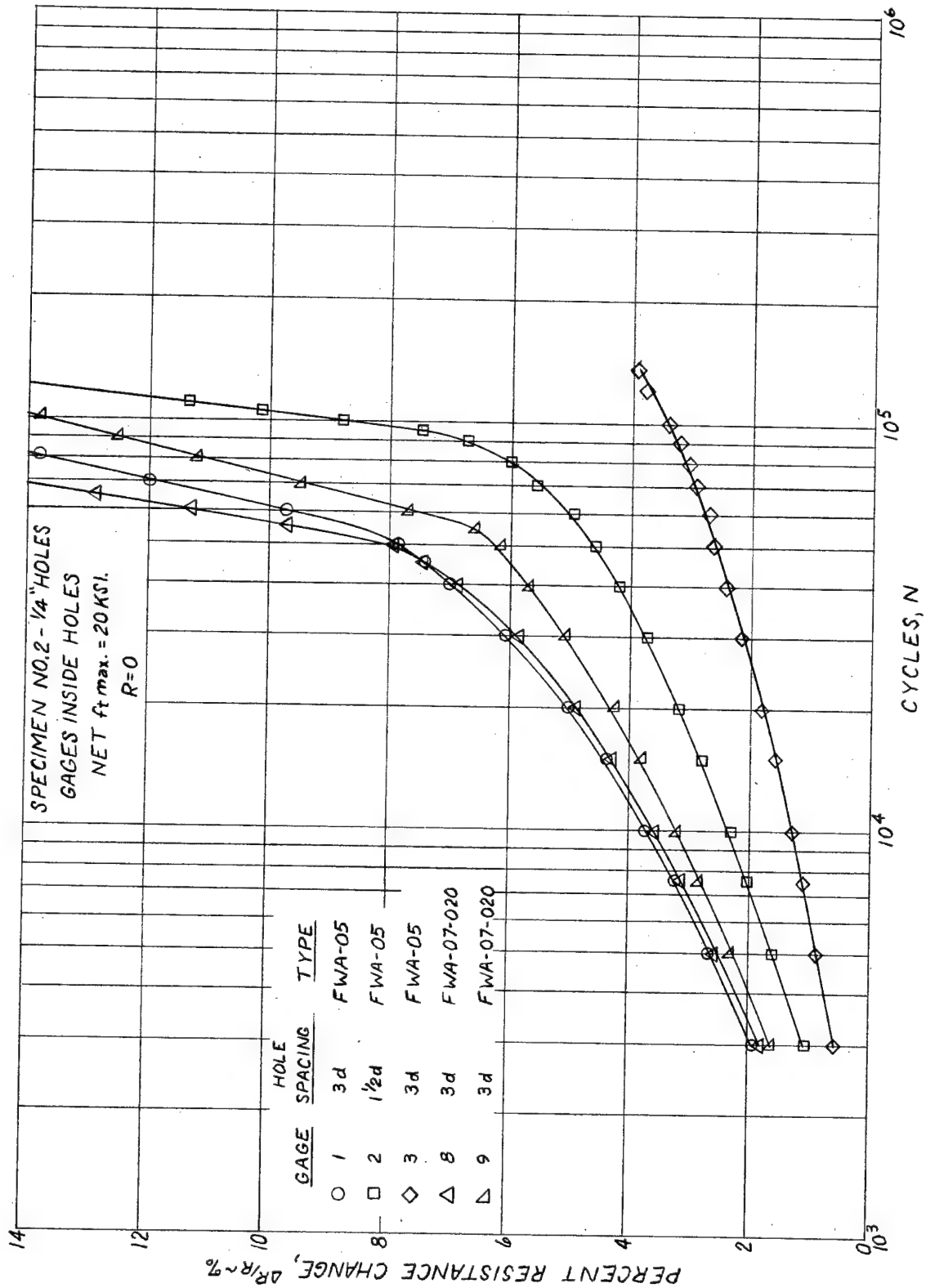

FIG. C-7 GAGE RESPONSE VS. NO. OF CYCLES

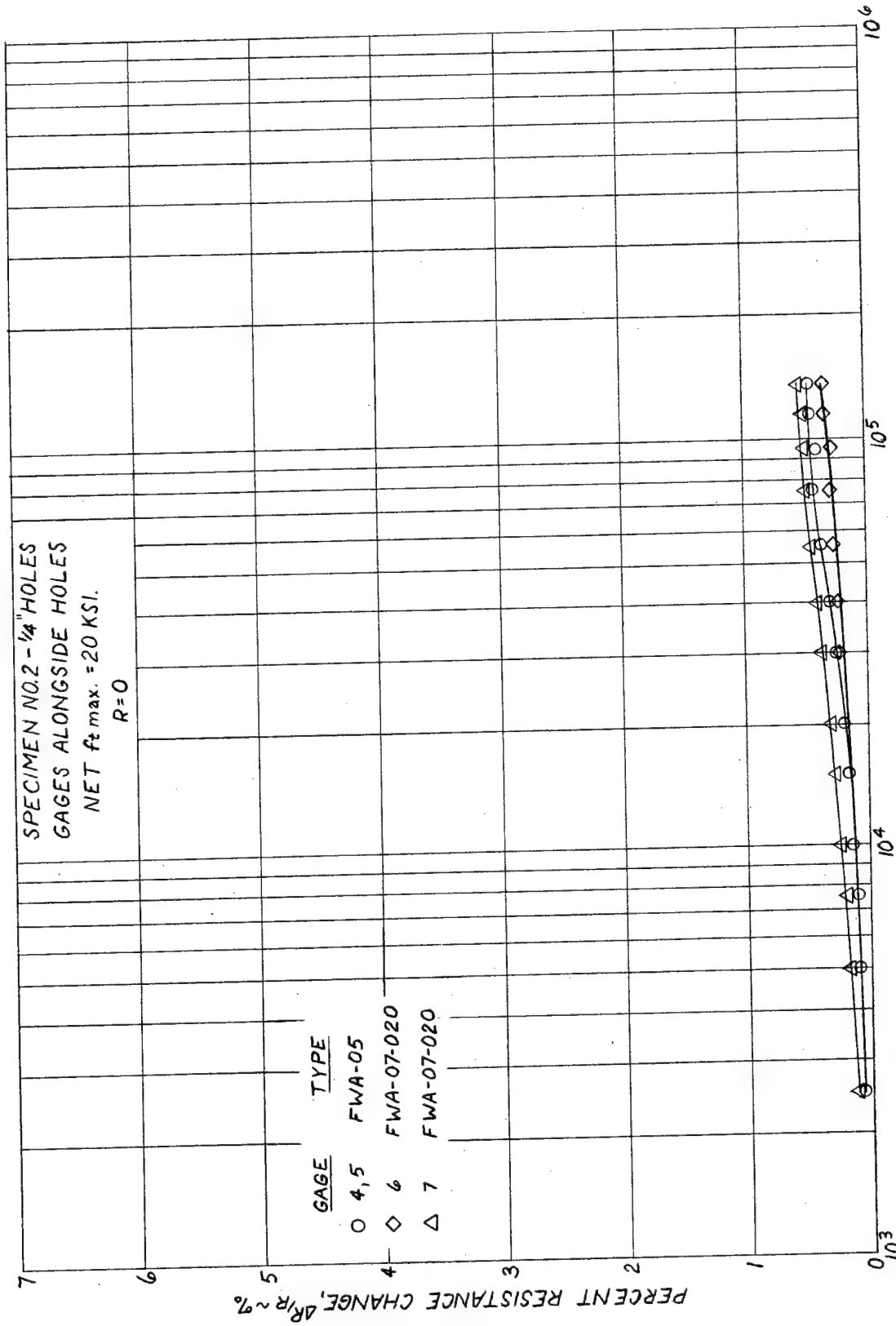

FIG. C-8 GAGE RESPONSE VS. NO. OF CYCLES

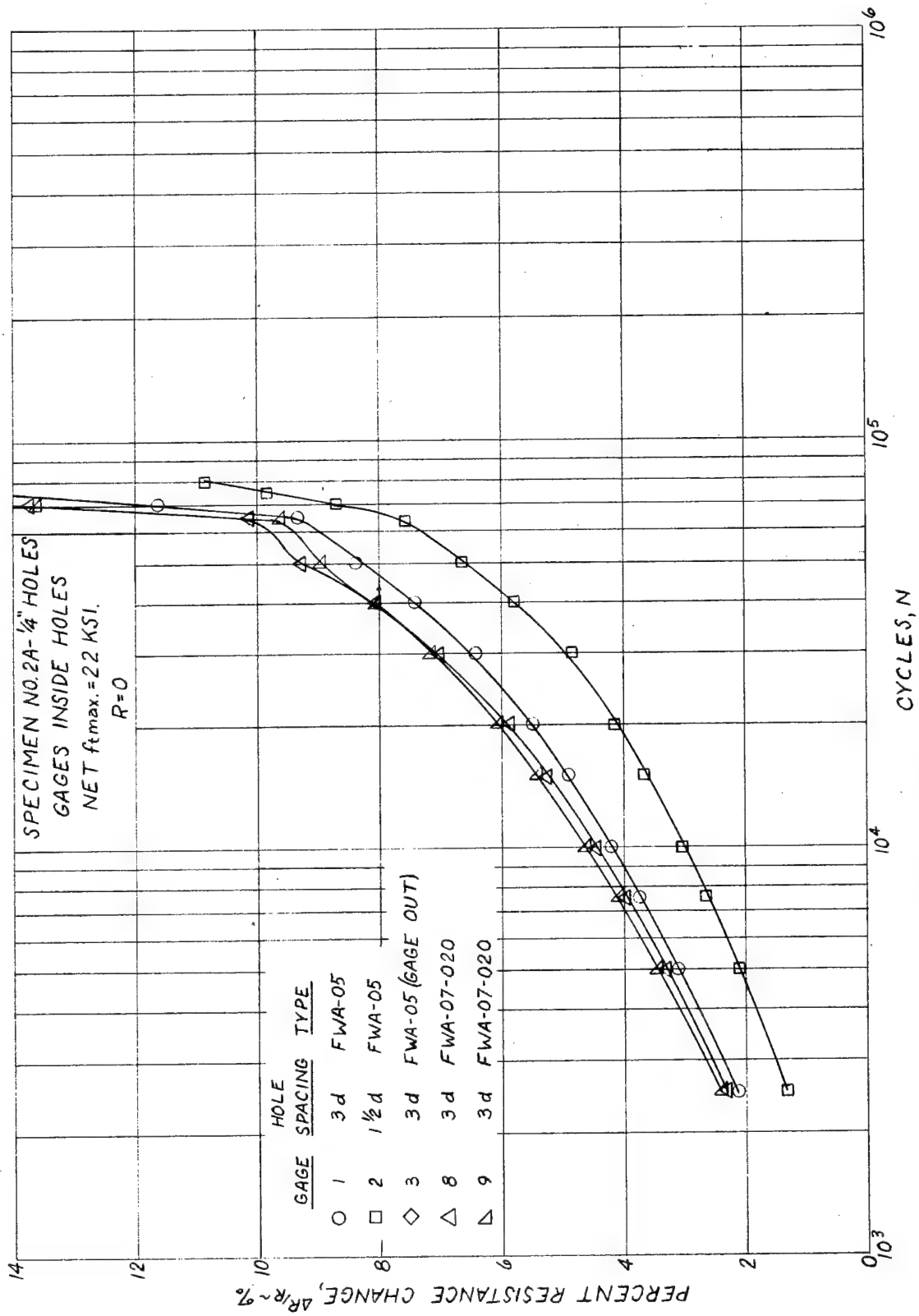

FIG. C-9 GAGE RESPONSE VS. NO. OF CYCLES

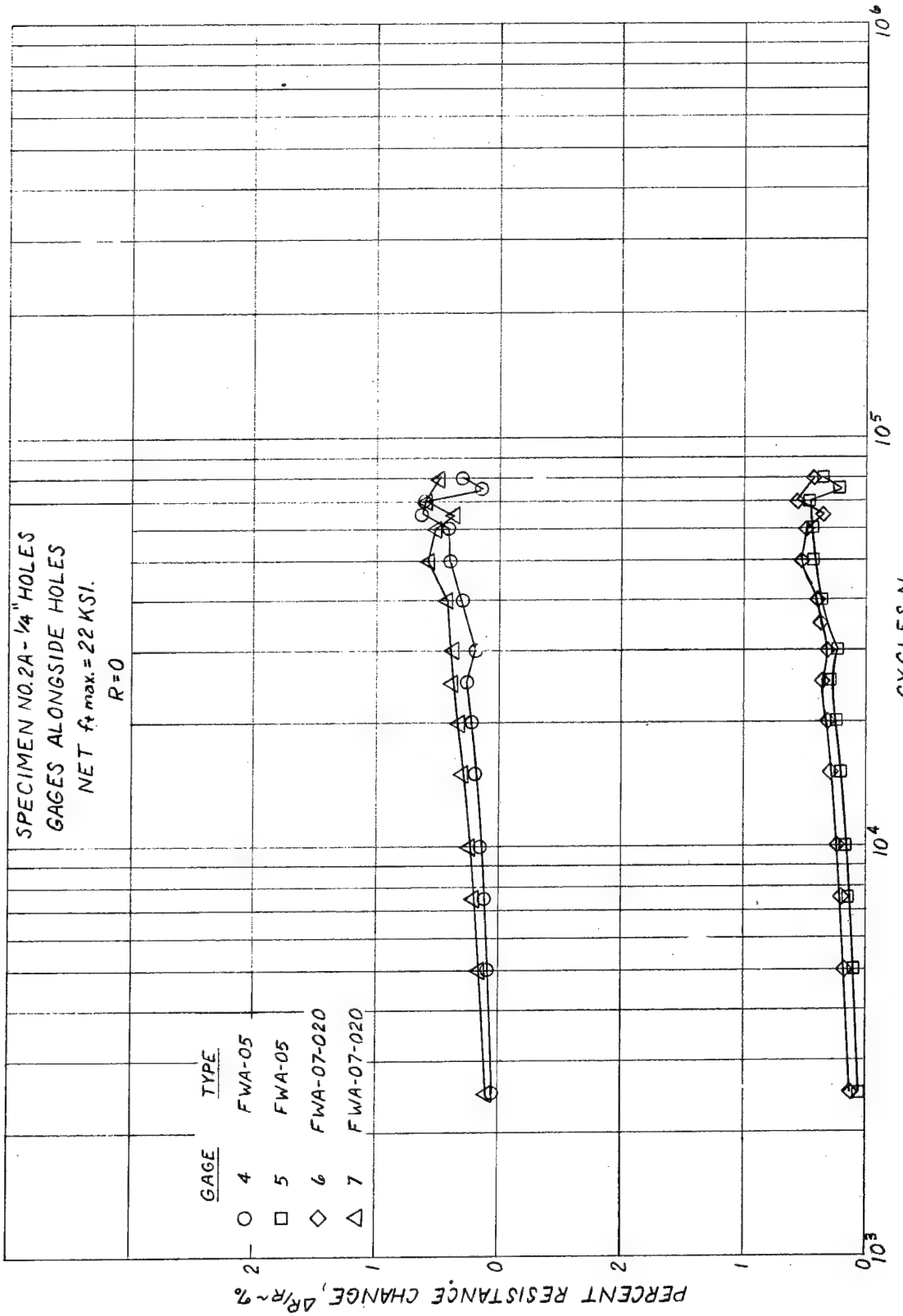

FIG. C-10 GAGE RESPONSE VS. NO. OF CYCLES

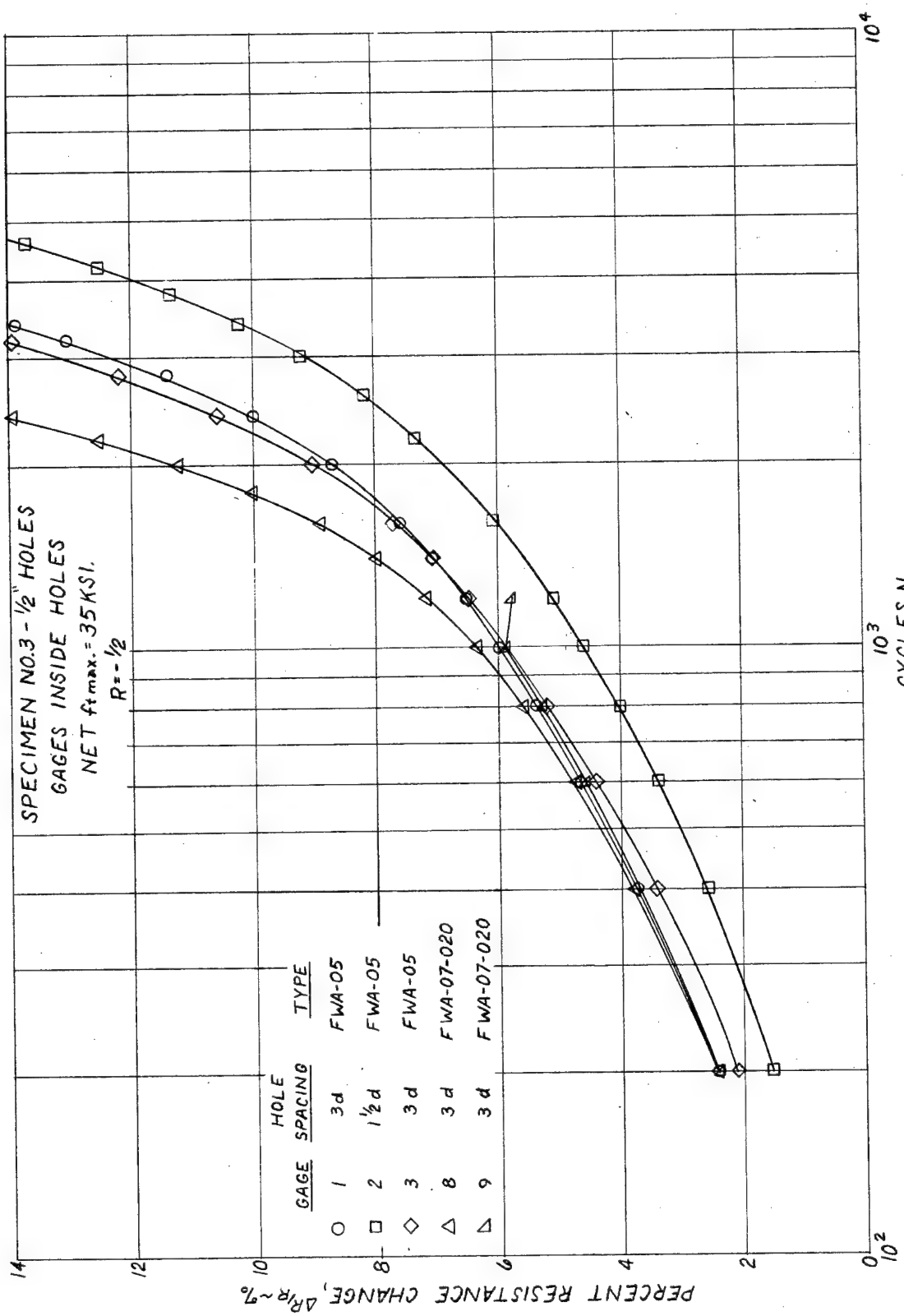

FIG. C-11 GAGE RESPONSE VS. NO. OF CYCLES

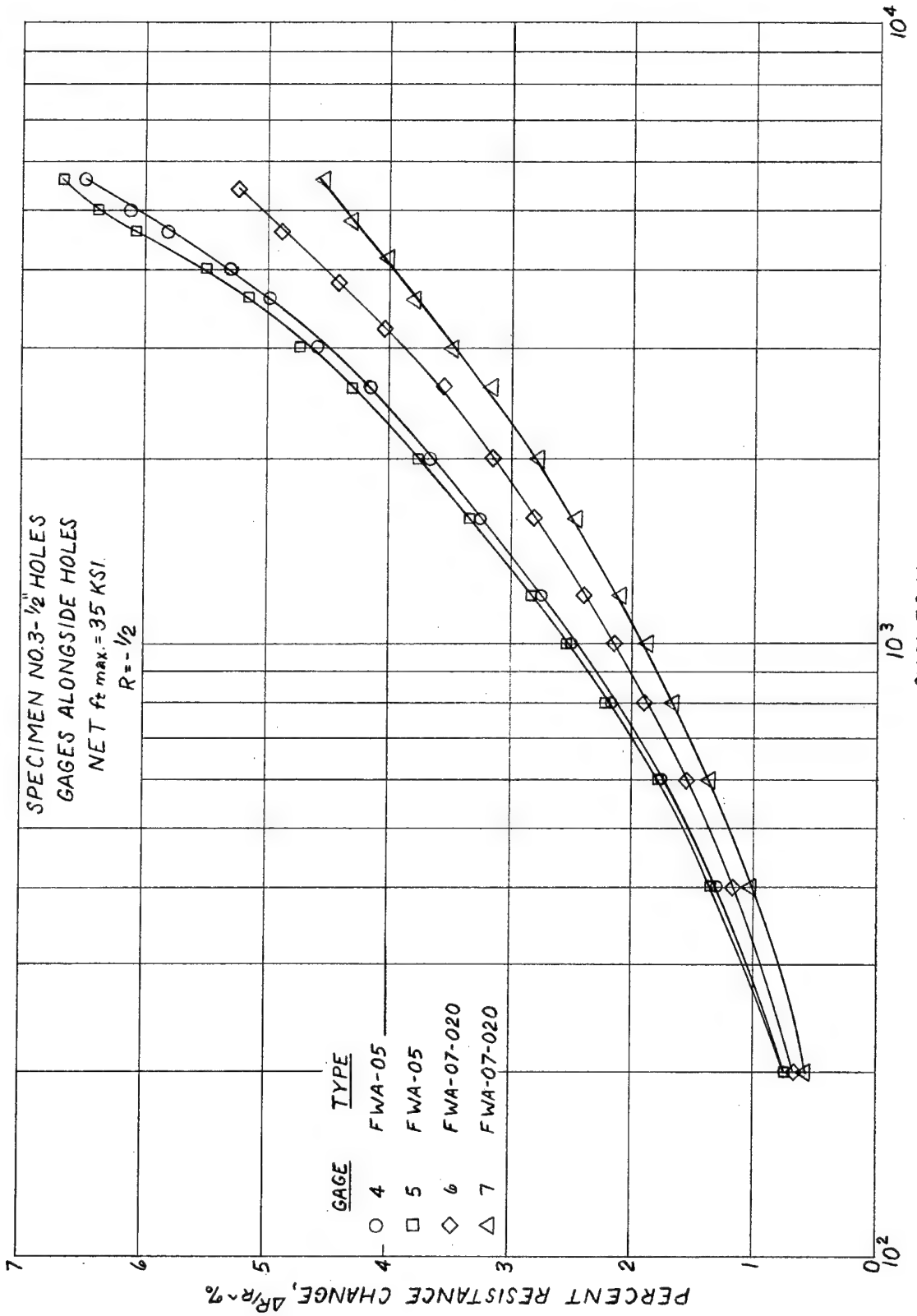

FIG. C-12 GAGE RESPONSE VS NO. OF CYCLES

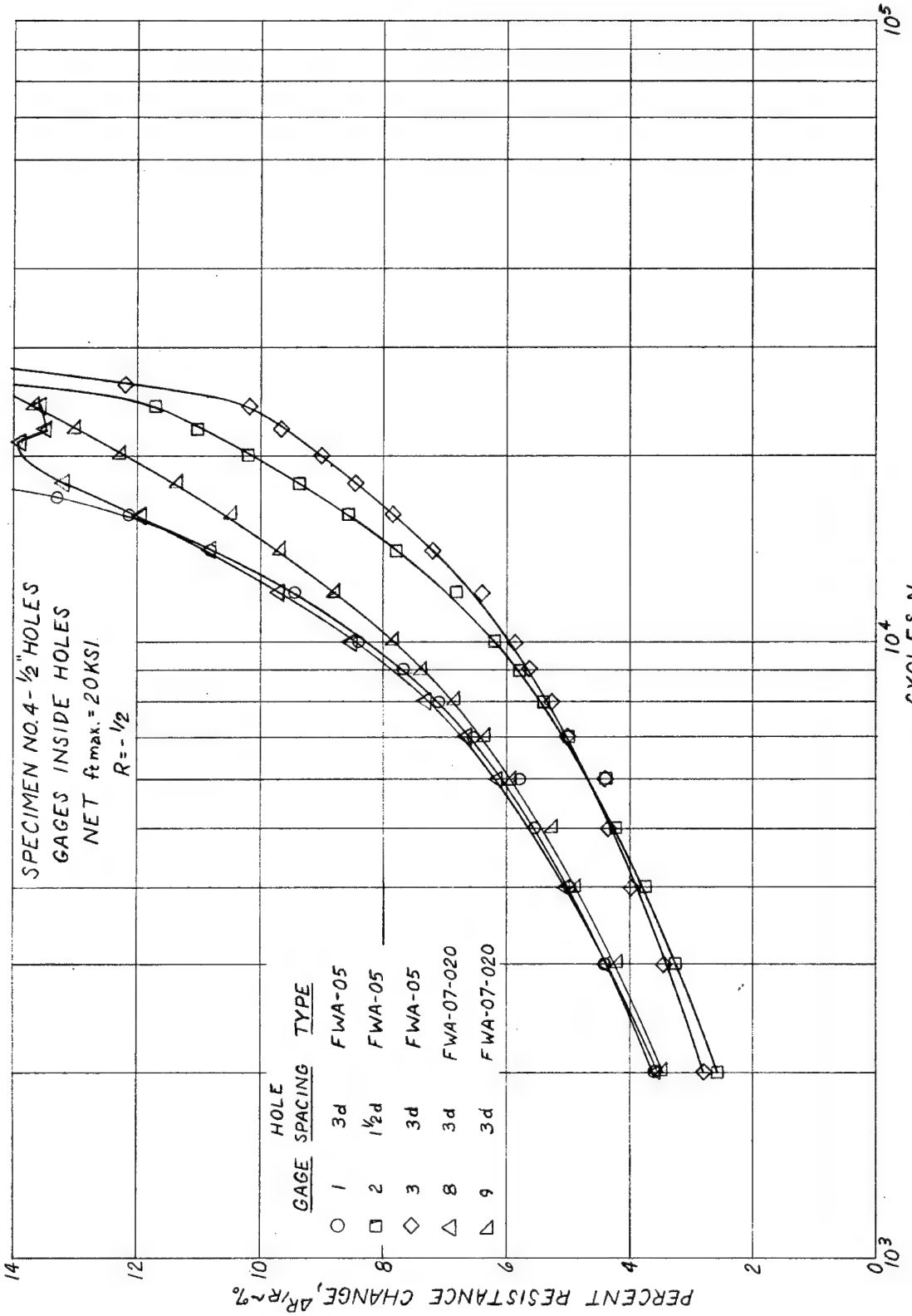

FIG. C-13 GAGE RESPONSE VS. NO. OF CYCLES

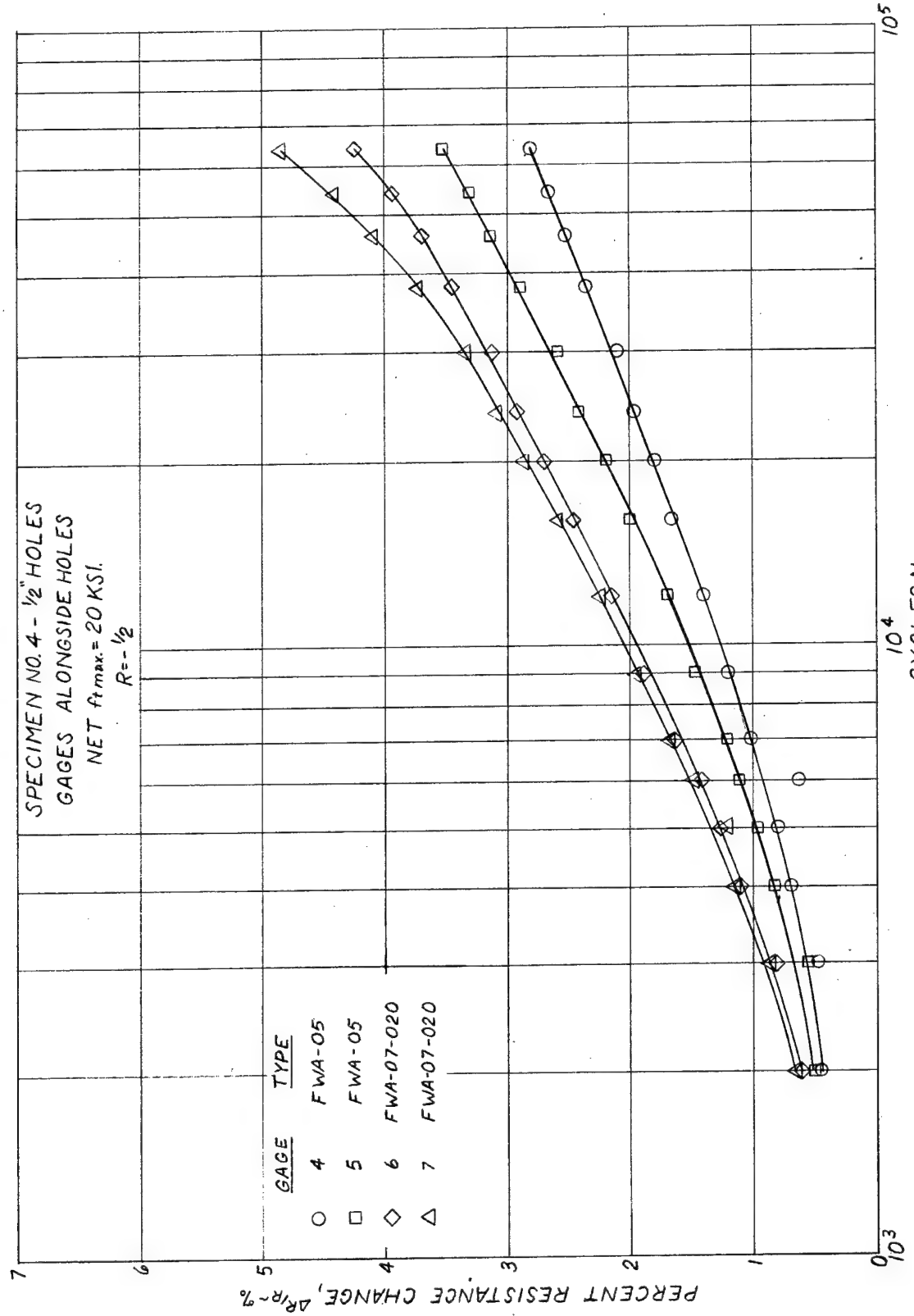

FIG. C-14 GAGE RESPONSE VS. NO. OF CYCLES

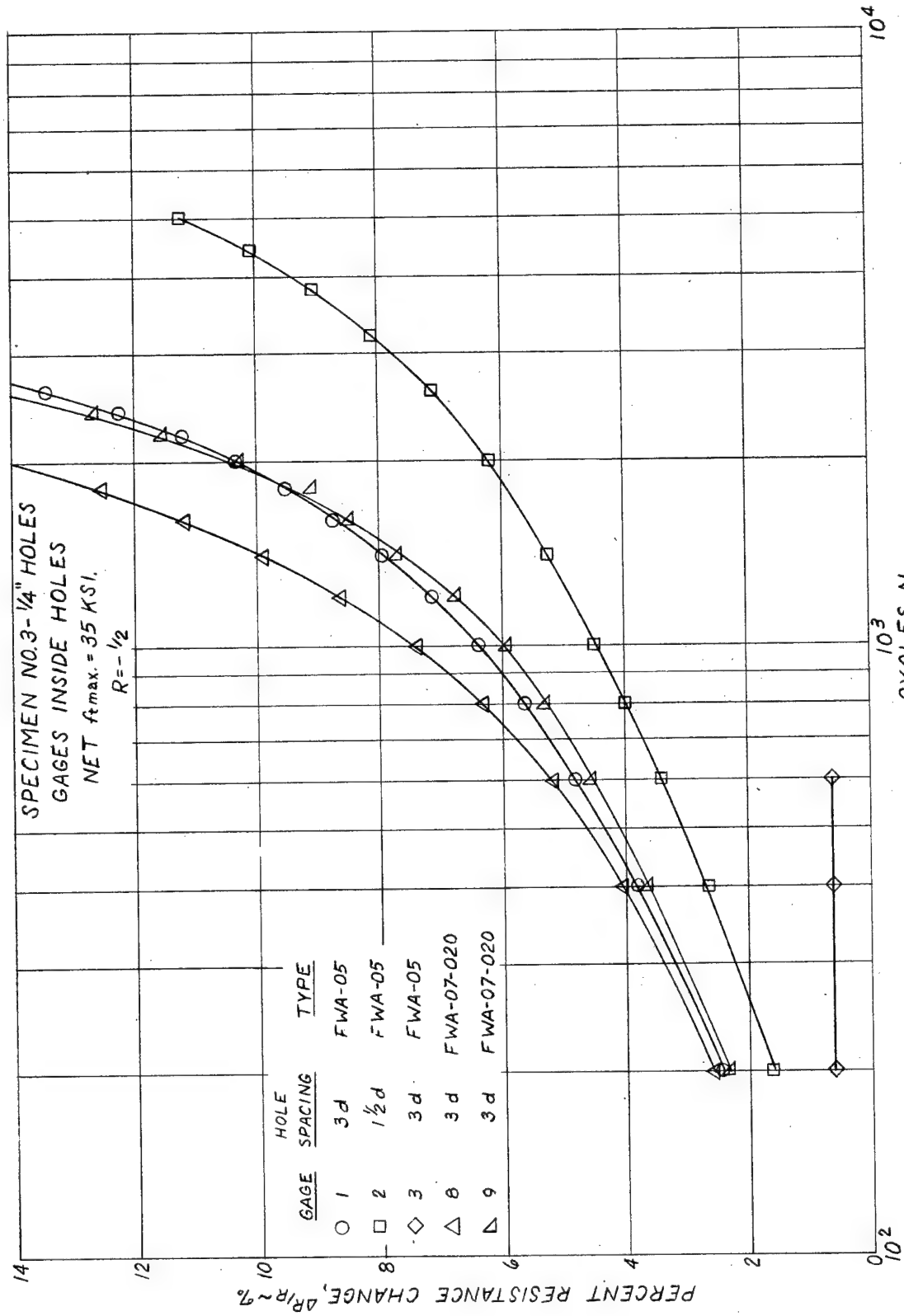

FIG. C-15 GAGE RESPONSE VS. NO. OF CYCLES

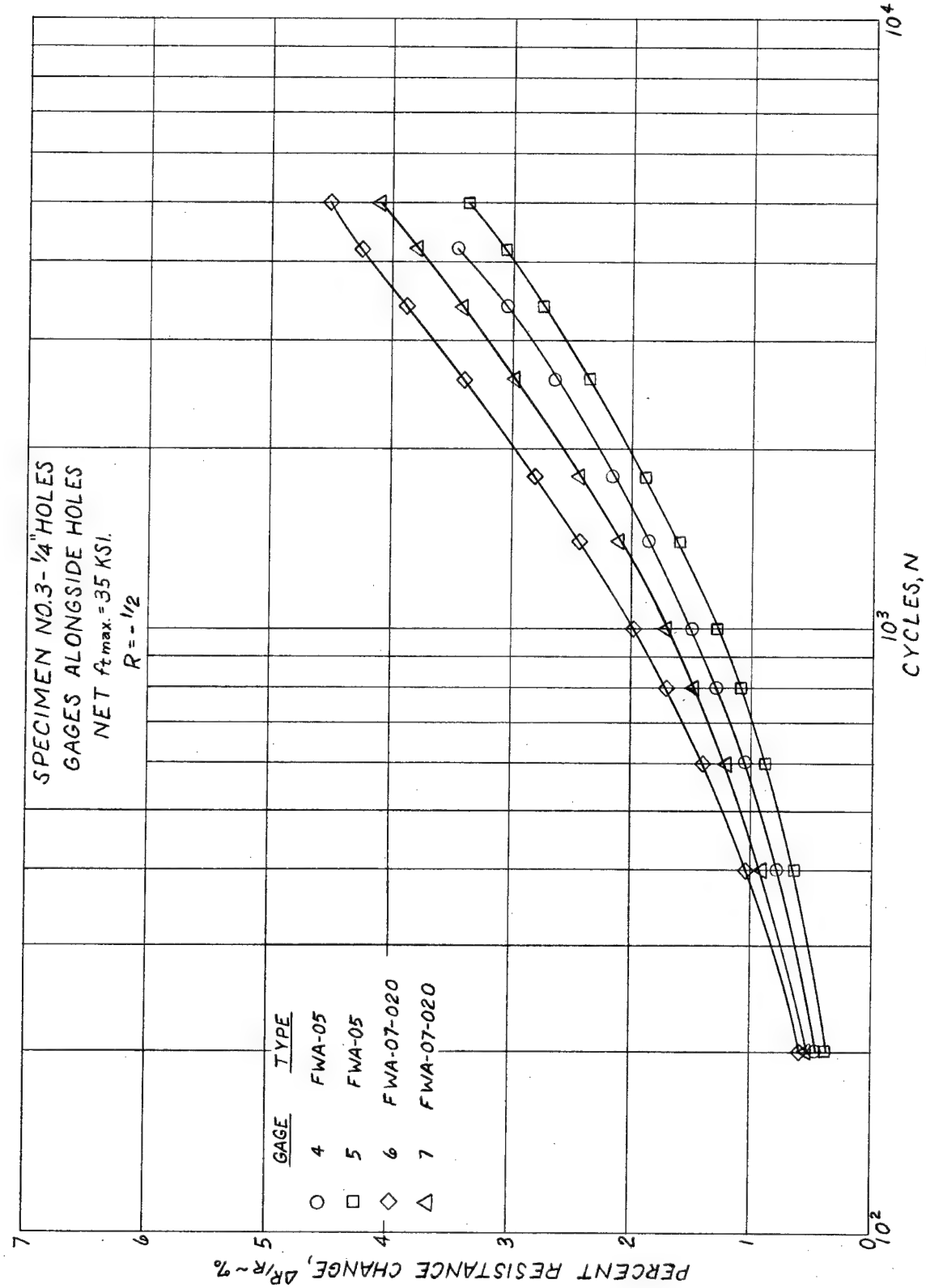

FIG. C-16 GAGE RESPONSE VS. NO. OF CYCLES

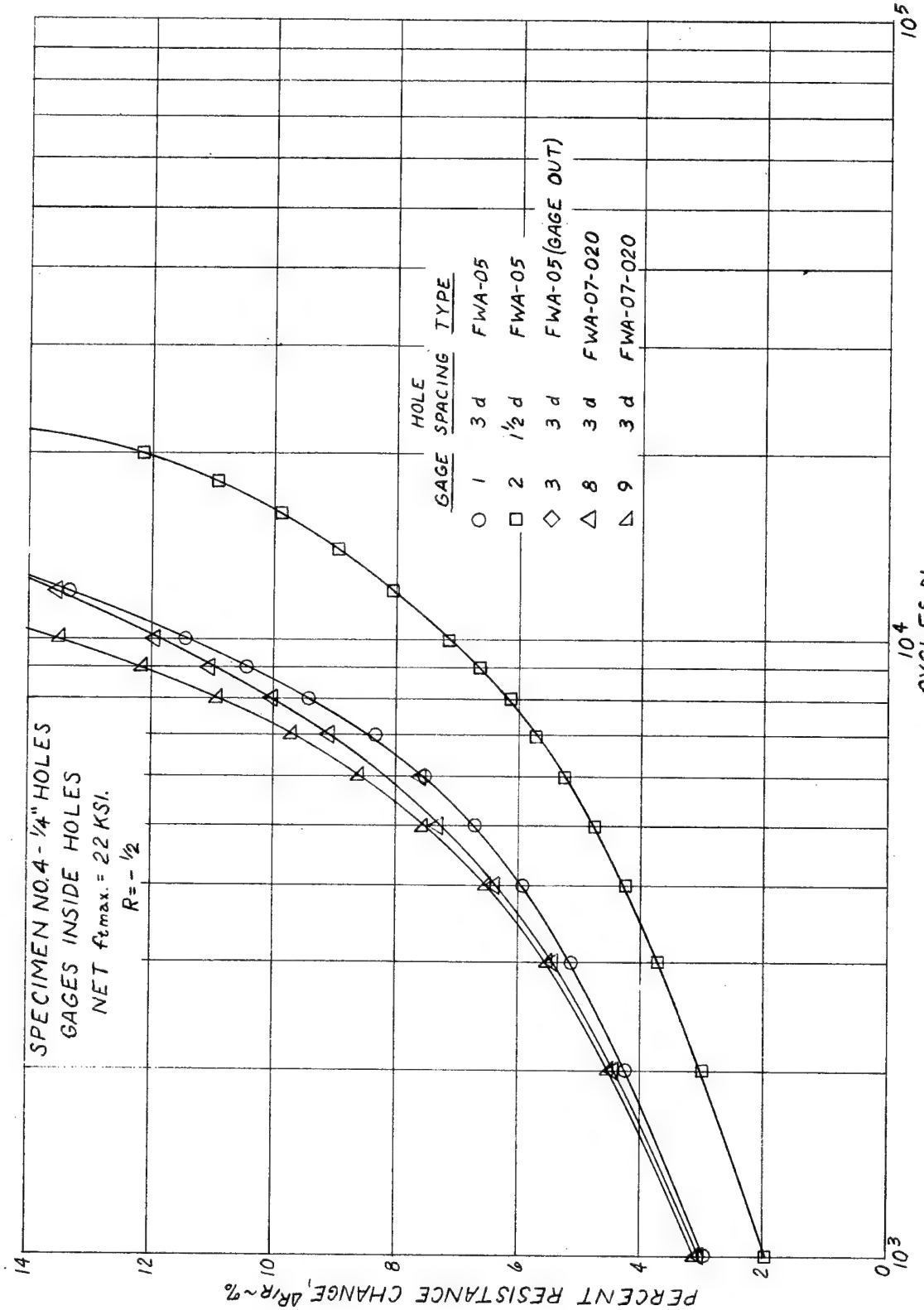

FIG. C-17 GAGE RESPONSE VS. NO. OF CYCLES

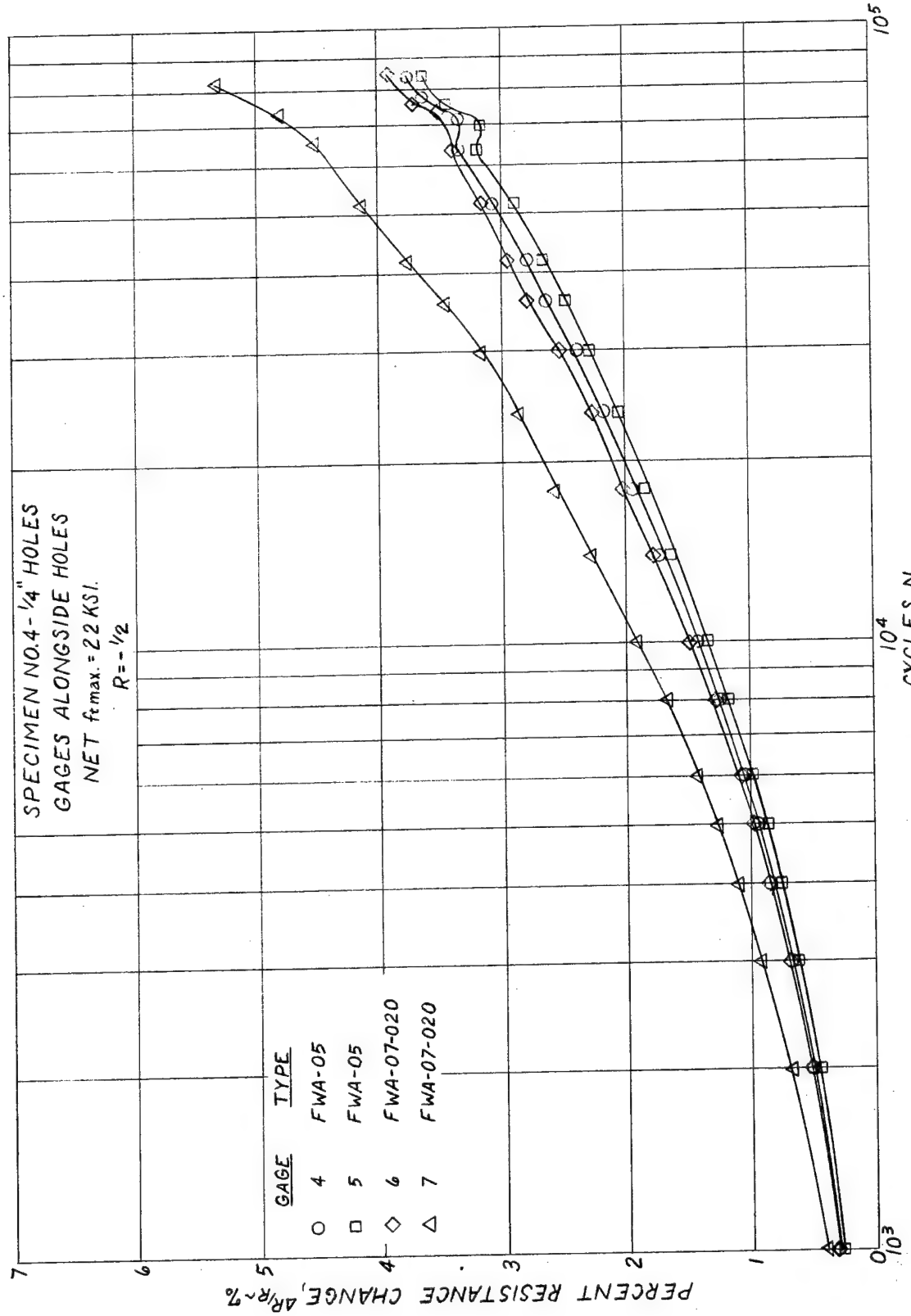

FIG. C-18 GAGE RESPONSE VS. NO. OF CYCLES

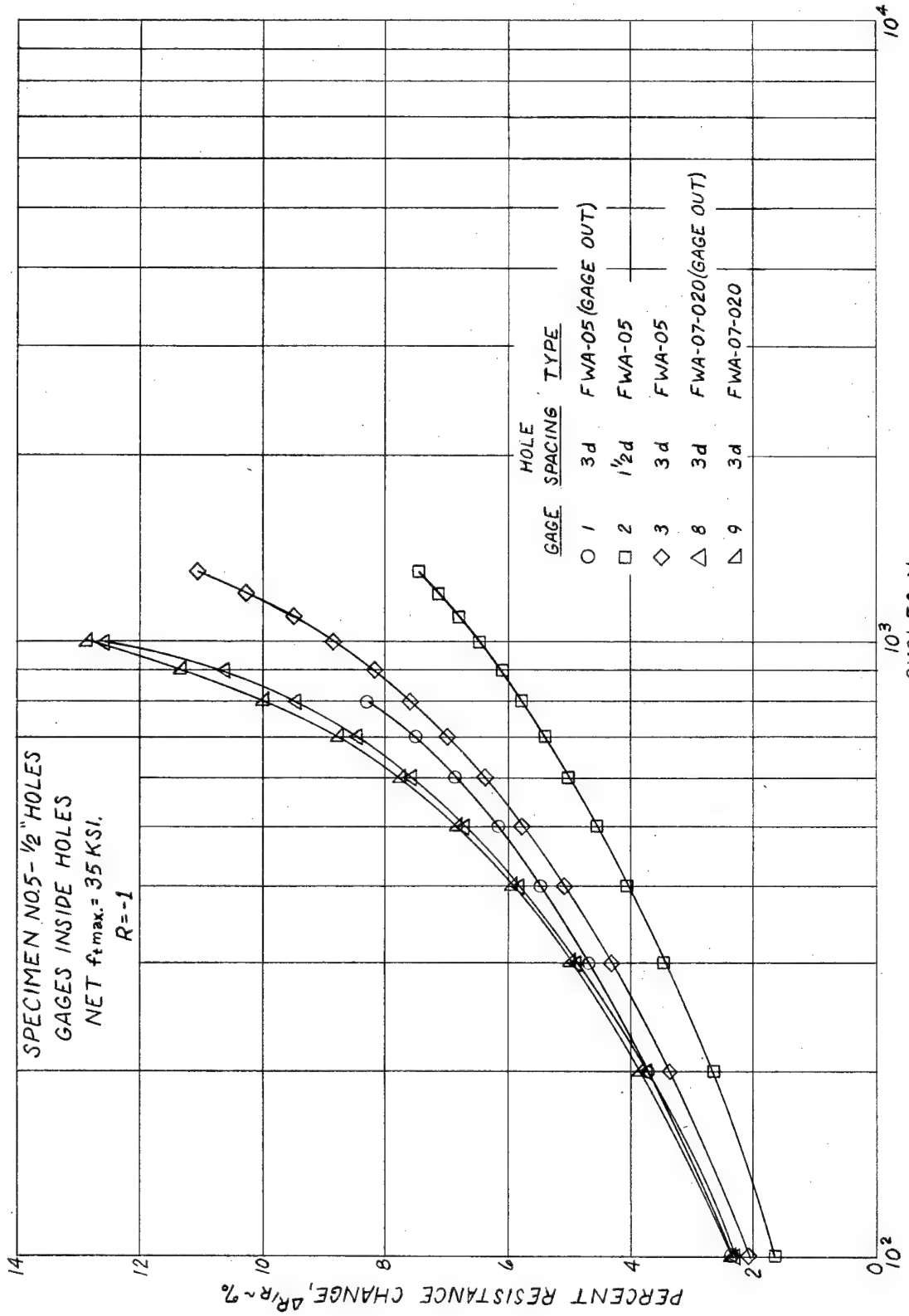

FIG. C-19 GAGE RESPONSE VS. NO. OF CYCLES

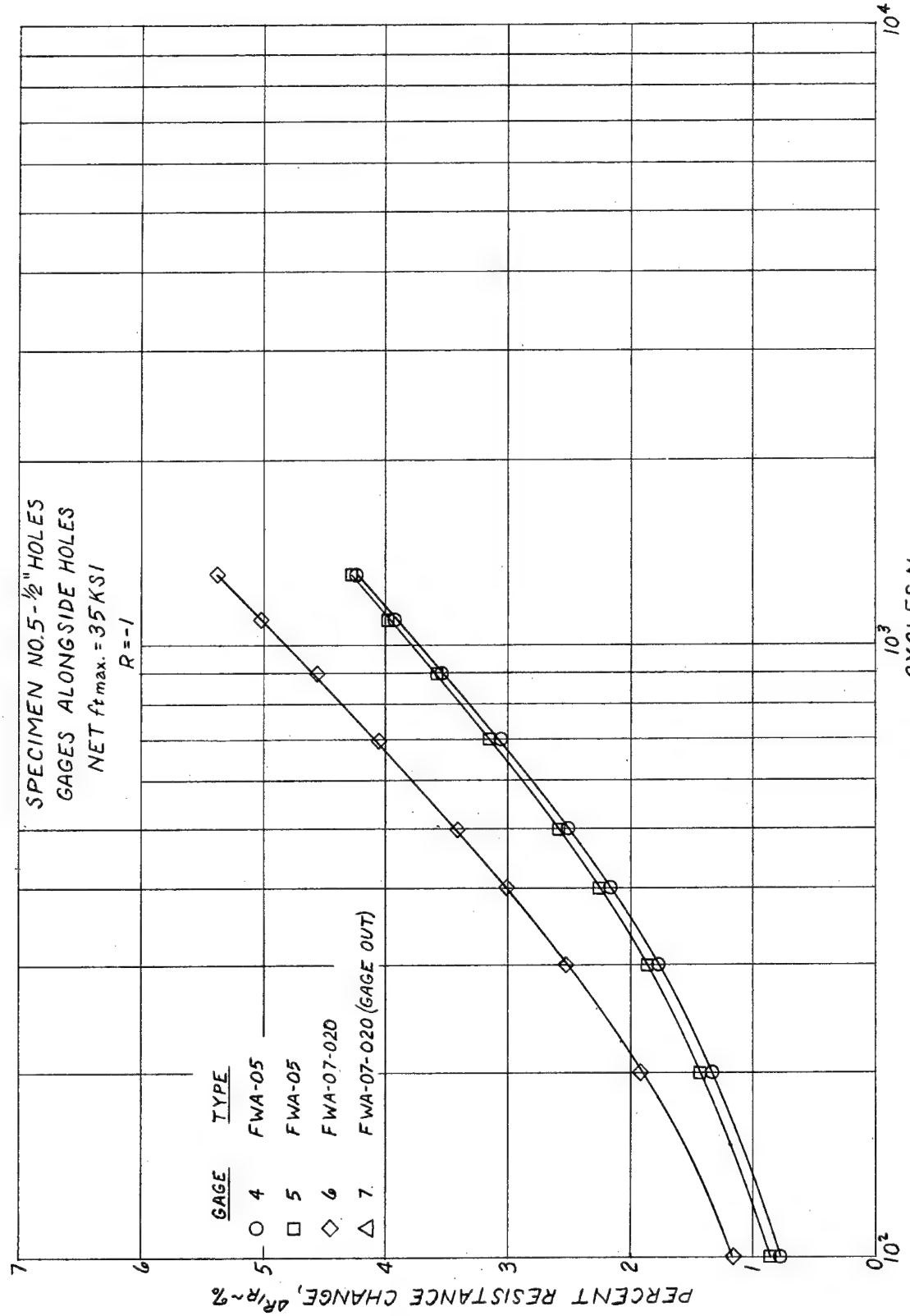

FIG. C-20 GAGE RESPONSE VS. NO. OF CYCLES

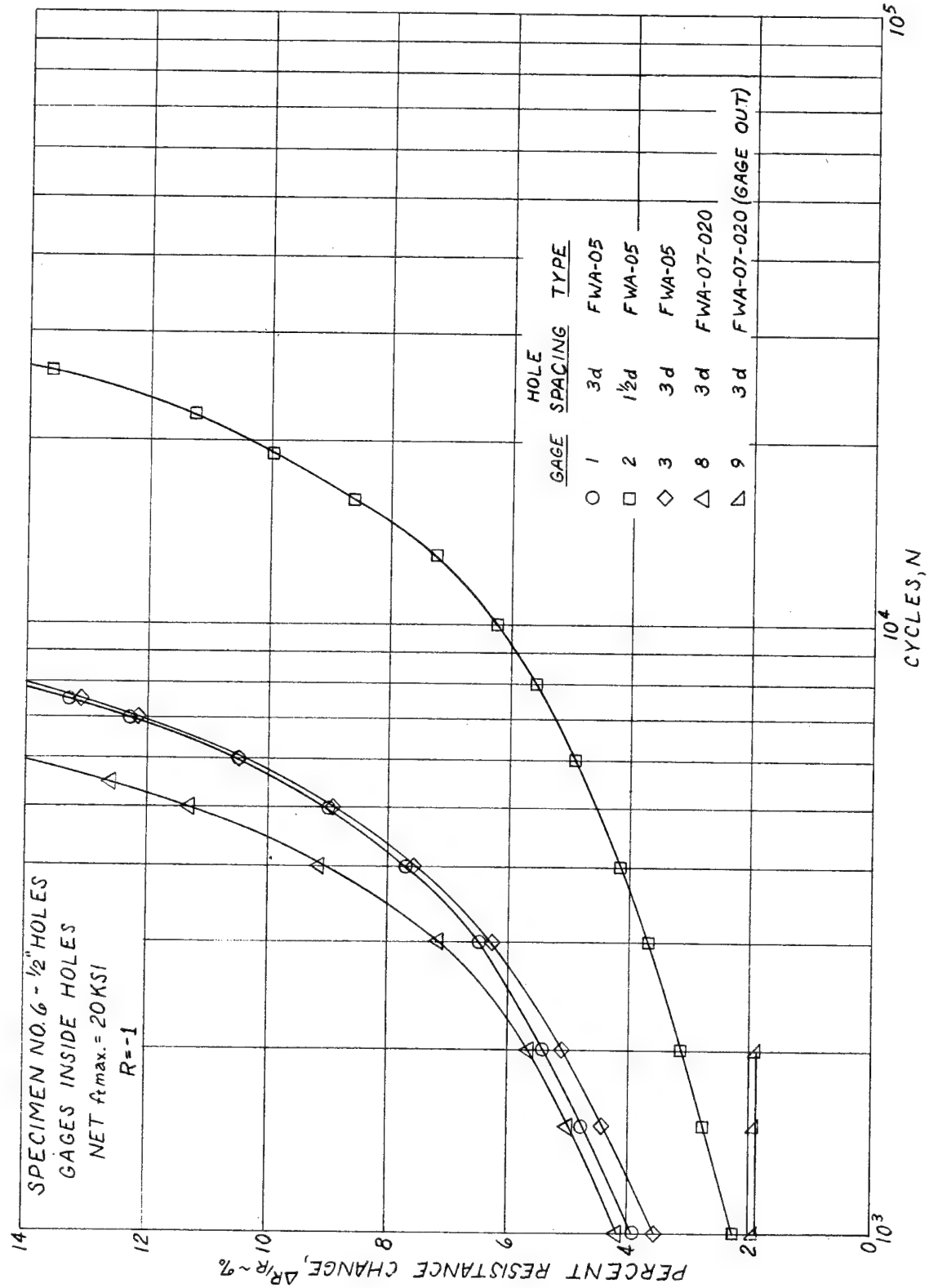

FIG. C-21 GAGE RESPONSE VS. NO. OF CYCLES

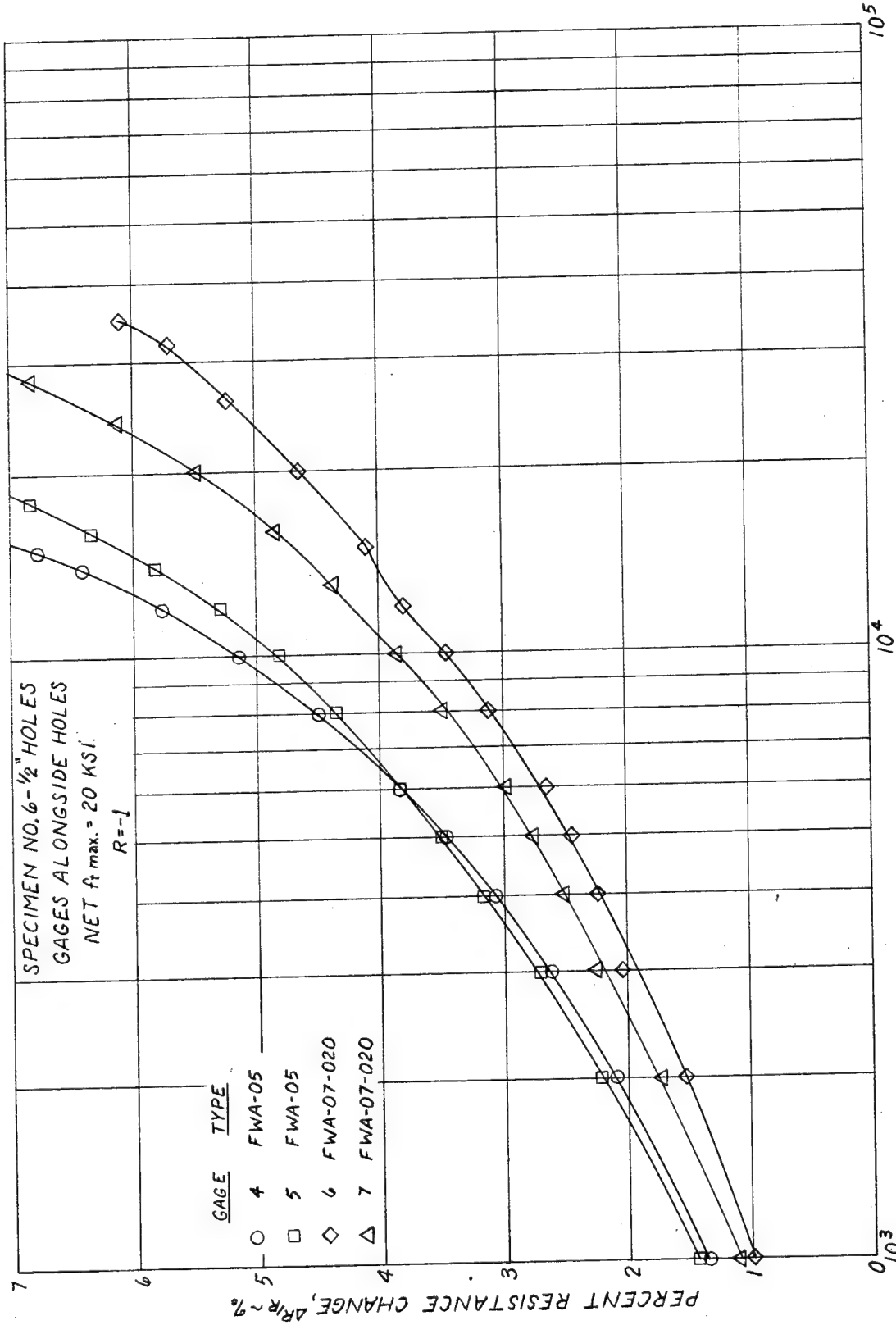

FIG. C-22 GAGE RESPONSE VS. NO. OF CYCLES

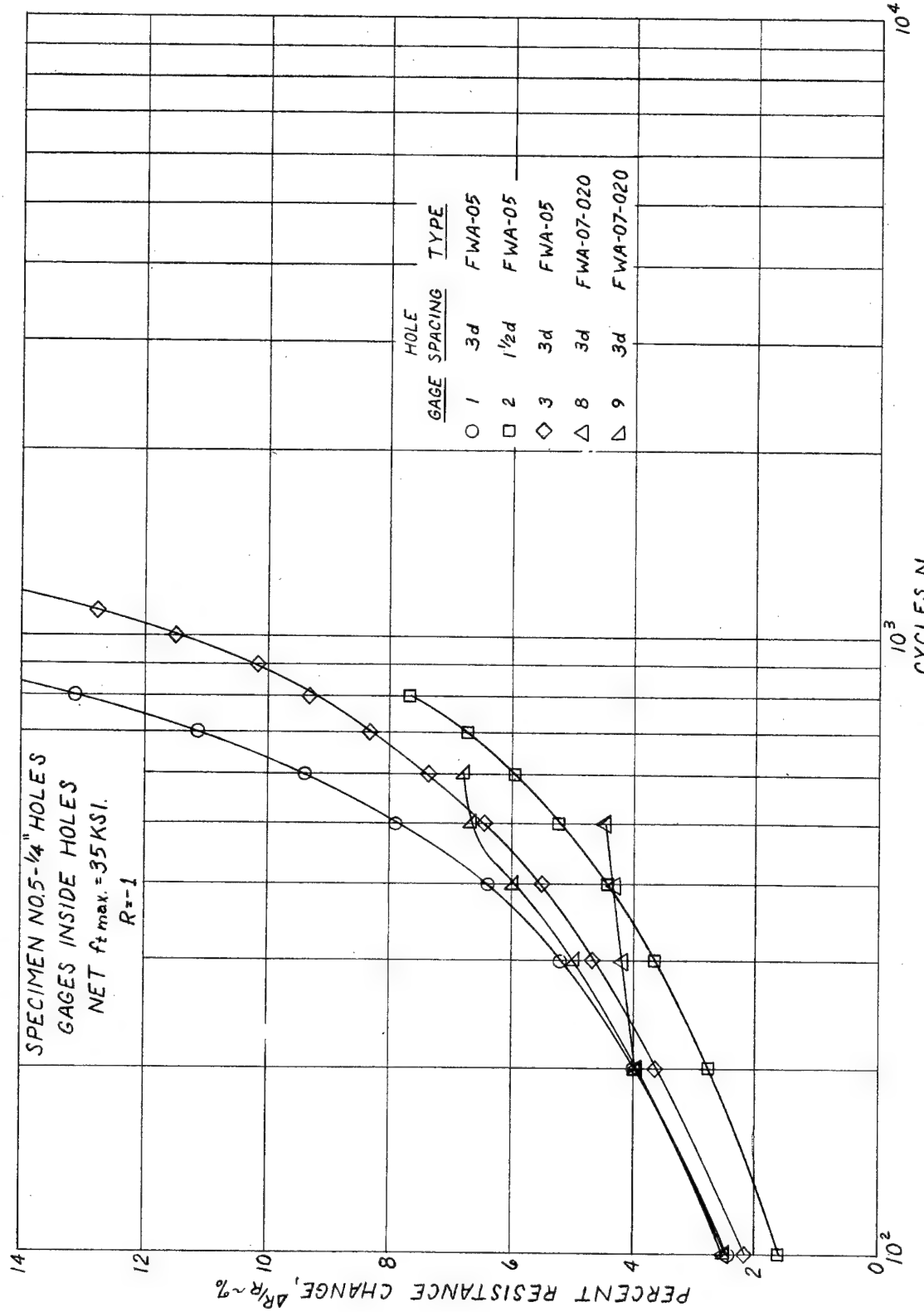

FIG. C-23 GAGE RESPONSE VS. NO. OF CYCLES

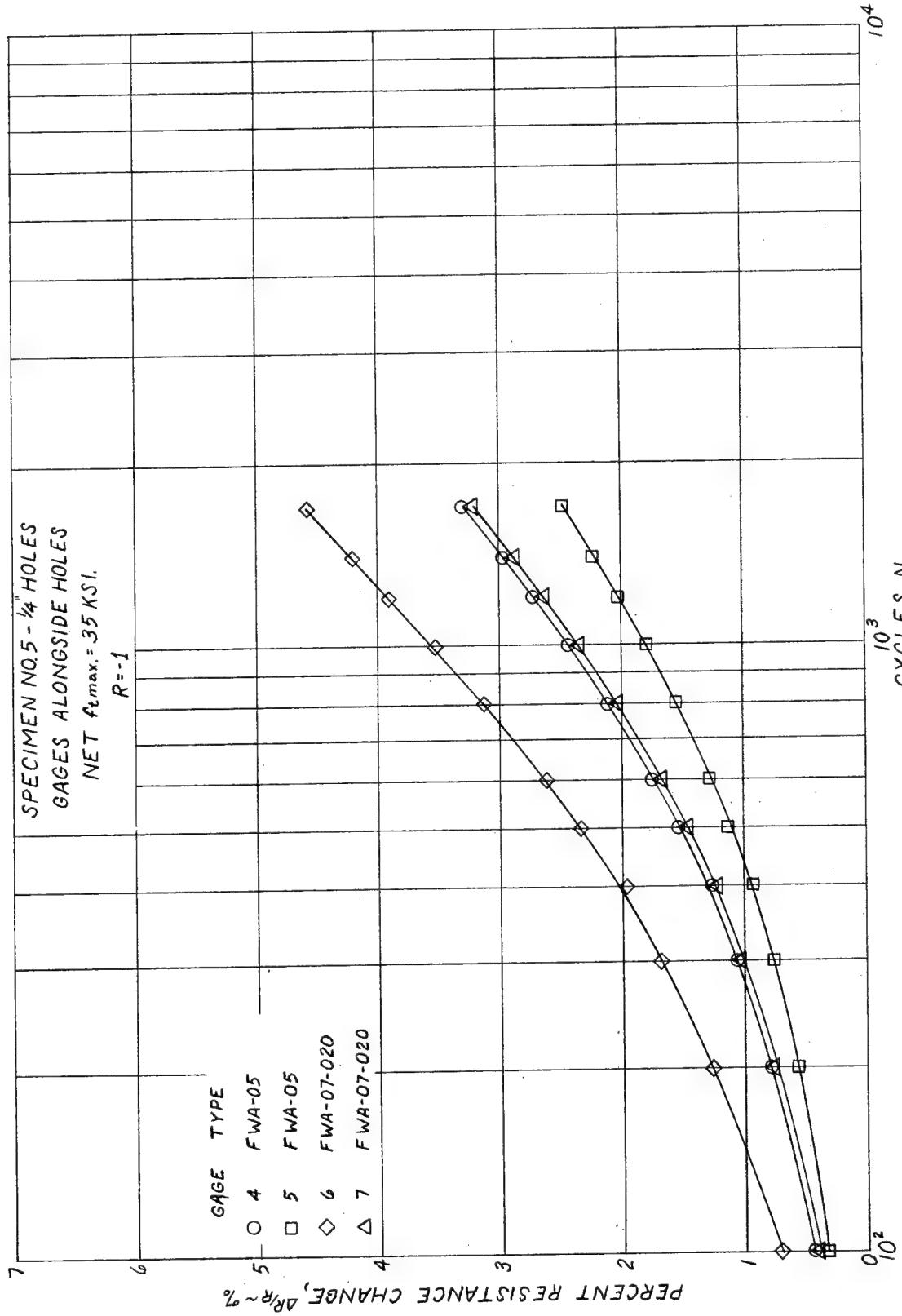

FIG. C-24 GAGE RESPONSE VS. NO. OF CYCLES.

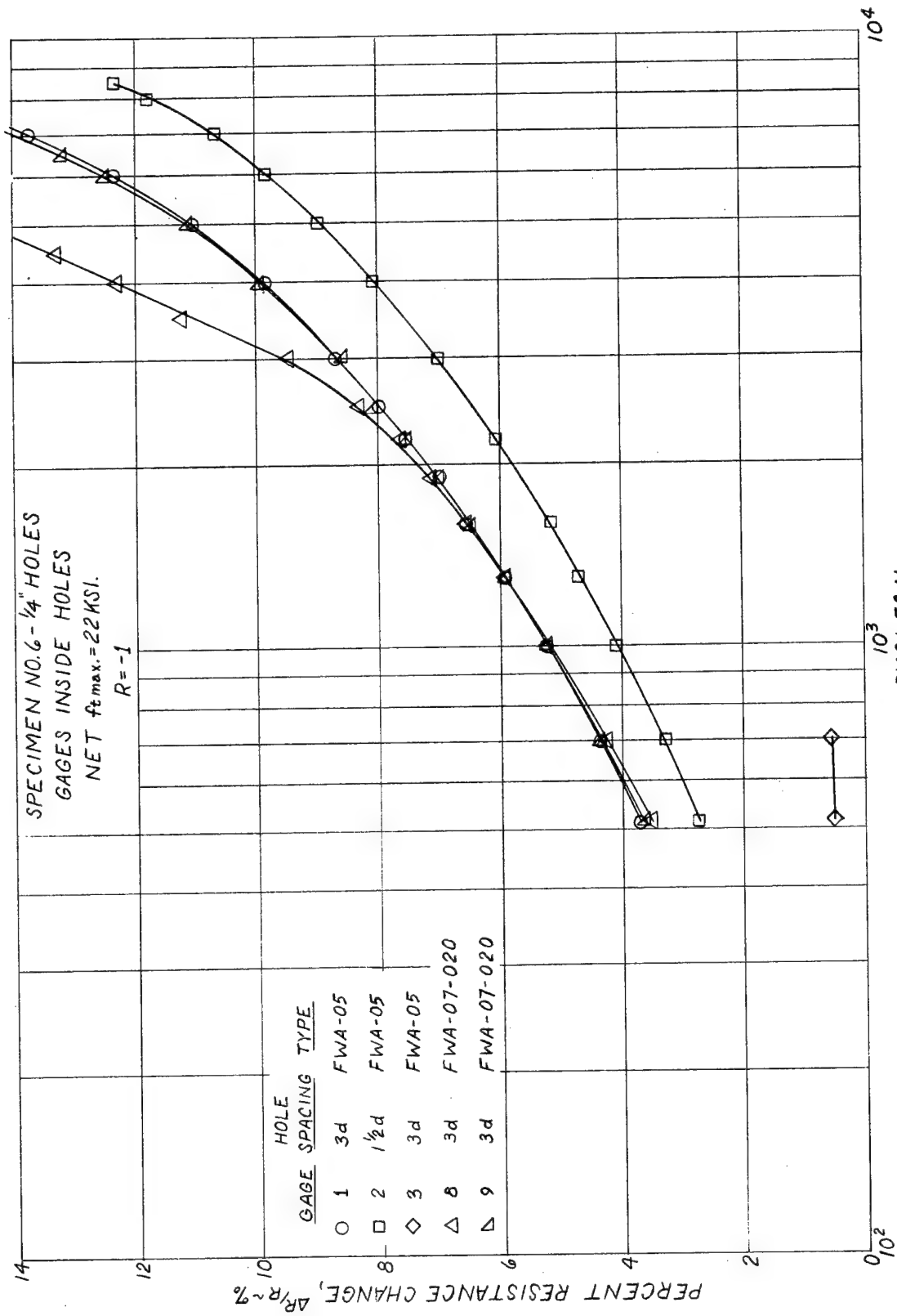

FIG. C-25 GAGE RESPONSE VS. NO. OF CYCLES

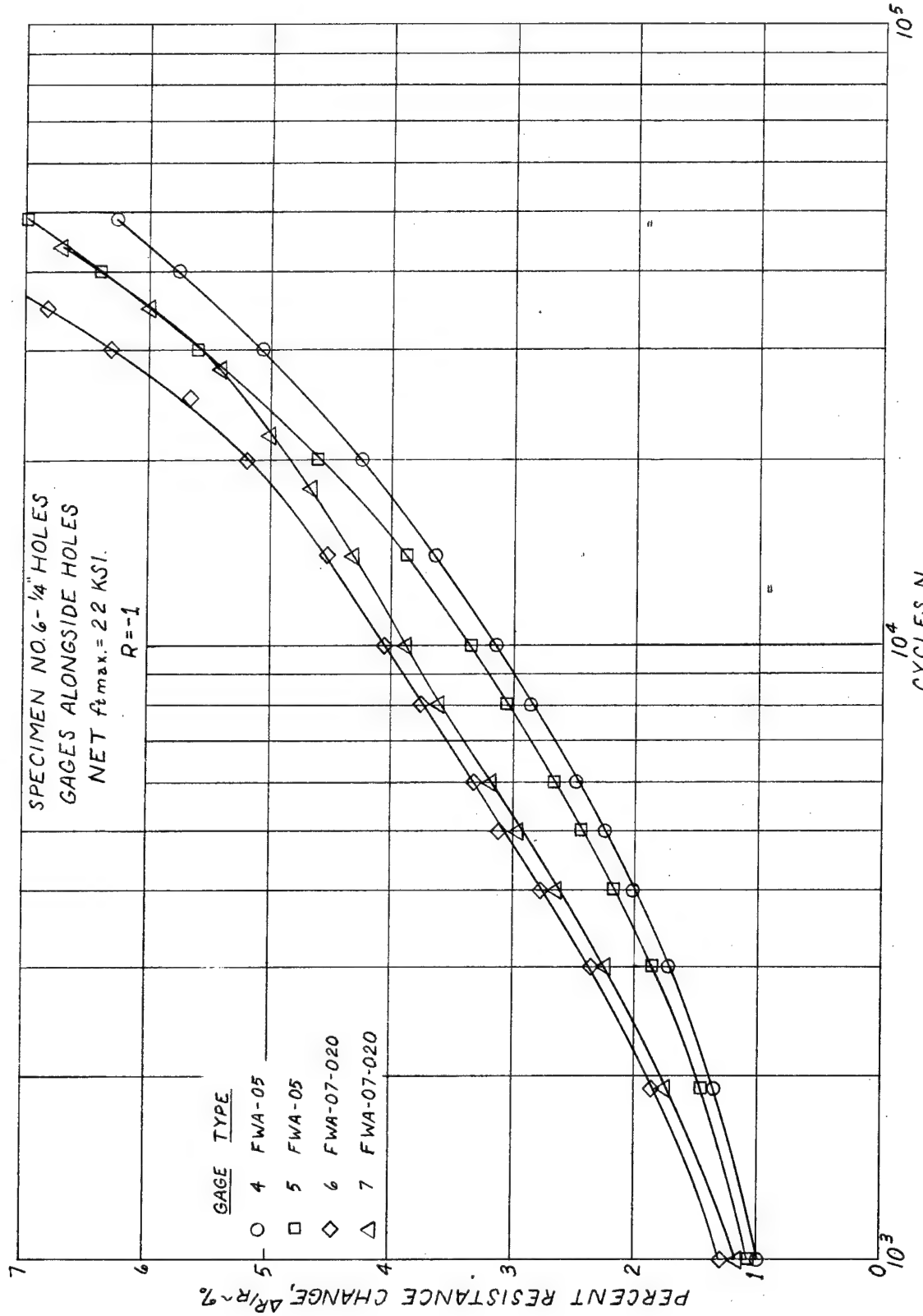

FIG. C-26 GAGE RESPONSE VS. NO. OF CYCLES

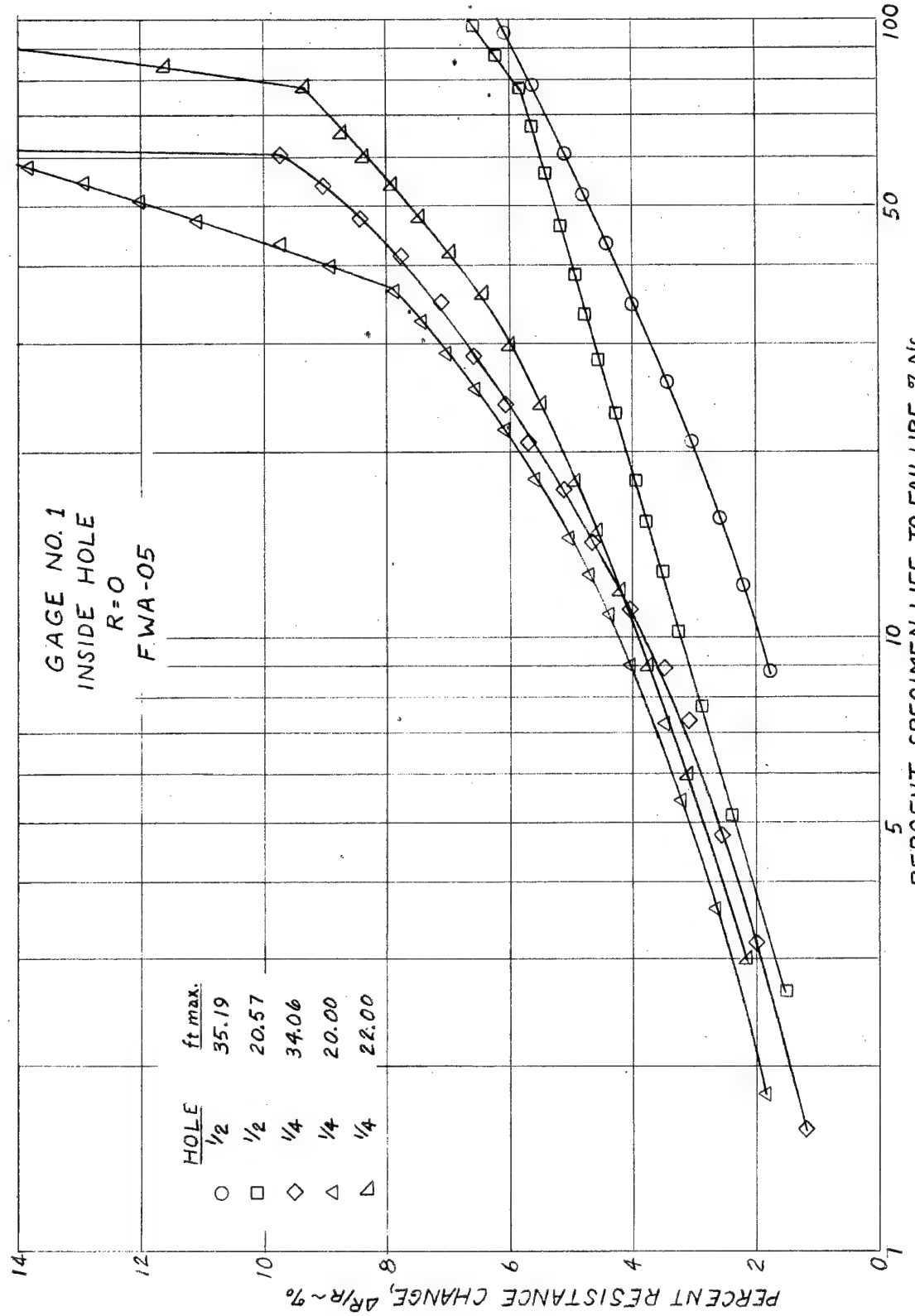

FIG. C-27 GAGE RESPONSE VS. SPECIMEN LIFE

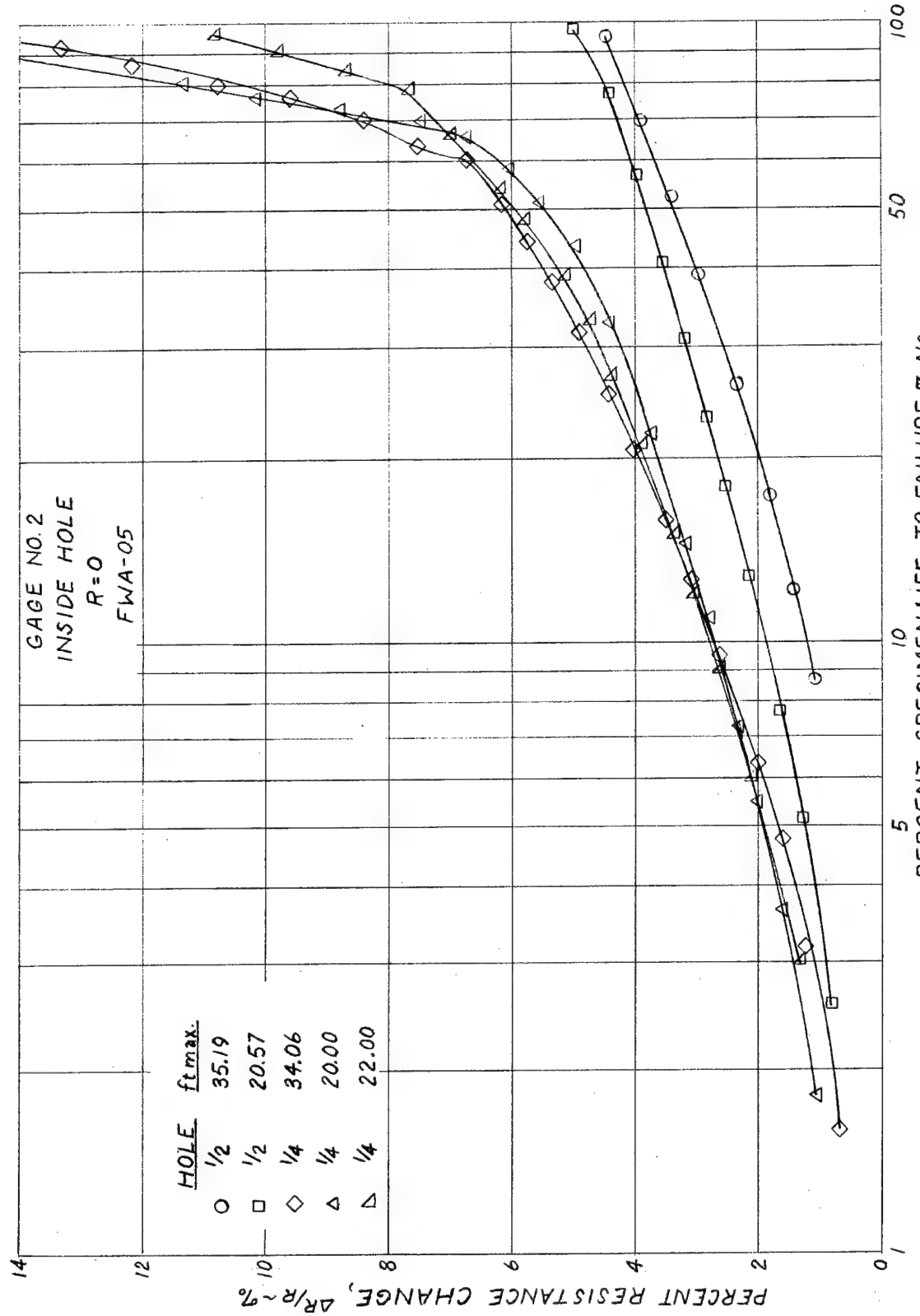

FIG. C-28 GAGE RESPONSE VS. SPECIMEN LIFE

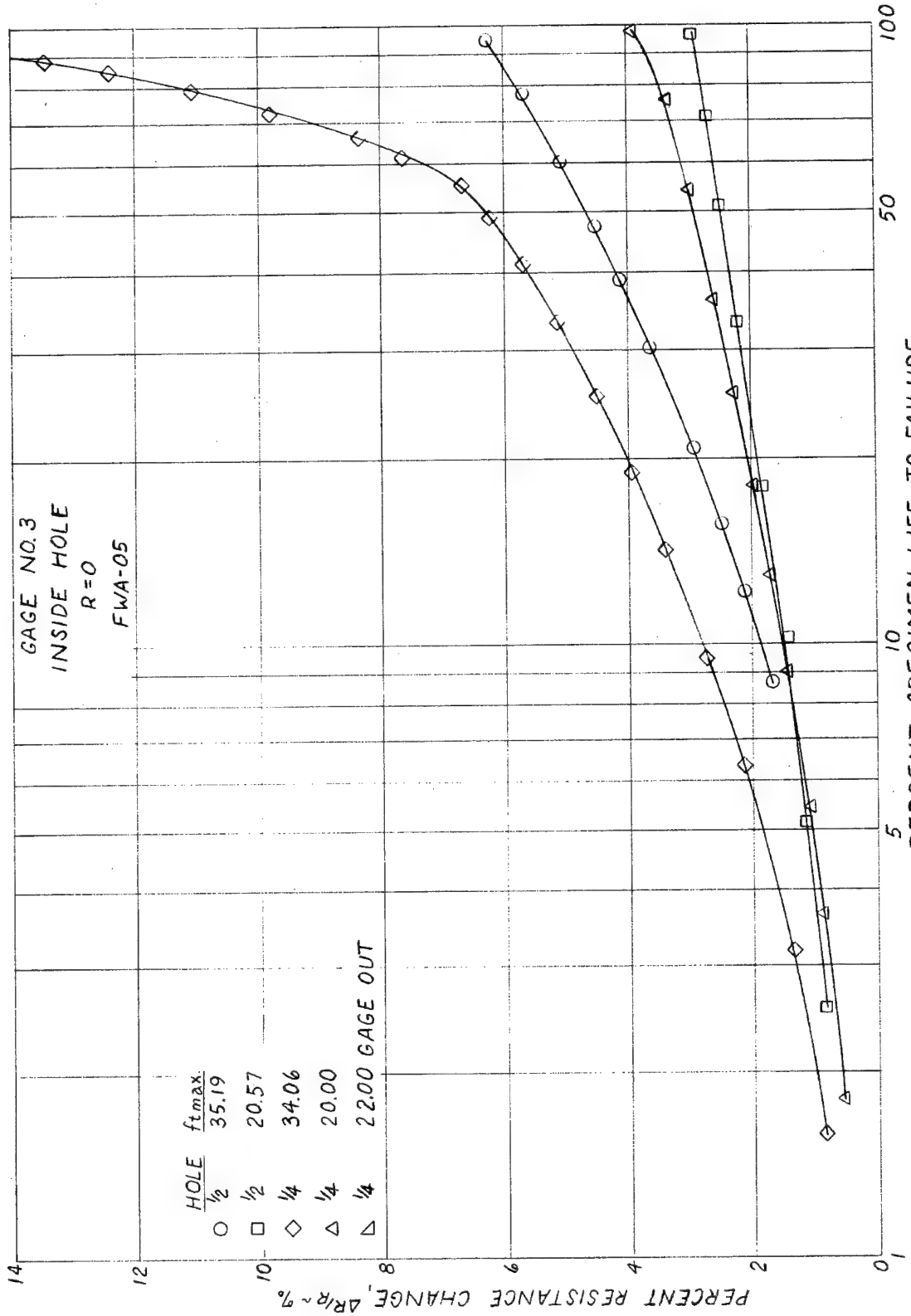

FIG.C29GAGE RESPONSE VS. SPECIMEN LIFE

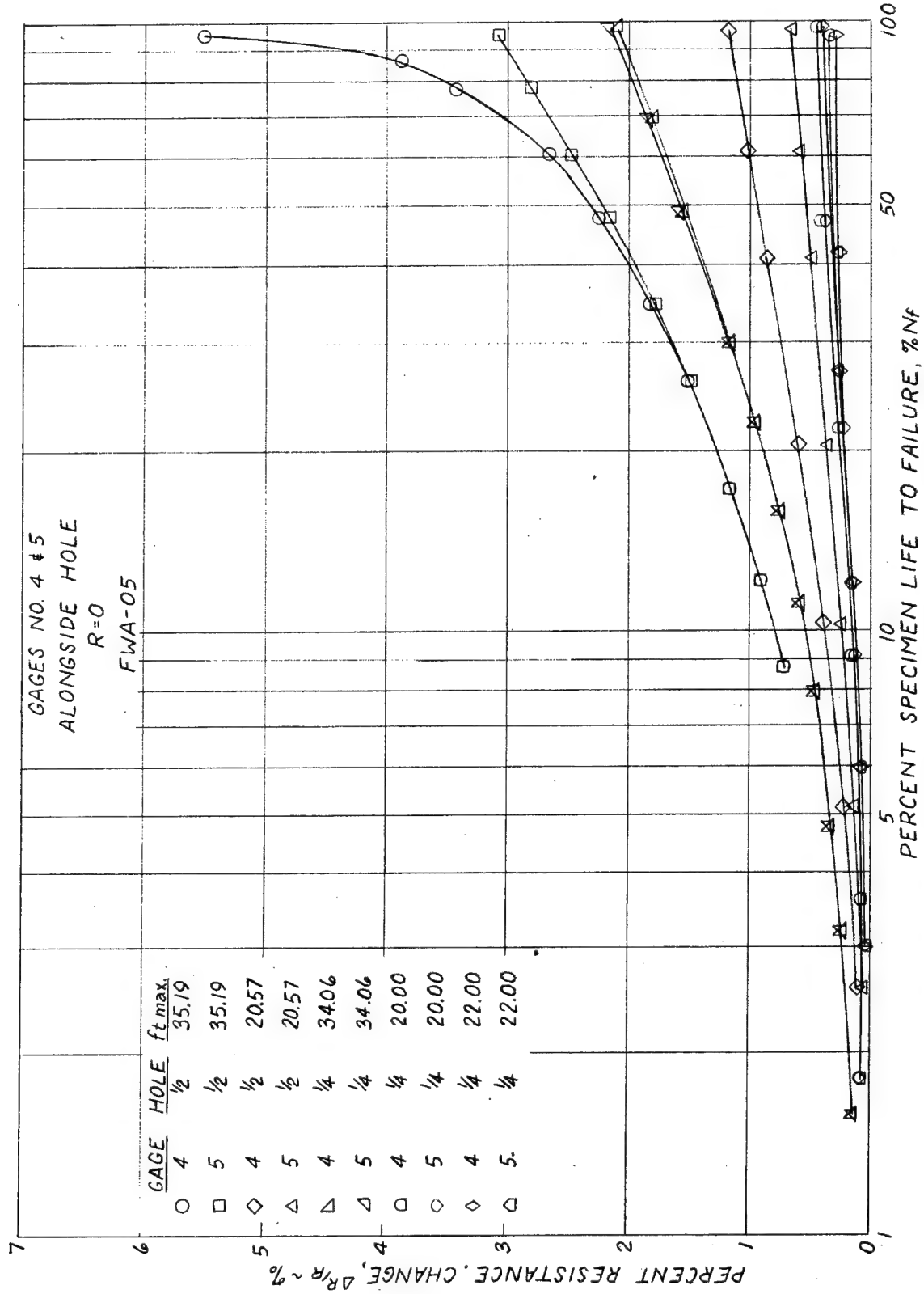

FIG.C-30 GAGE RESPONSE VS. SPECIMEN LIFE

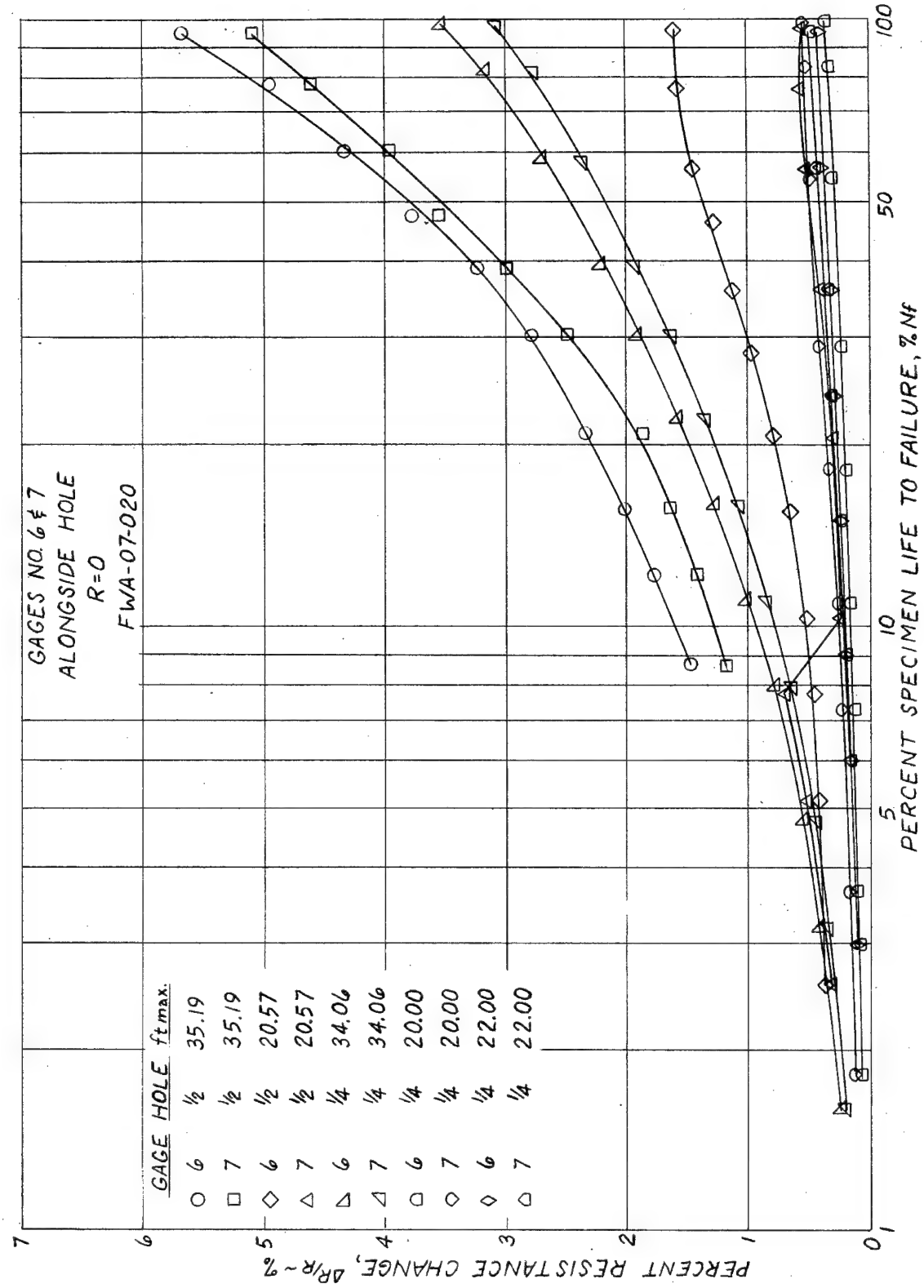

FIG.C-31 GAGE RESPONSE VS. SPECIMEN LIFE

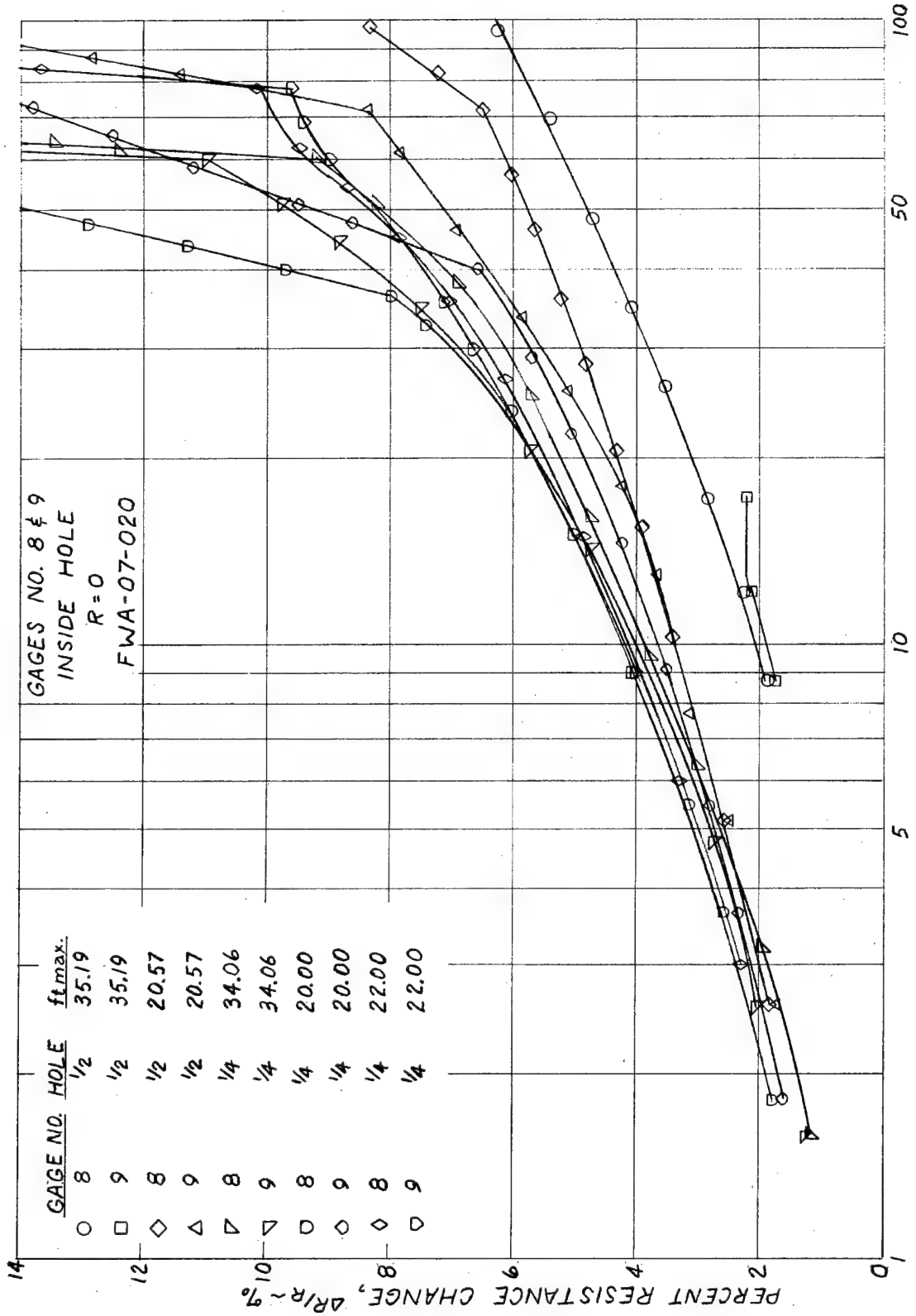

FIG.C-32 GAGE RESPONSE VS. SPECIMEN LIFE

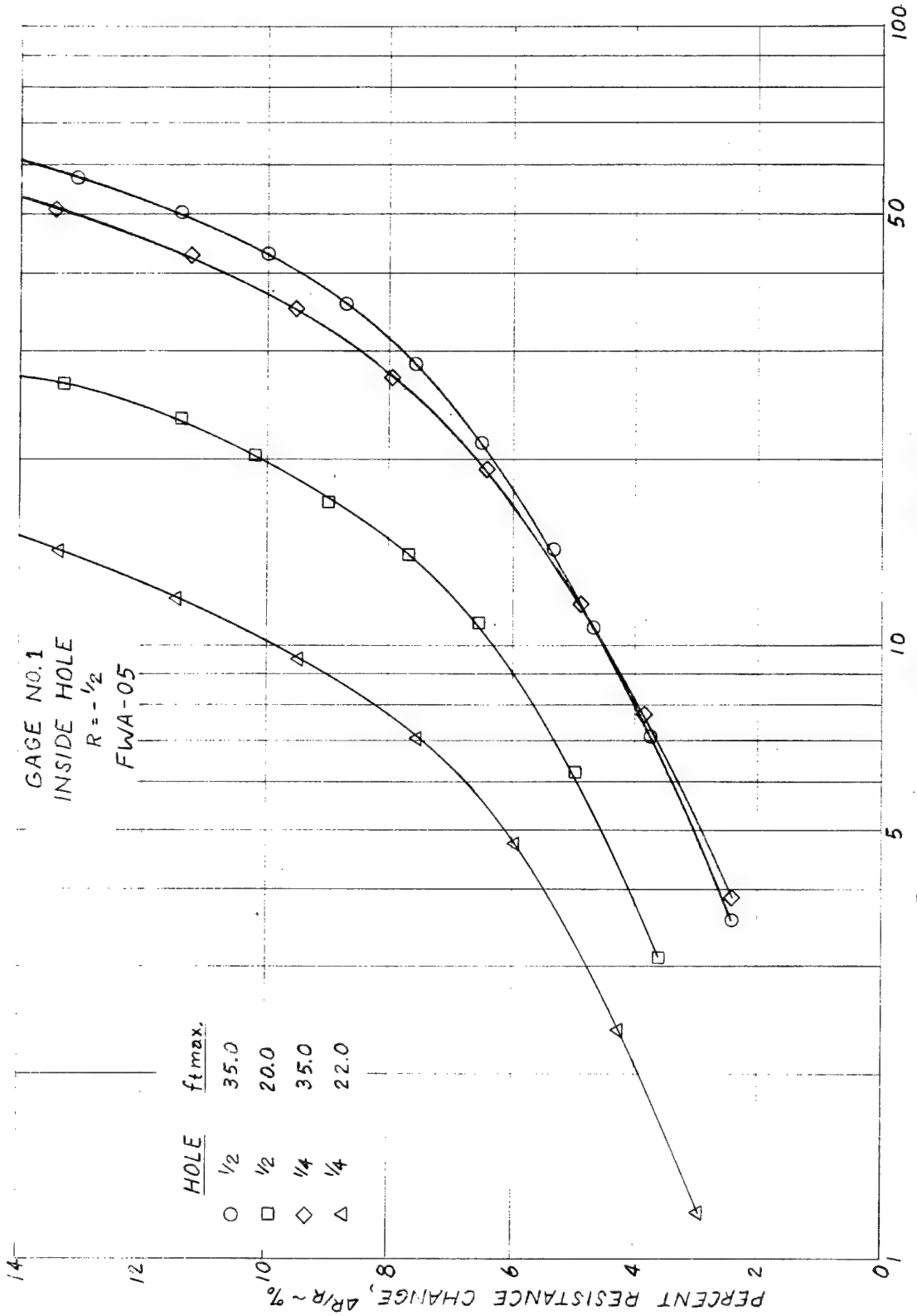

FIG.C-33 GAGE RESPONSE VS. SPECIMEN LIFE

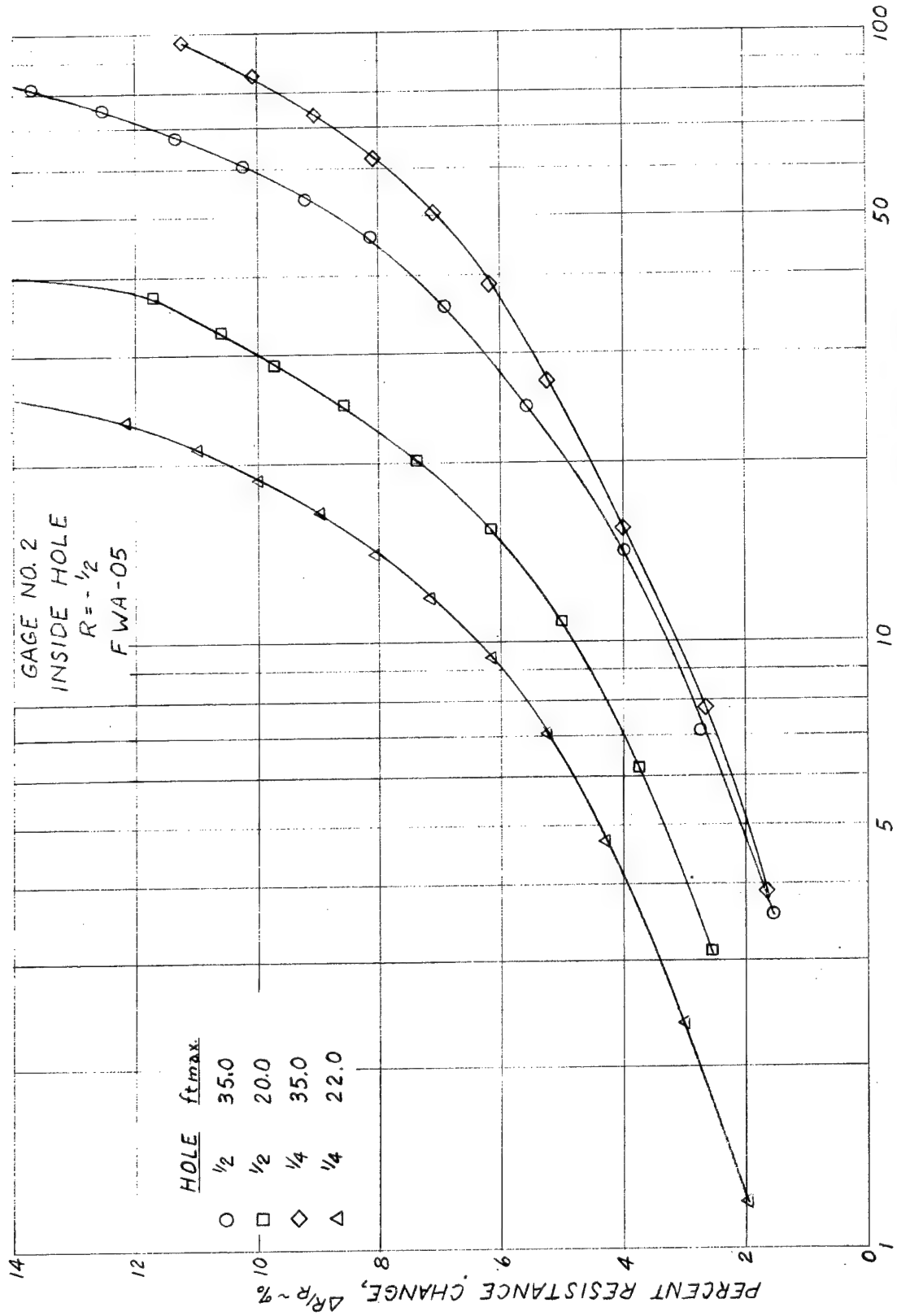

FIG. C-34 GAGE RESPONSE VS. SPECIMEN LIFE

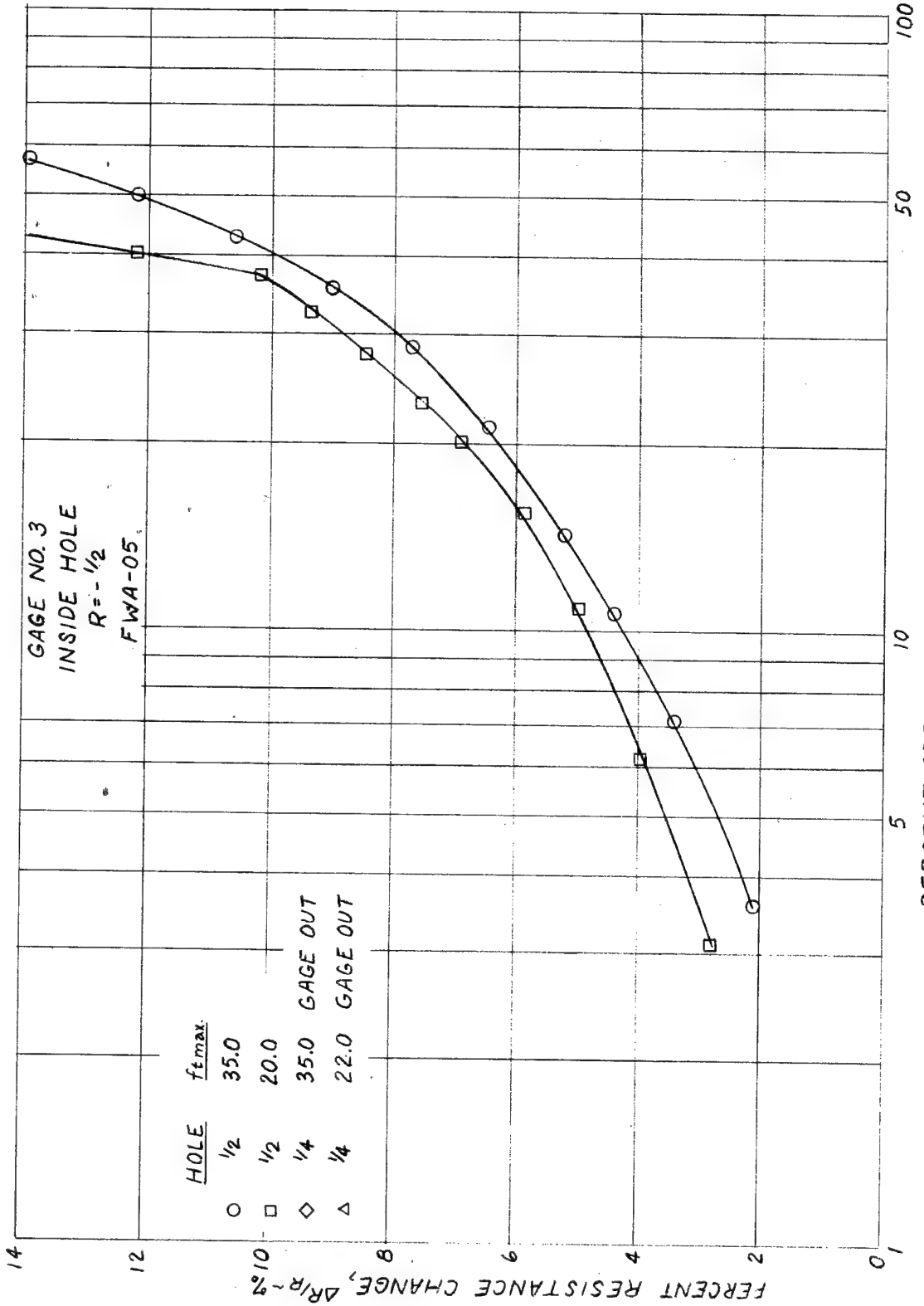

FIG. C-35 GAGE RESPONSE VS. SPECIMEN LIFE

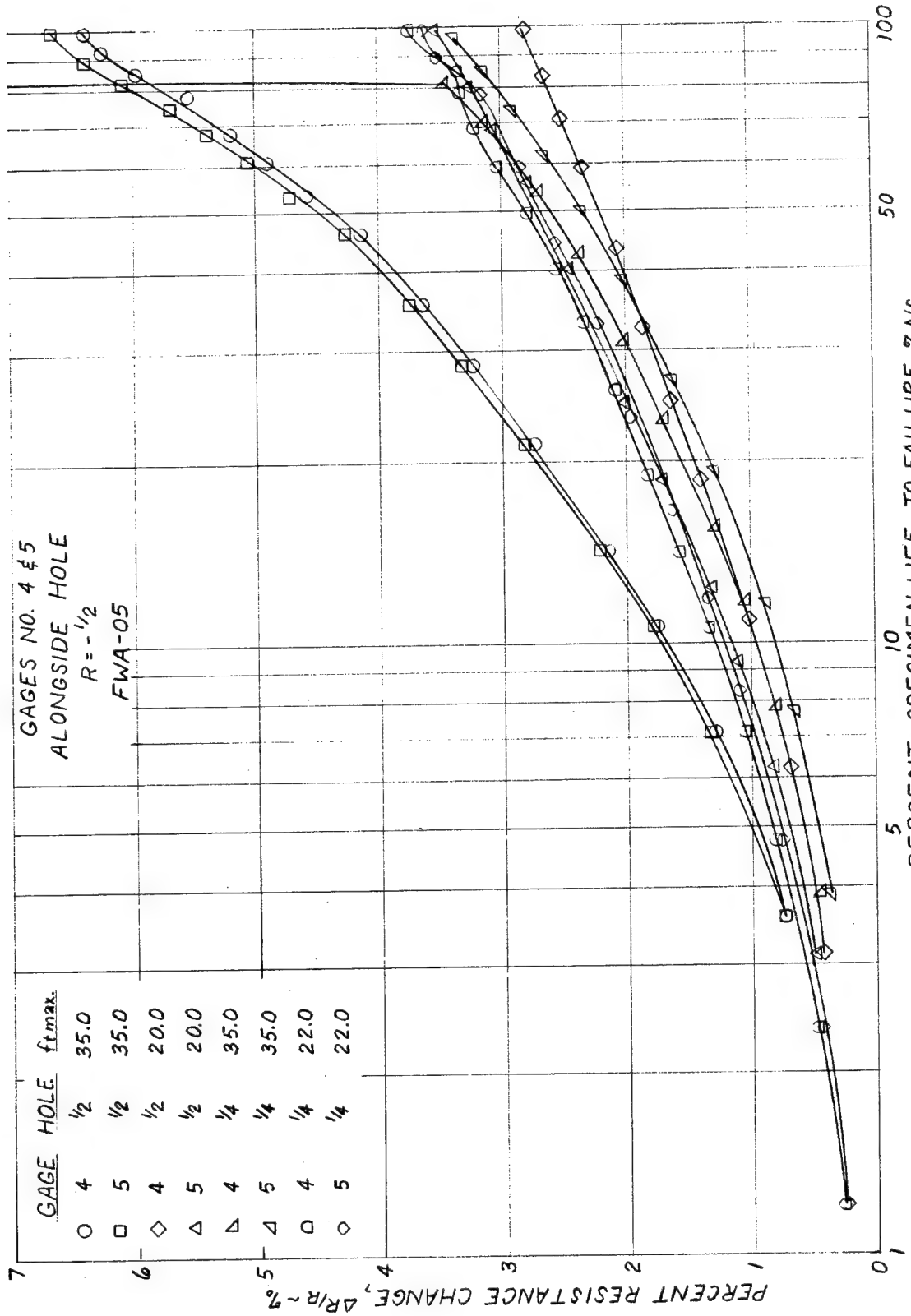

FIG C-36 GAGE RESPONSE VS. SPECIMEN LIFE

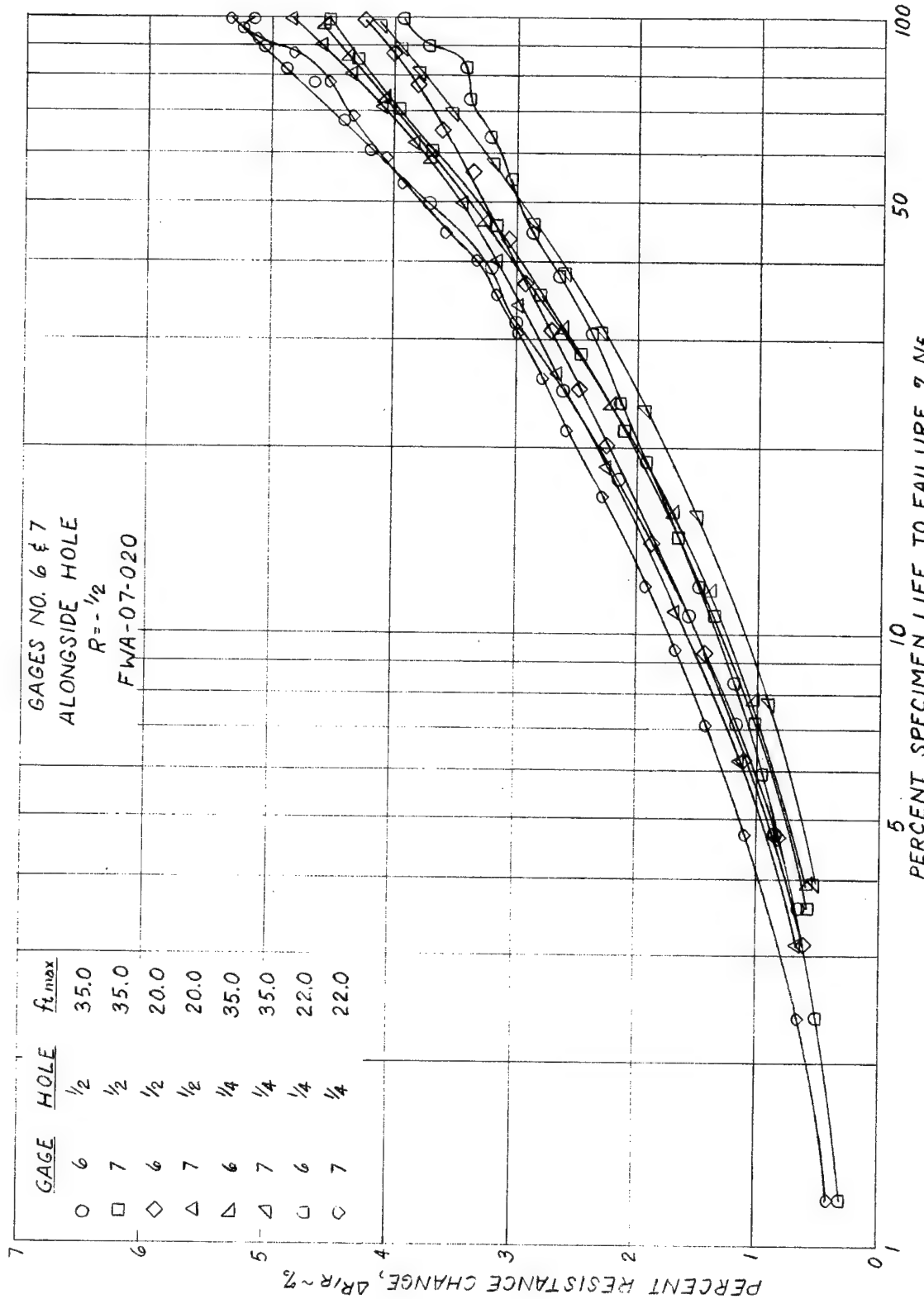

FIG. C-37 GAGE RESPONSE VS. SPECIMEN LIFE

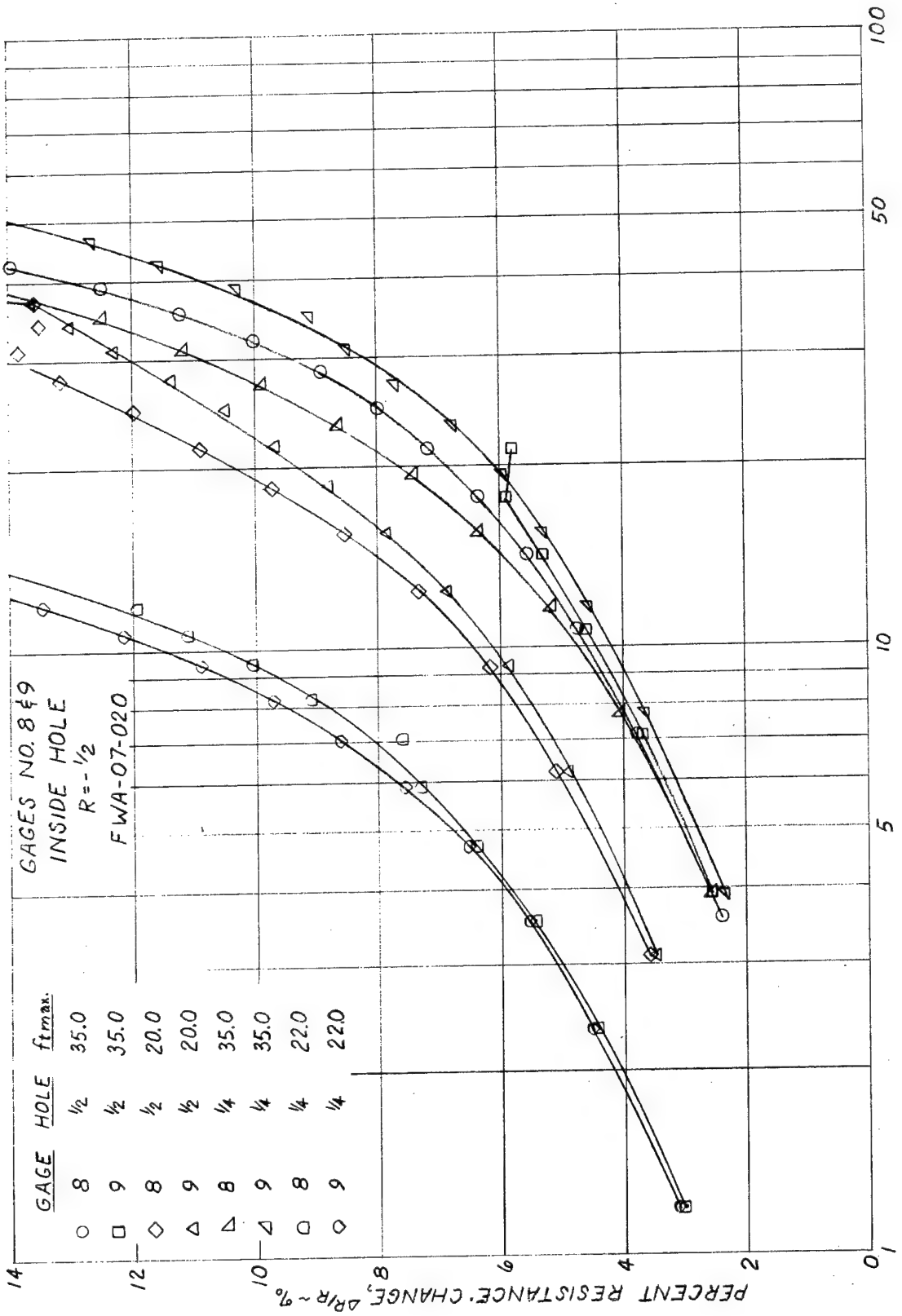

FIG. C-38 GAGE RESPONSE VS. SPECIMEN LIFE

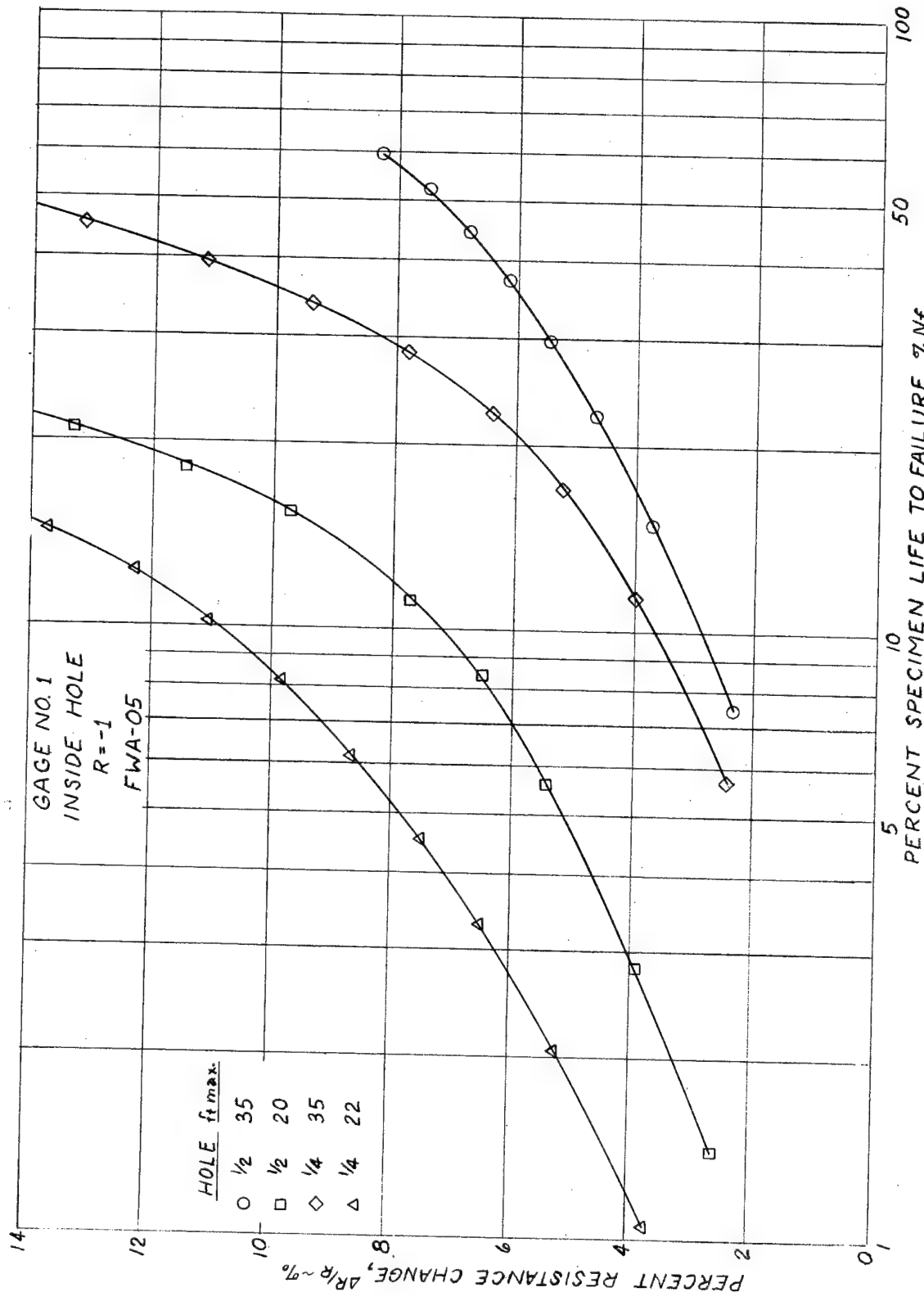

FIG. C-39 GAGE RESPONSE VS. SPECIMEN LIFE

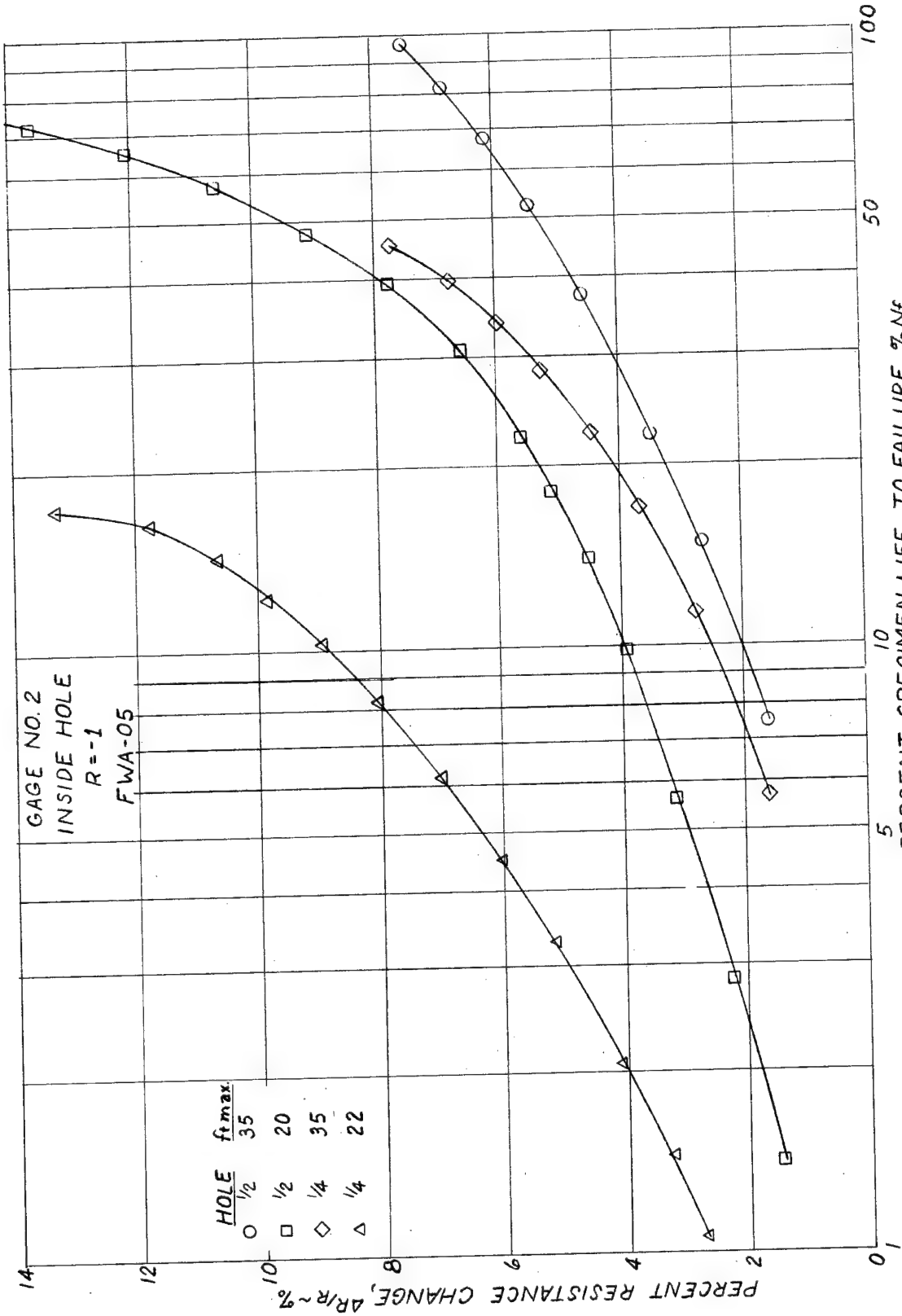

FIG. C-40 GAGE RESPONSE VS. SPECIMEN LIFE

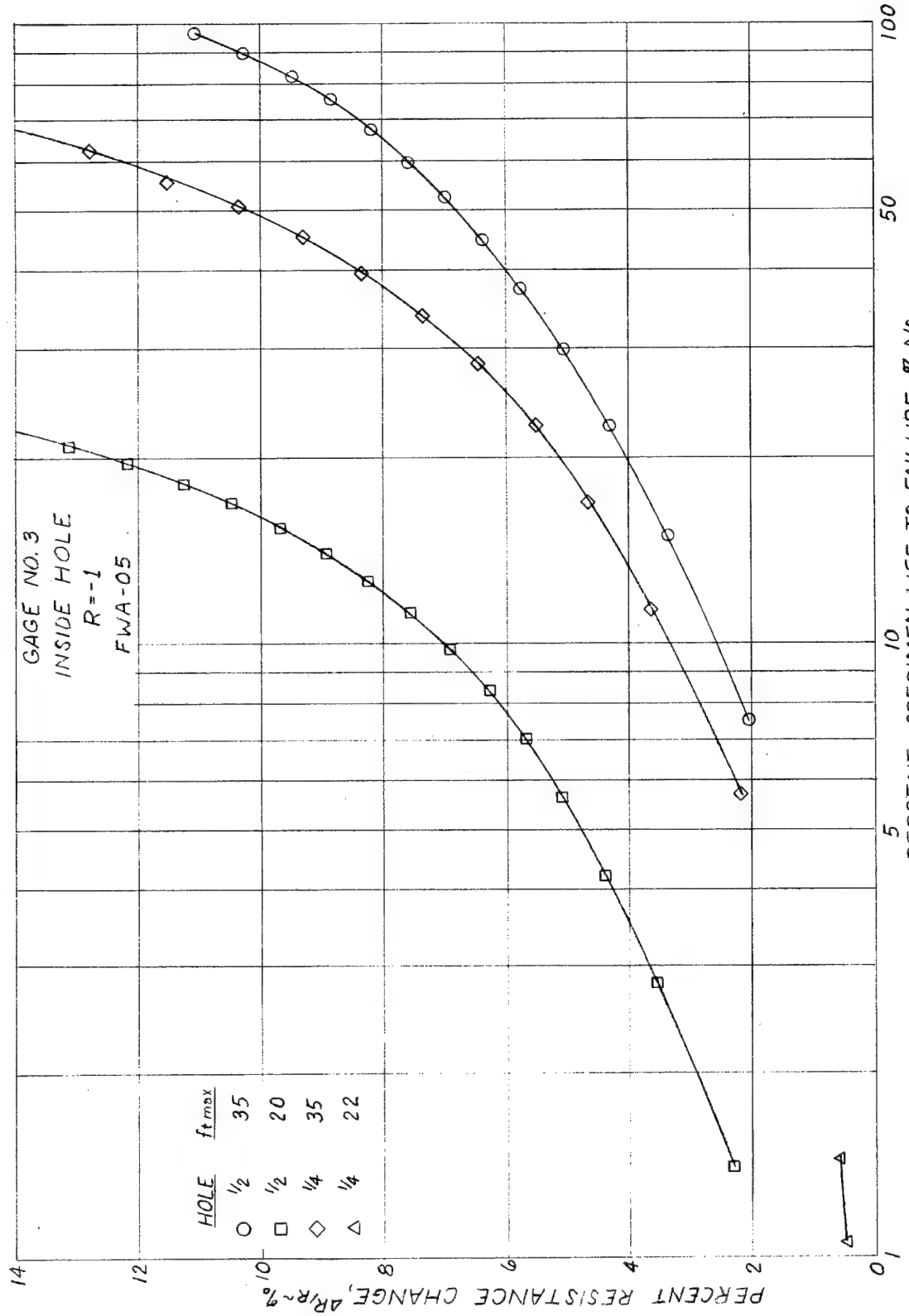

FIG. C-41 GAGE RESPONSE VS. SPECIMEN LIFE

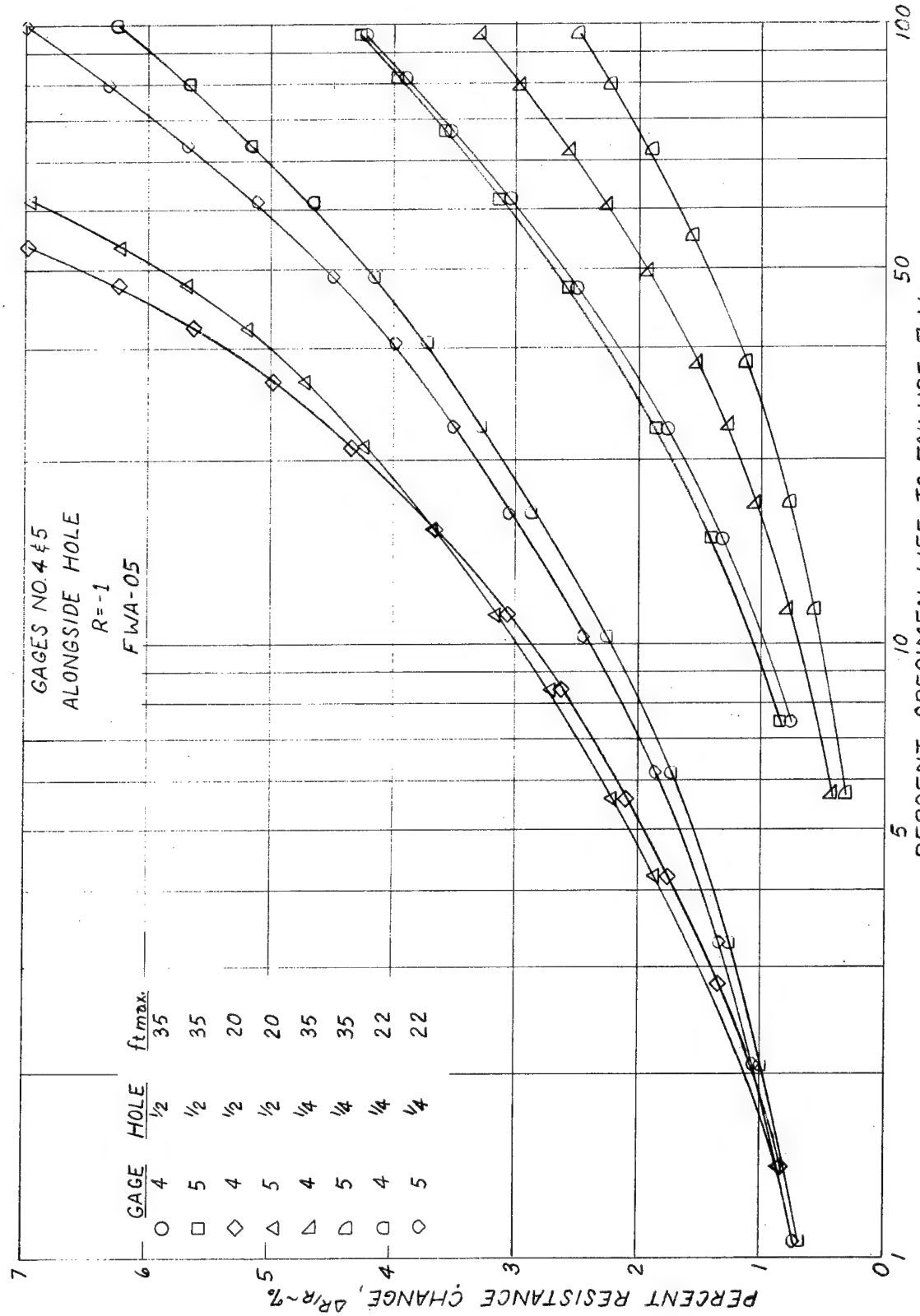

FIG. C-42 GAGE RESPONSE VS. SPECIMEN LIFE

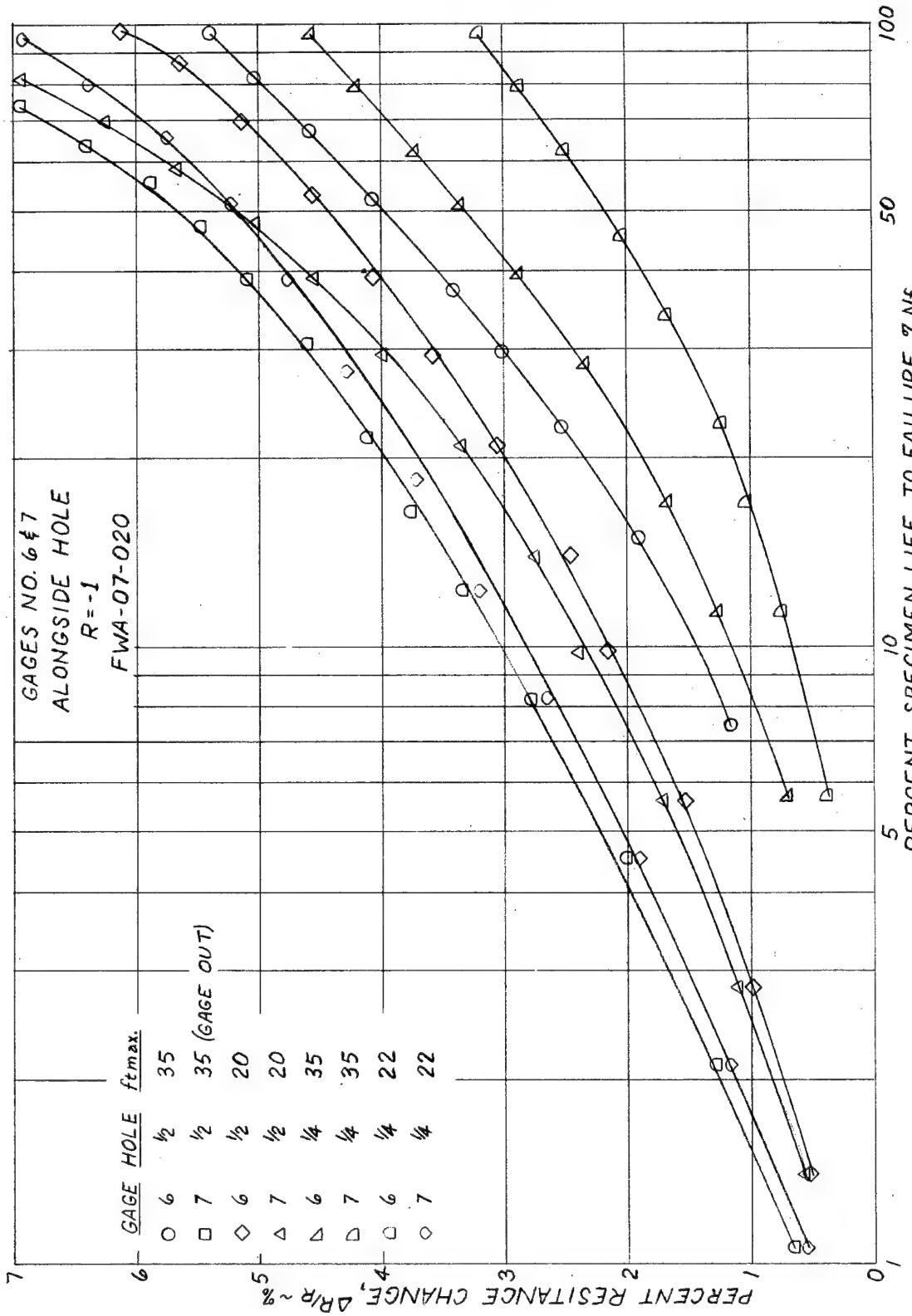

FIG C-43 GAGE RESPONSE VS. SPECIMEN LIFE

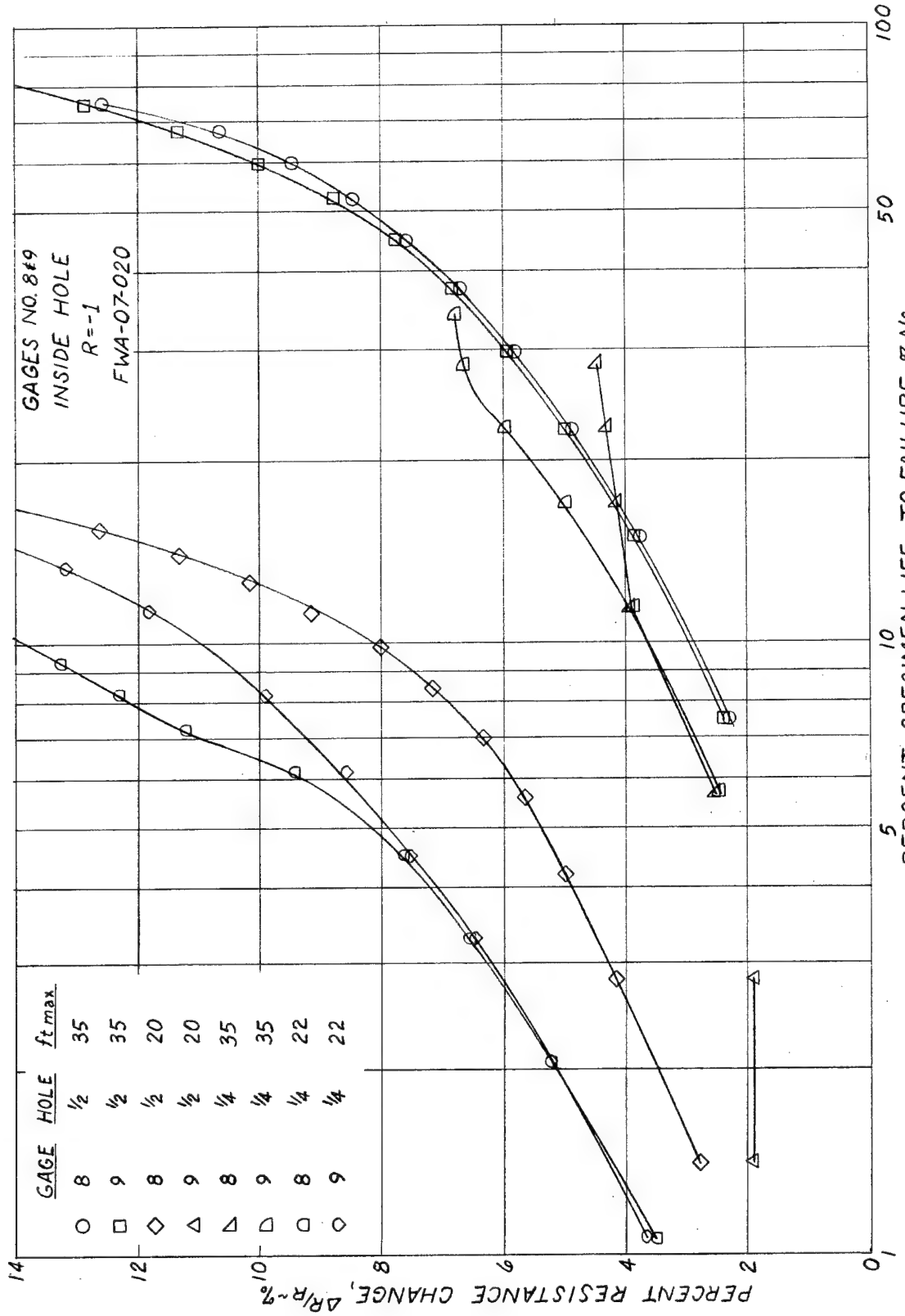

FIG. C-44 GAGE RESPONSE VS. SPECIMEN LIFE

APPENDIX D

VARIABLE AMPLITUDE TEST DATA

LIST OF FIGURES

LIST OF FIGURES

The variable amplitude test data are plotted in Figures D-1 to D-18 using percent of specimen life as the abscissa. Two additional tests were performed (specimen 3A for the complete spectrum A and specimen 1B for the positive loads of spectrum B) but the data are not shown because these specimens failed prematurely due to test machine control problems. All tests were performed for a nominal net section stress of 30 ksi. at 100% limit load.

The data from specimens 2A, 4A, 5A, and 6A are plotted in Figures D-19 to D-29 using the number of 50-hour test loading blocks as the abscissa; this abscissa is proportional to the simulated service time since each block simulates 50 hours of anticipated service experience. Thus the results from identical tests for four nominally identical specimens are compared in these figures.

The same data contained in Figures D-1 to D-18 were replotted in Figures D-30 to D-36 to compare the results for comparable gage installations for the four nominally identical specimens under the same test conditions.

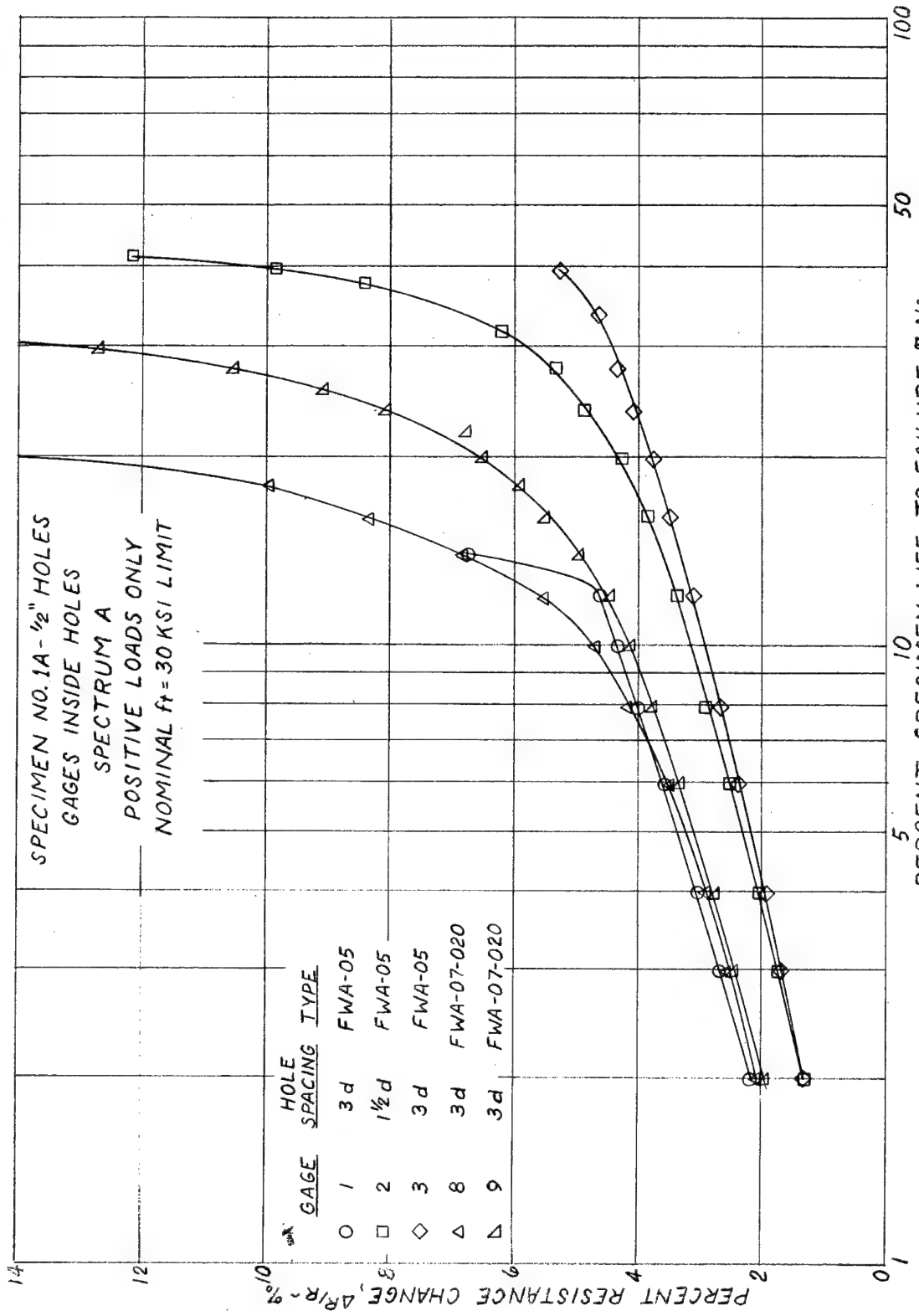

FIG. D-1 GAGE RESPONSE VS. SPECIMEN LIFE

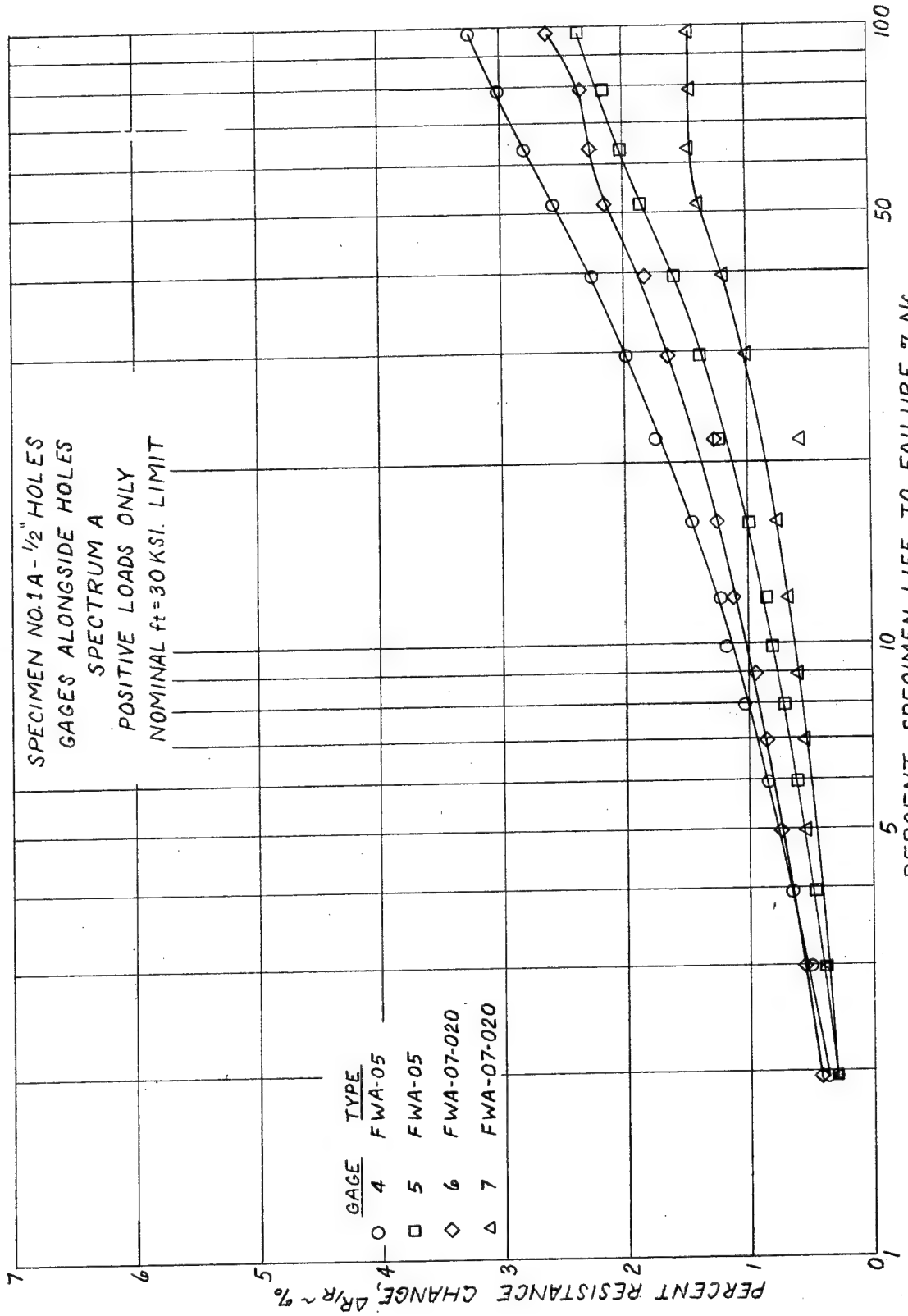

FIG. D-2 GAGE RESPONSE VS. SPECIMEN LIFE

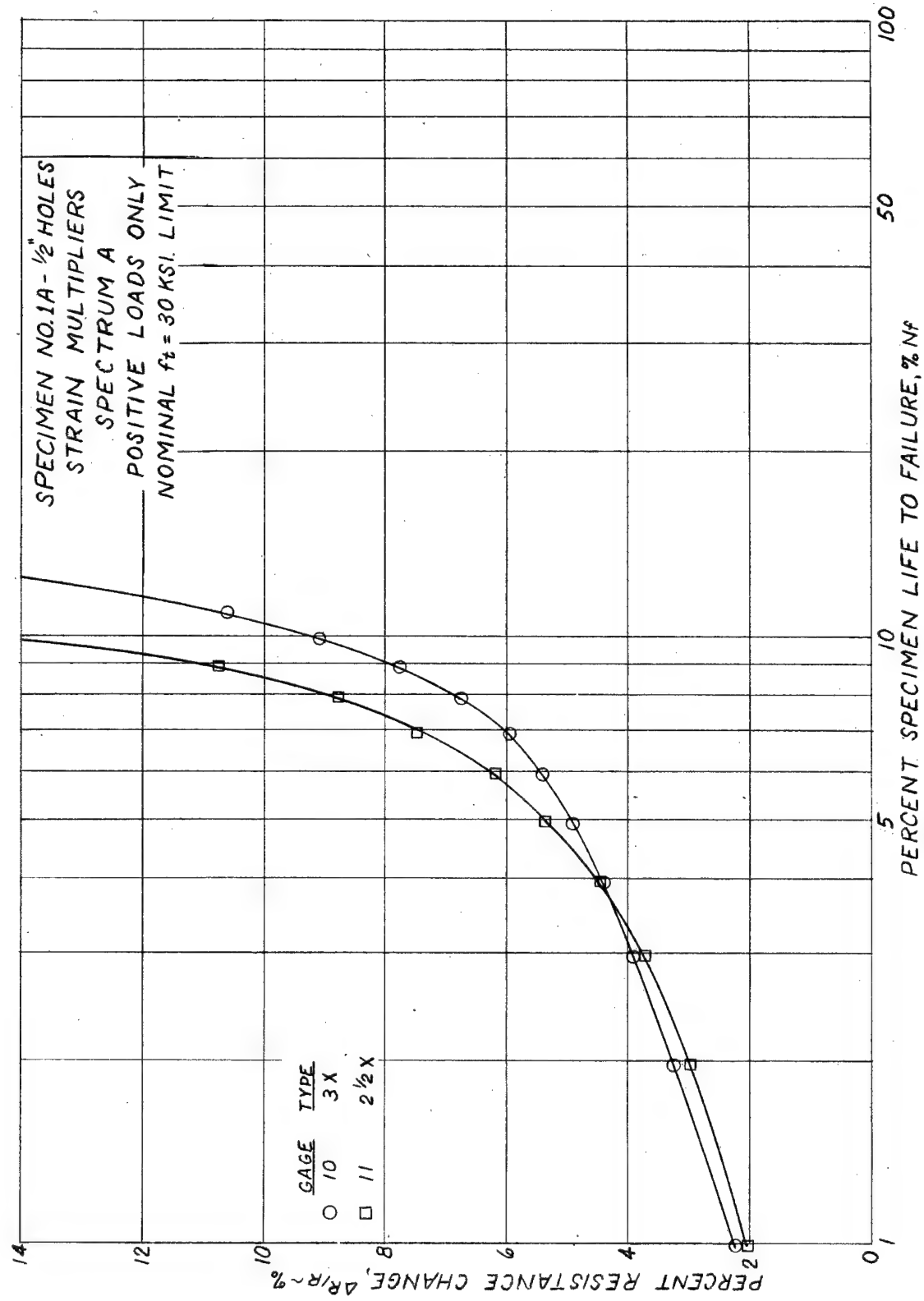

FIG D-3 GAGE RESPONSE VS. SPECIMEN LIFE

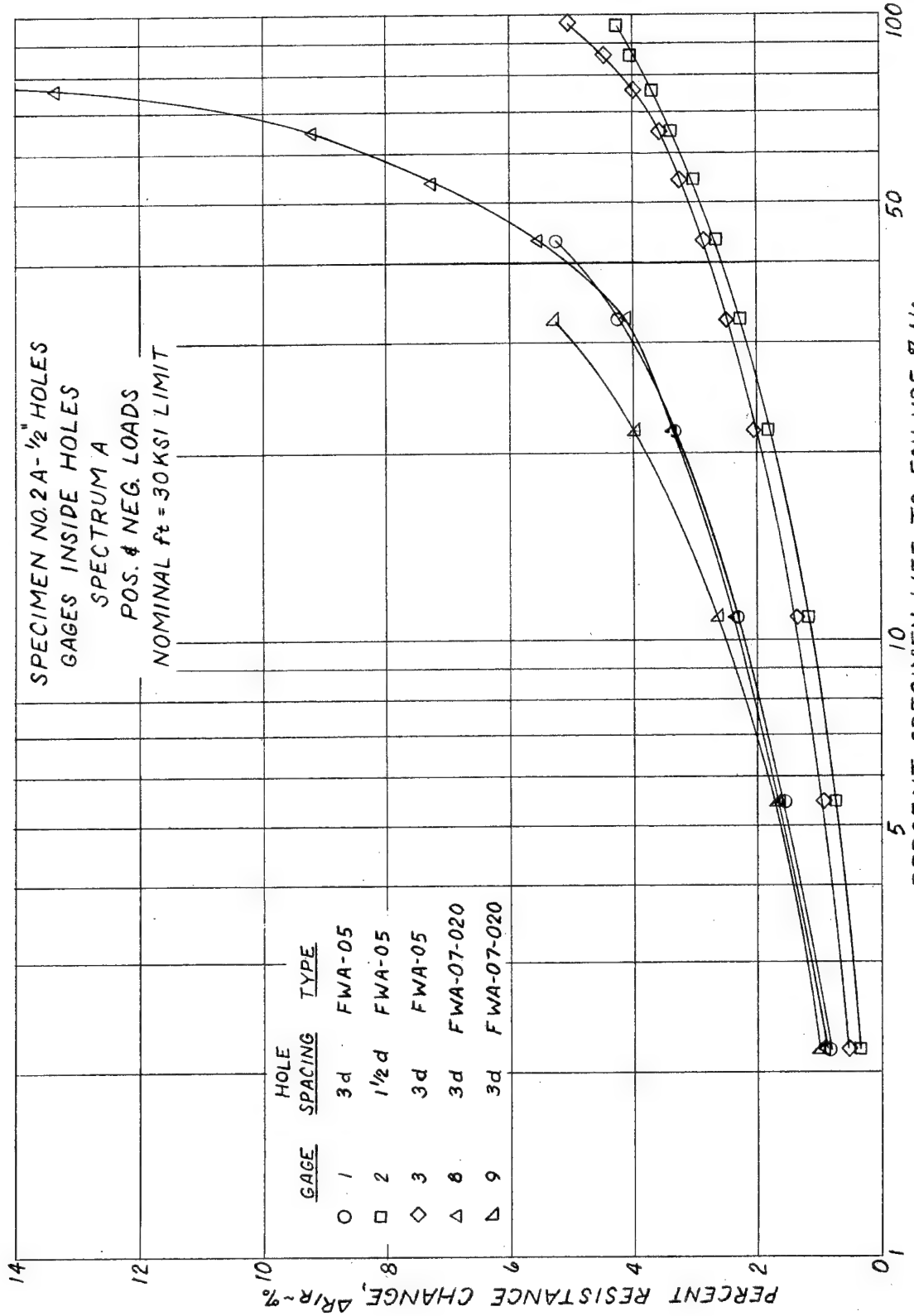

FIG. D-4 GAGE RESPONSE VS. SPECIMEN LIFE

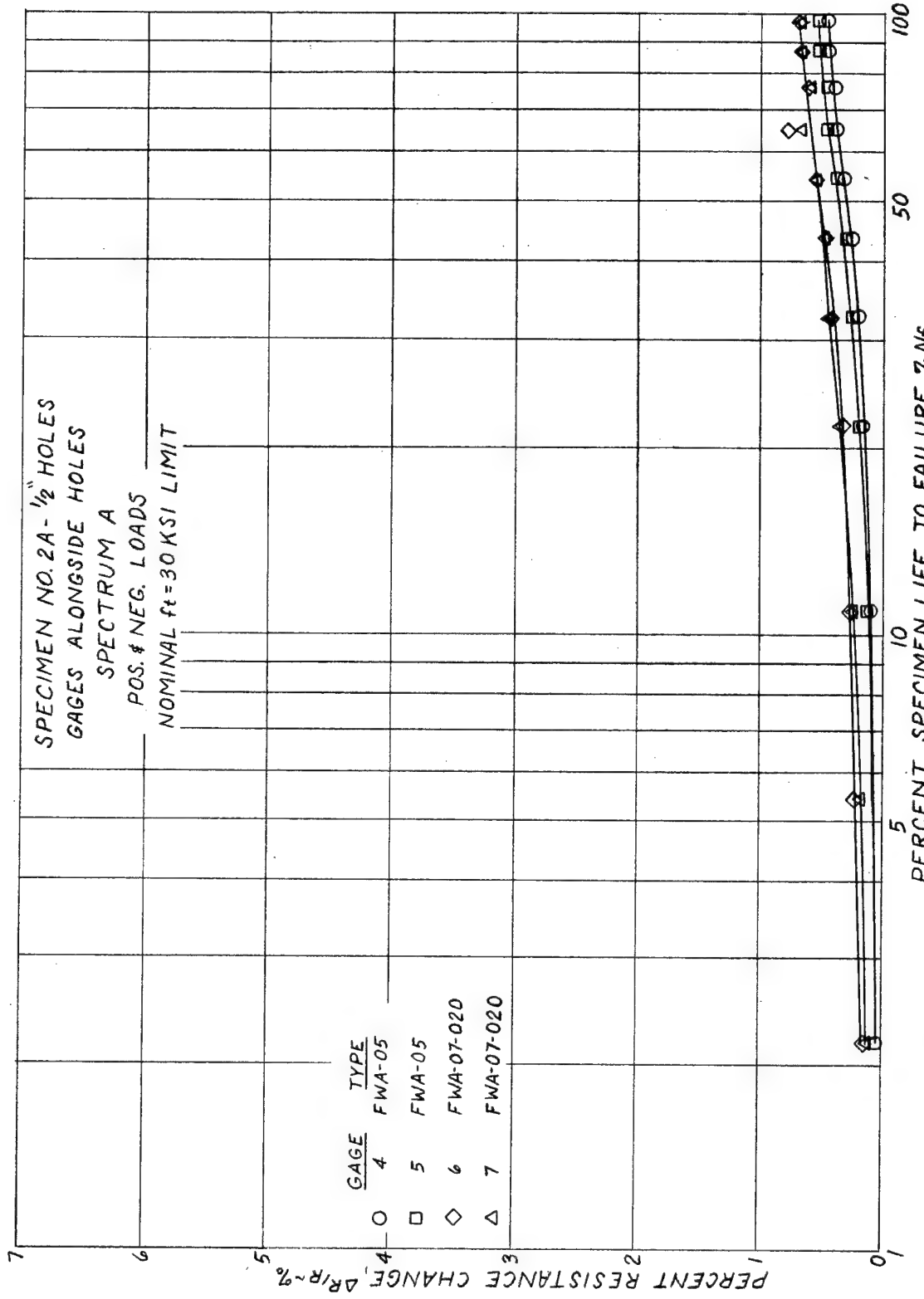

FIG. D-5 GAGE RESPONSE VS. SPECIMEN LIFE

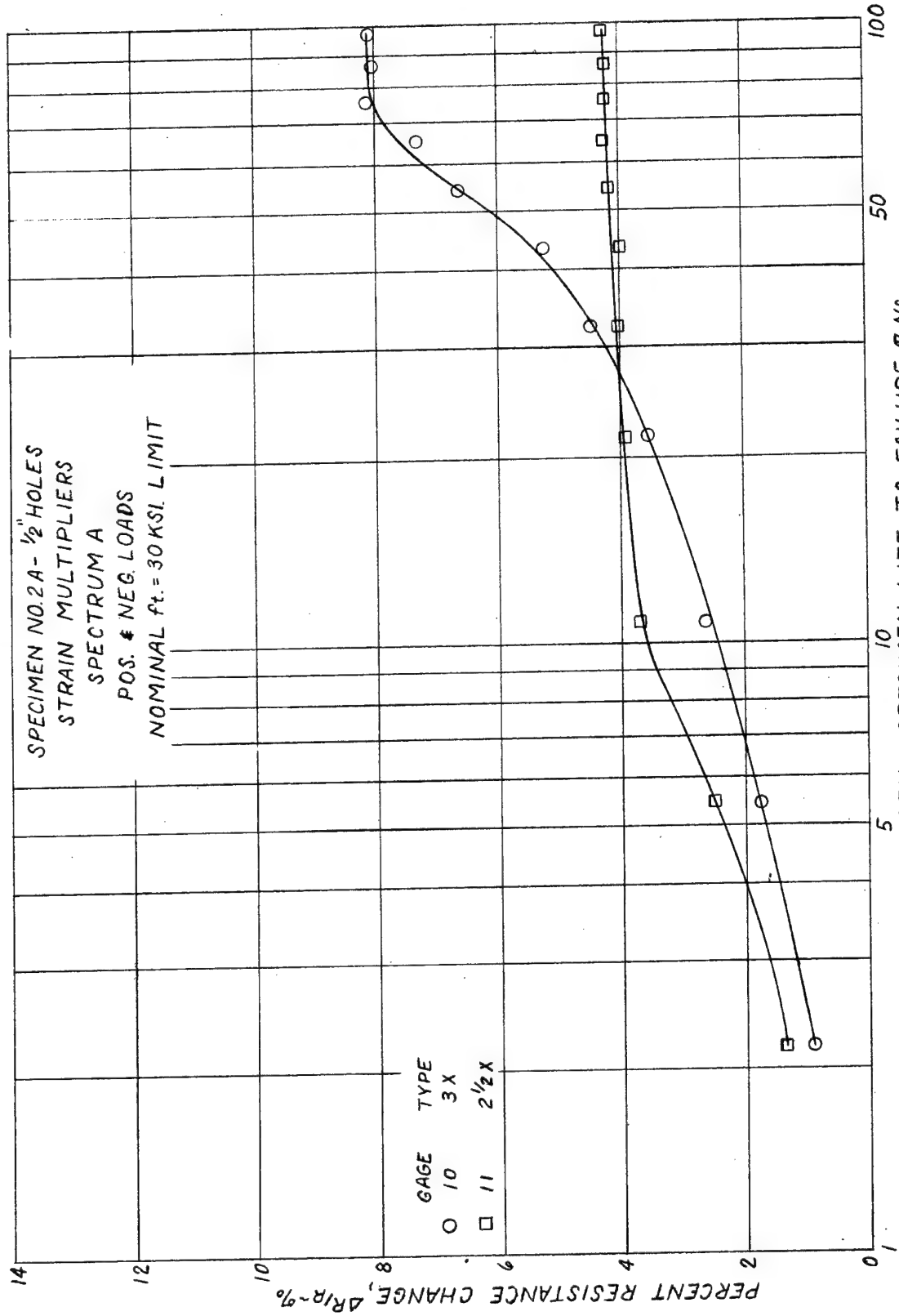

FIG.D-6 GAGE RESPONSE VS. SPECIMEN LIFE

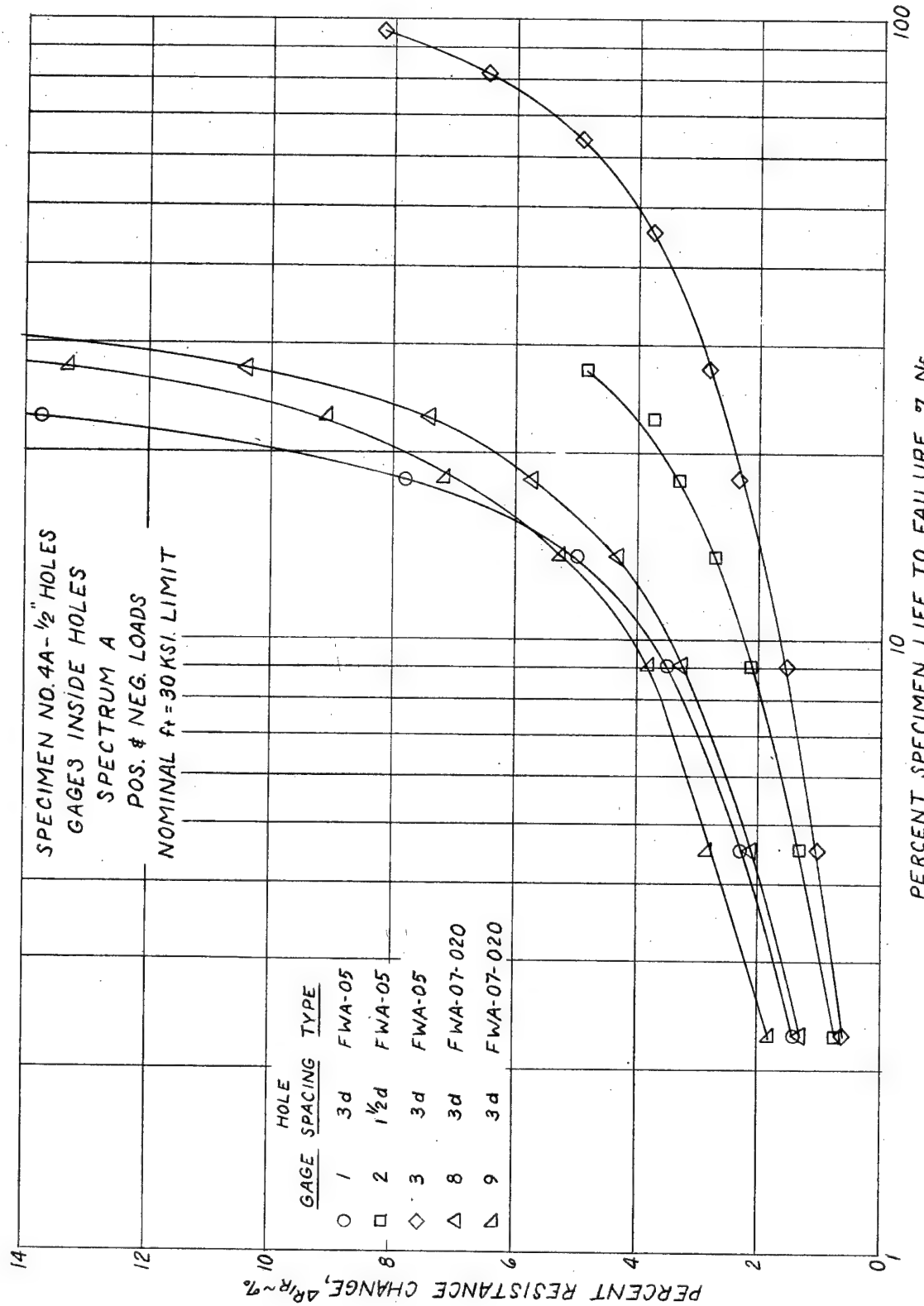

FIG. D-7 GAGE RESPONSE VS. SPECIMEN LIFE

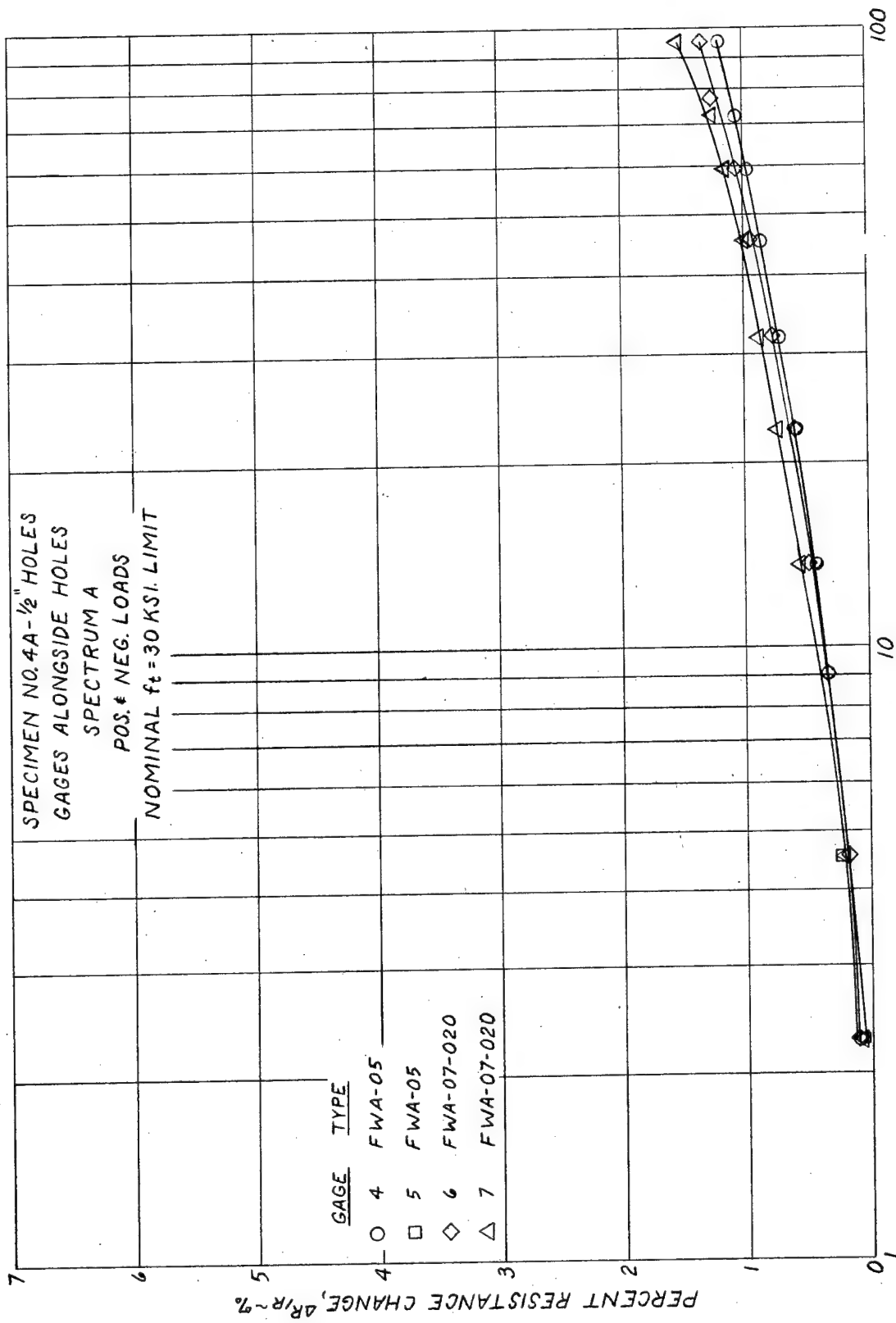

FIG. D-8 GAGE RESPONSE VS. SPECIMEN LIFE

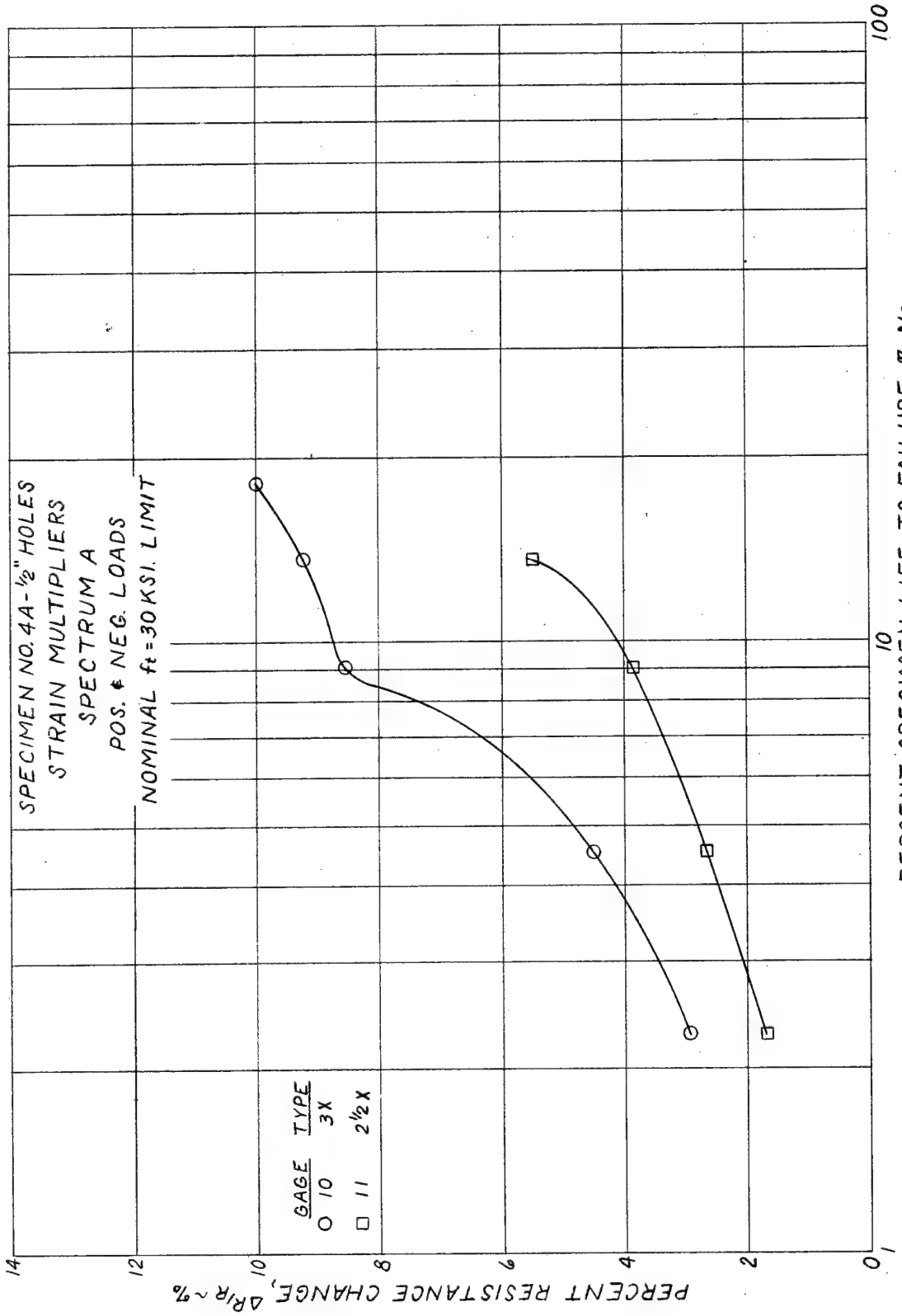

FIG. D-9 GAGE RESPONSE VS. SPECIMEN LIFE

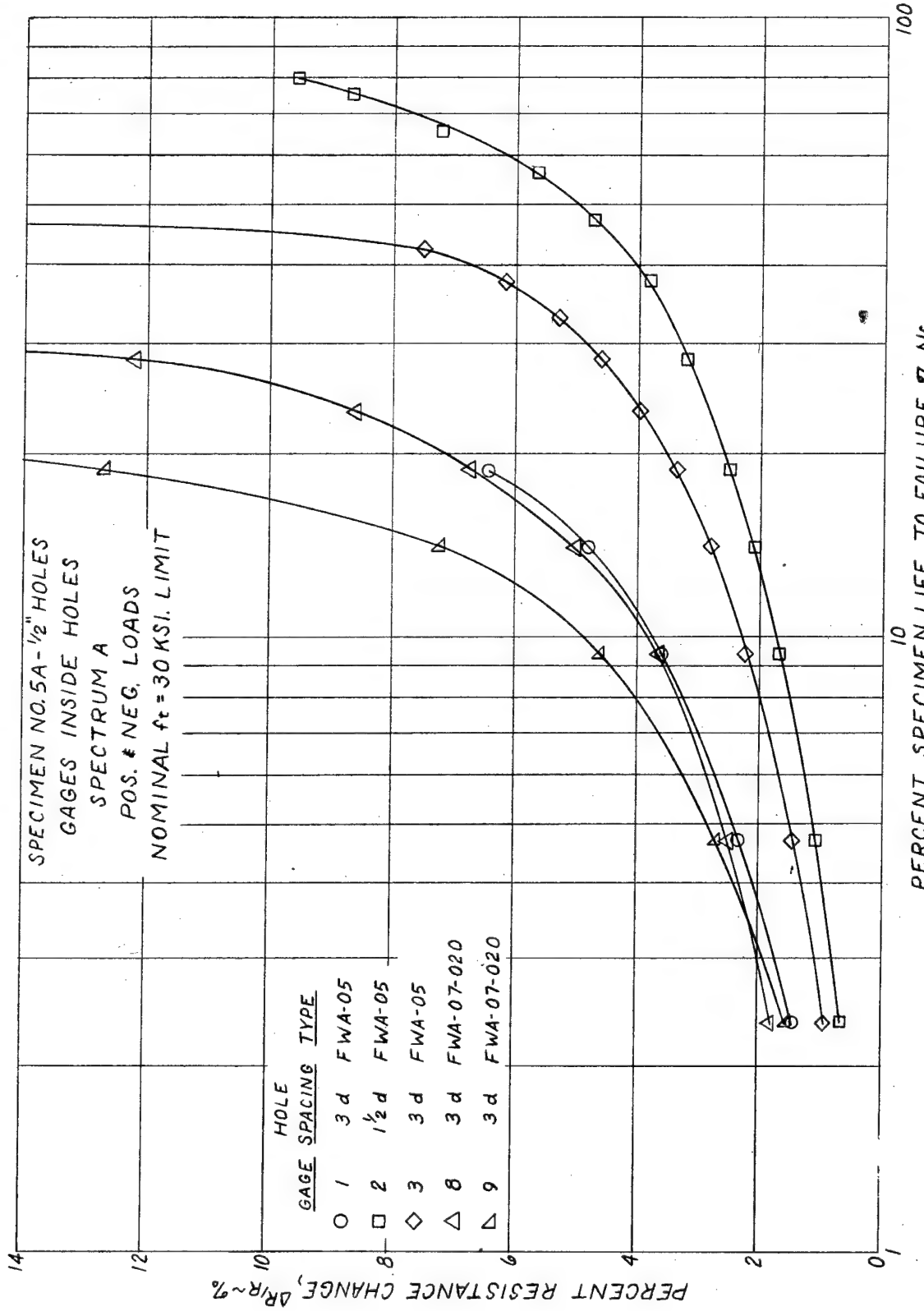

FIG. D-10 GAGE RESPONSE VS. SPECIMEN LIFE

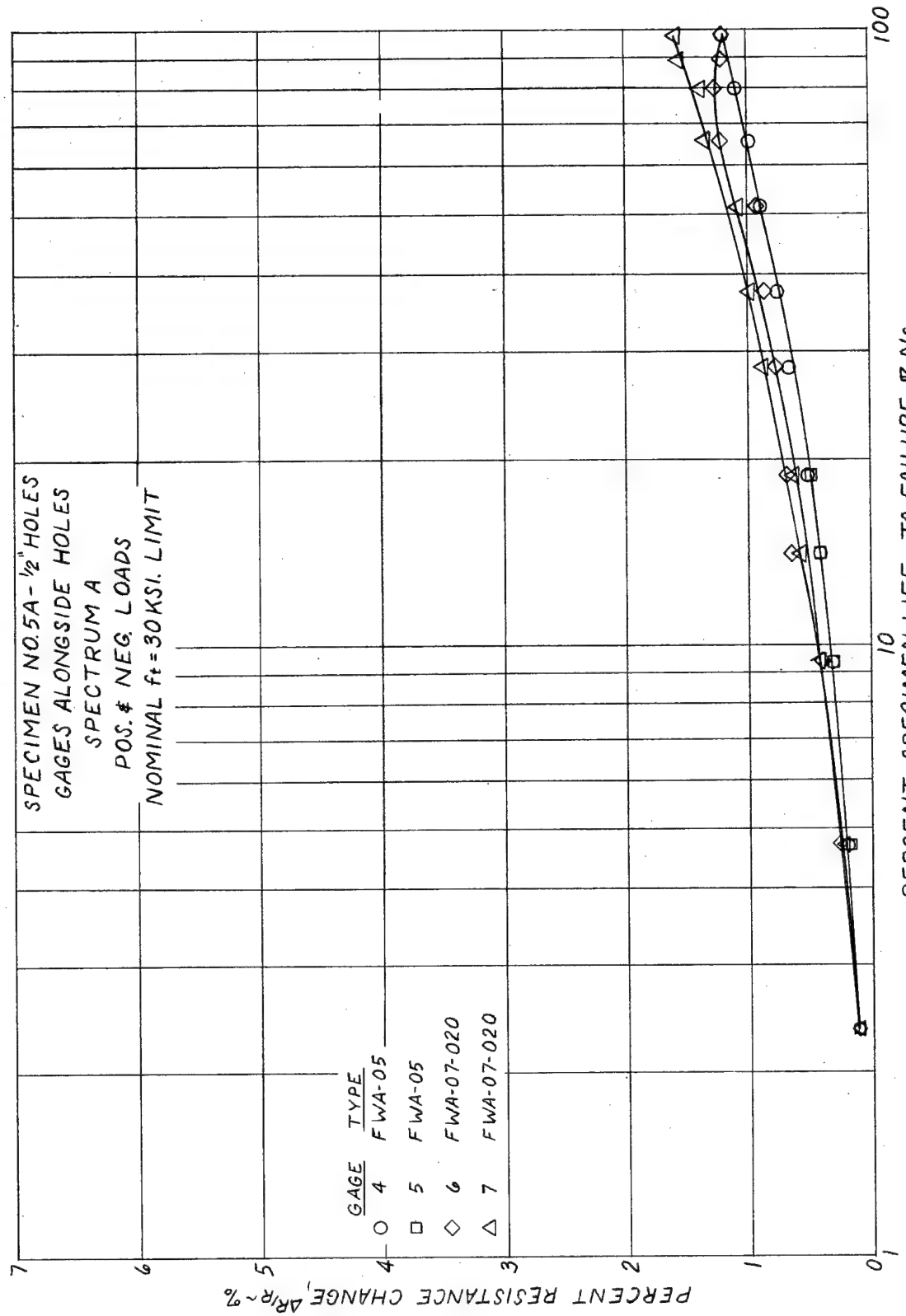

FIG. D-11 GAGE RESPONSE VS. SPECIMEN LIFE

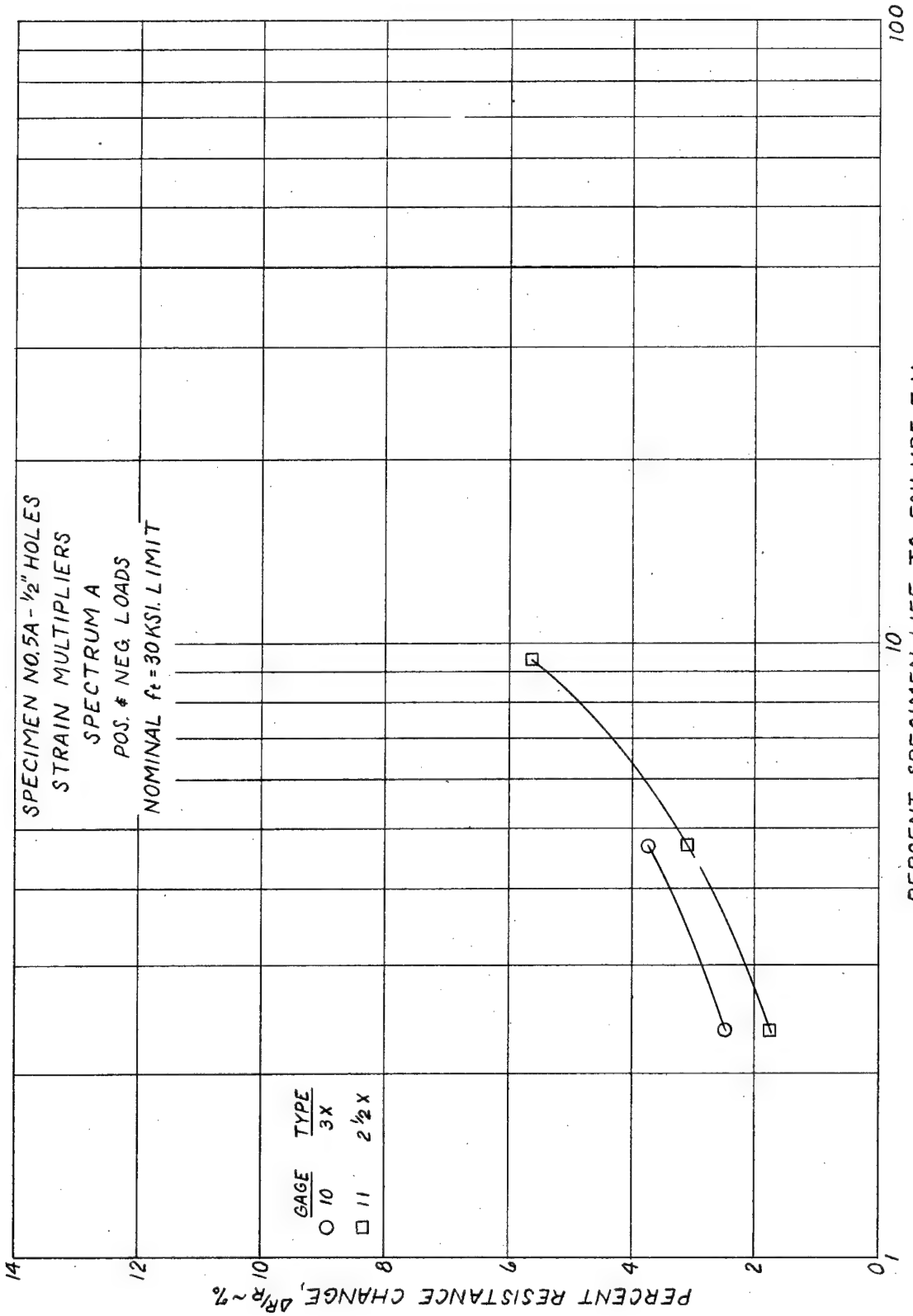

FIG. D-12 GAGE RESPONSE VS. SPECIMEN LIFE

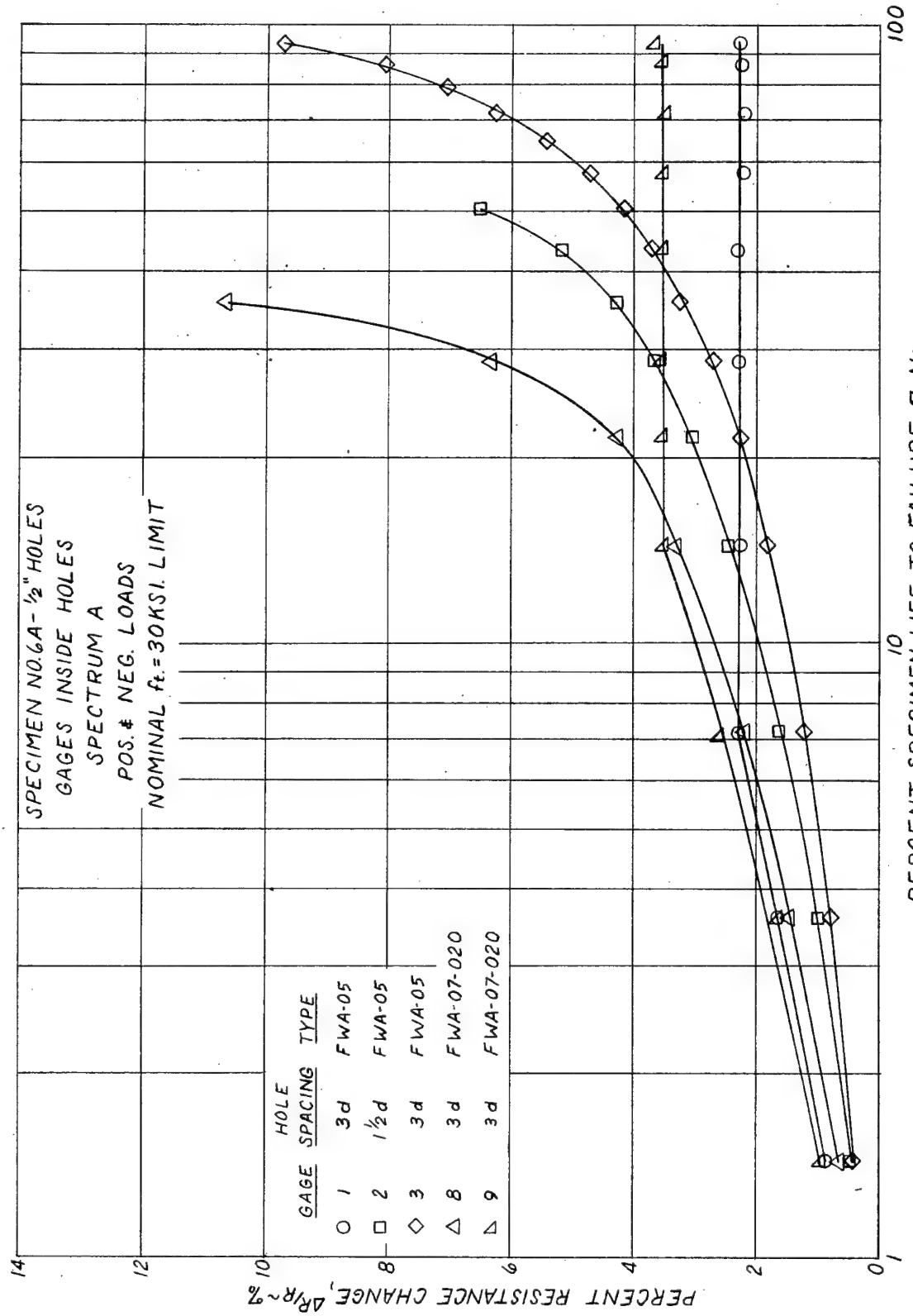

FIG. D-13 GAGE RESPONSE VS. SPECIMEN LIFE

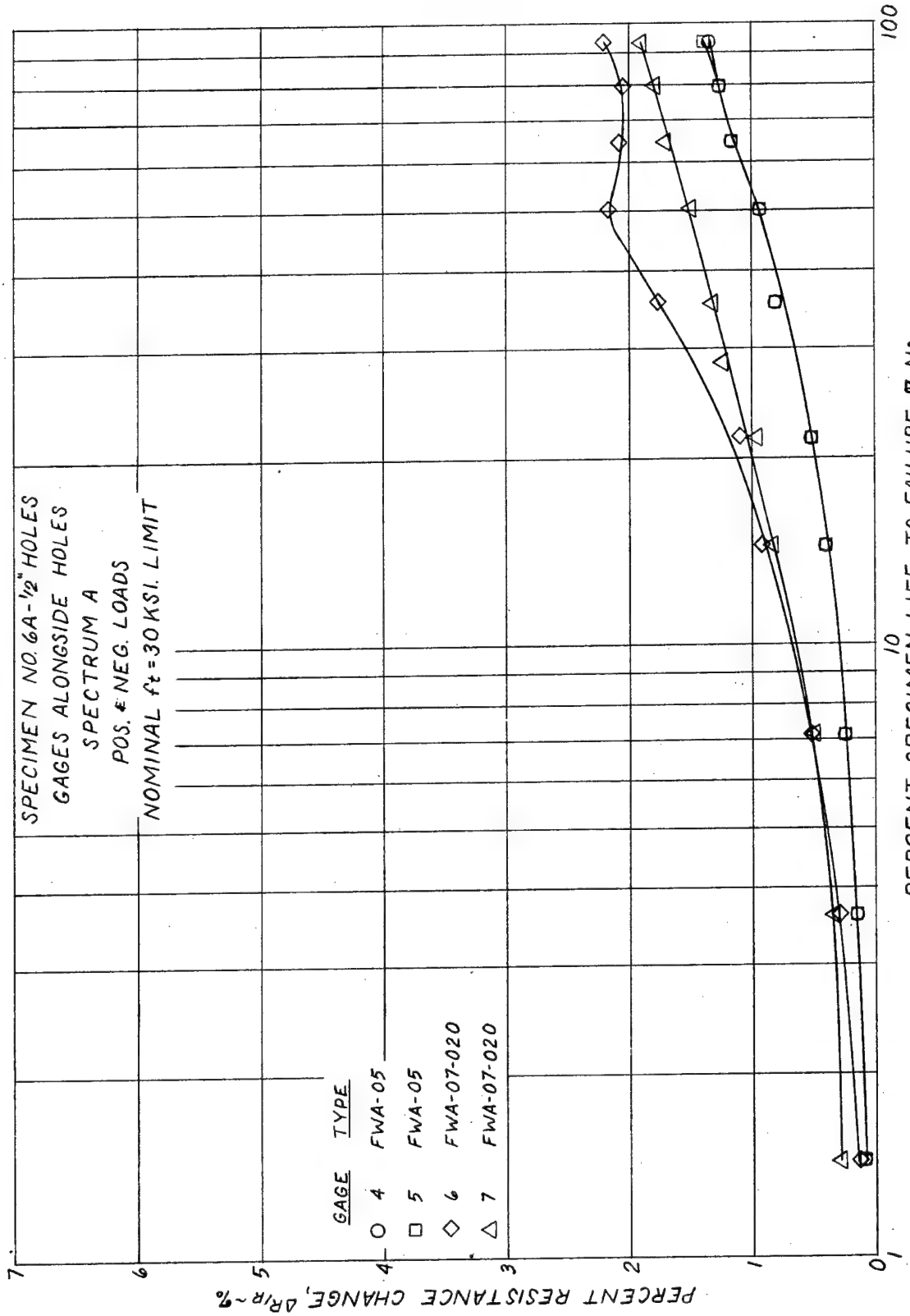

FIG. D-14 GAGE RESPONSE VS. SPECIMEN LIFE

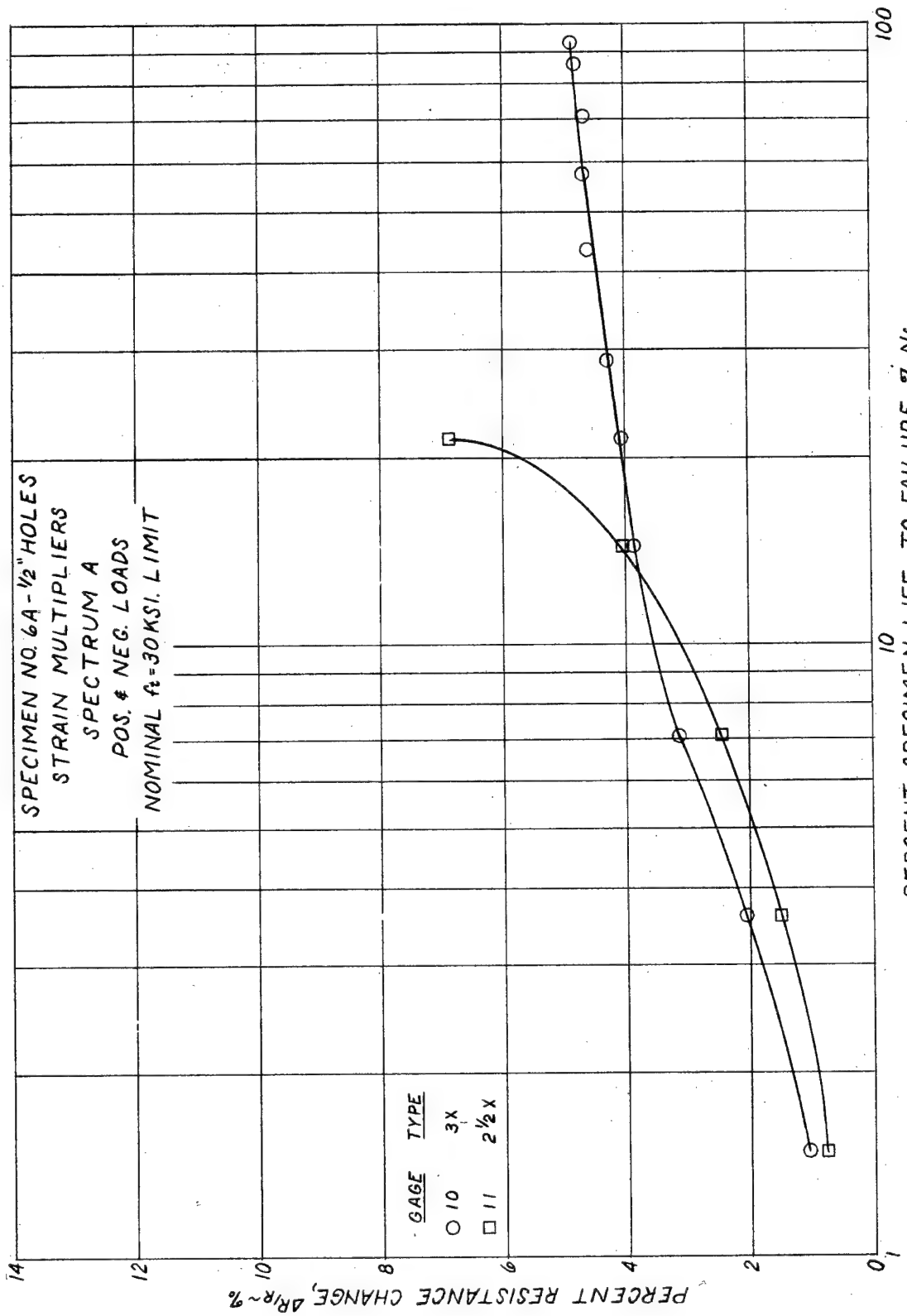

FIG. D-15 GAGE RESPONSE VS. SPECIMEN LIFE

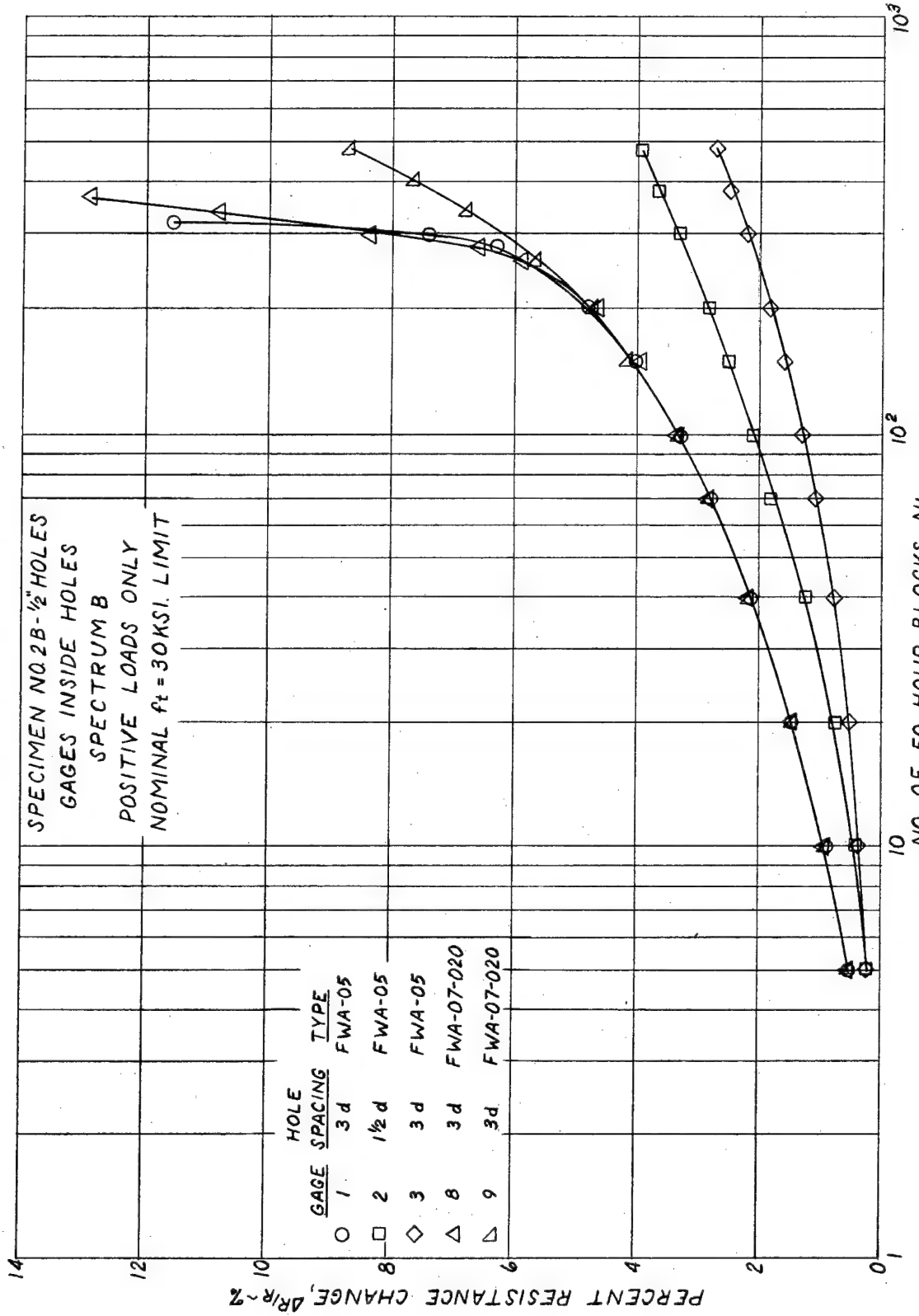

FIG. D-16 GAGE RESPONSE VS. NO. OF BLOCKS

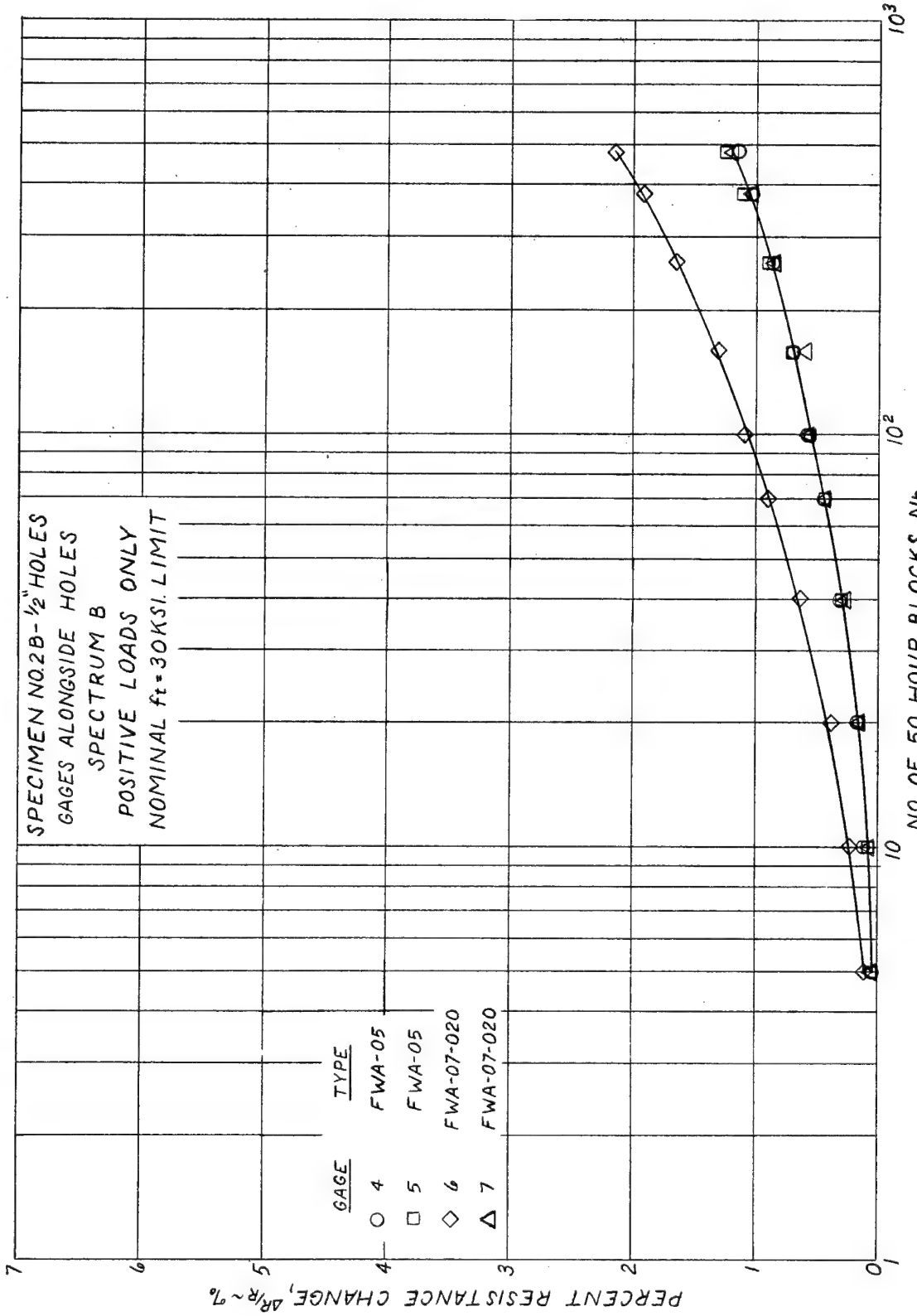

FIG. D-17 GAGE RESPONSE VS. NO. OF BLOCKS

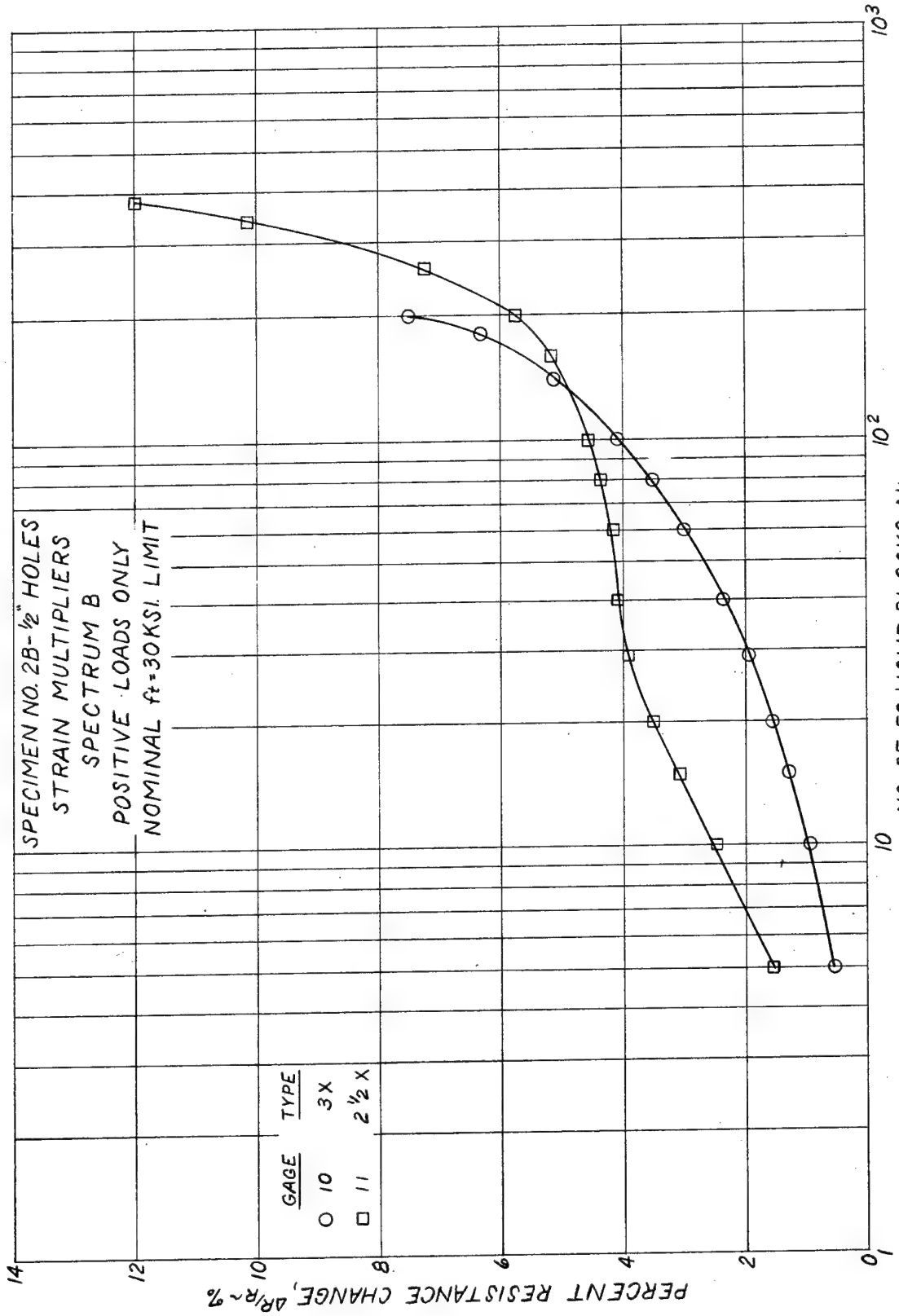

FIG. D-18 GAGE RESPONSE VS. NO. OF BLOCKS

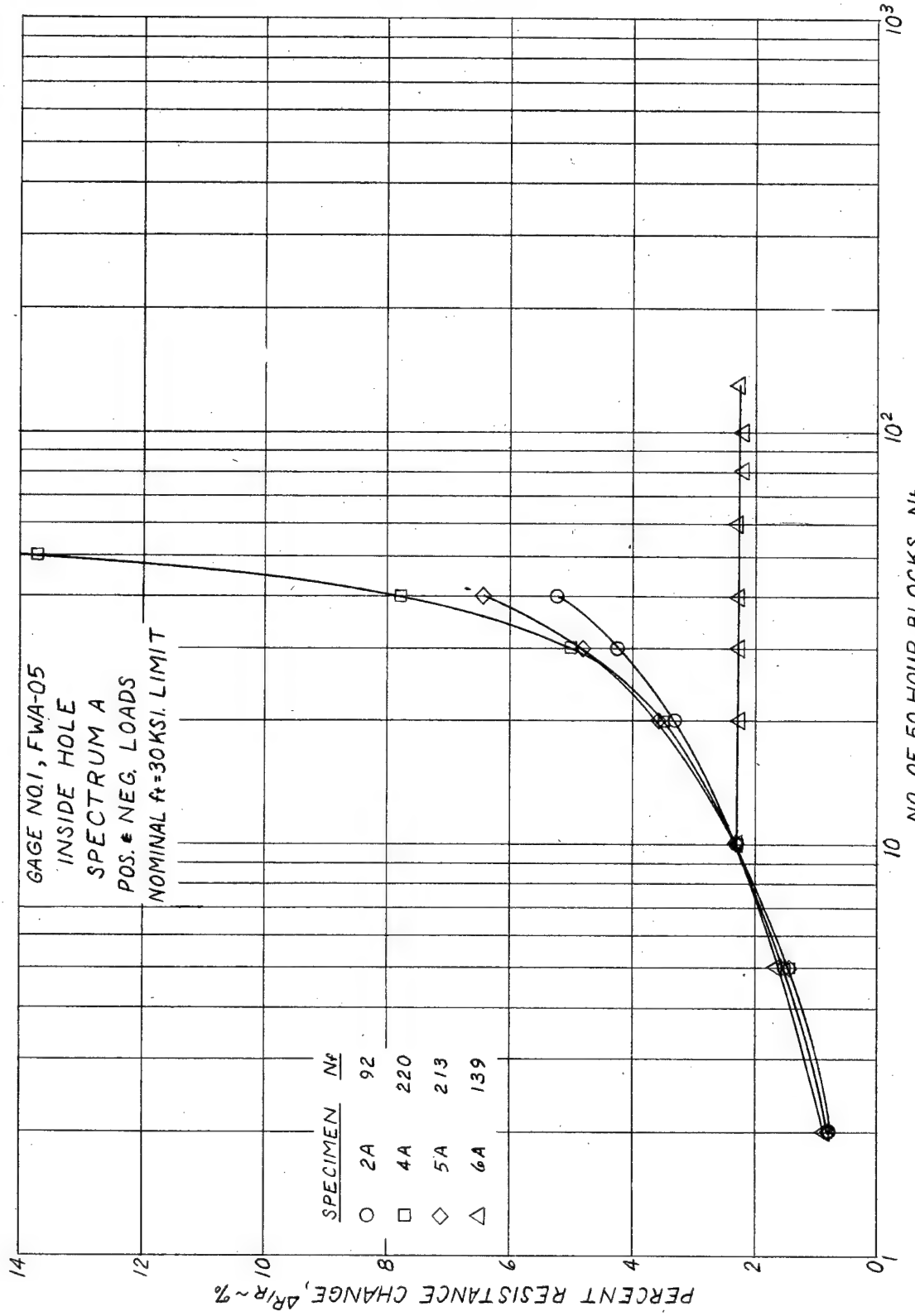

FIG. D-19 GAGE RESPONSE VS. NO. OF BLOCKS

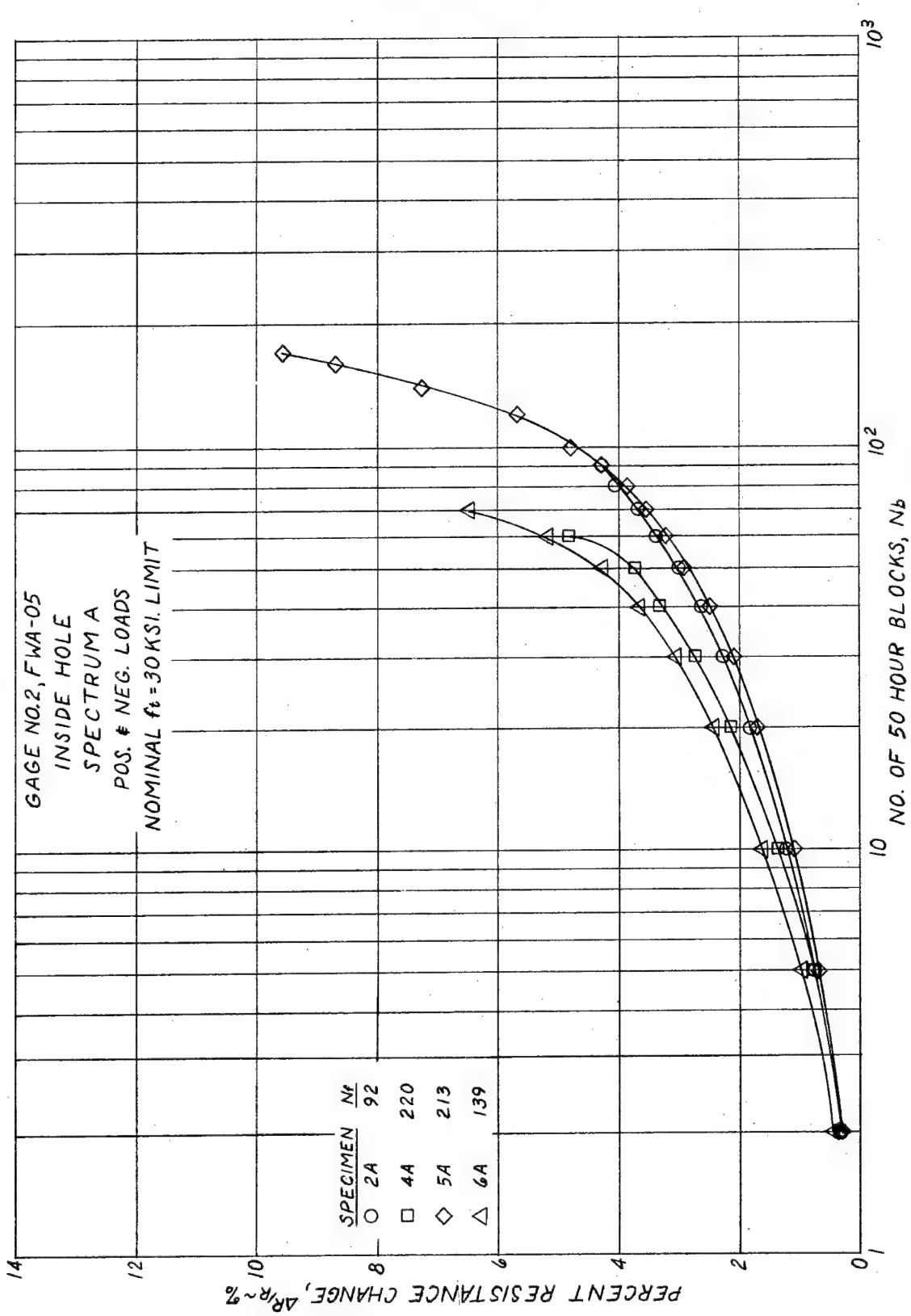

FIG. D-20 GAGE RESPONSE VS NO. OF BLOCKS

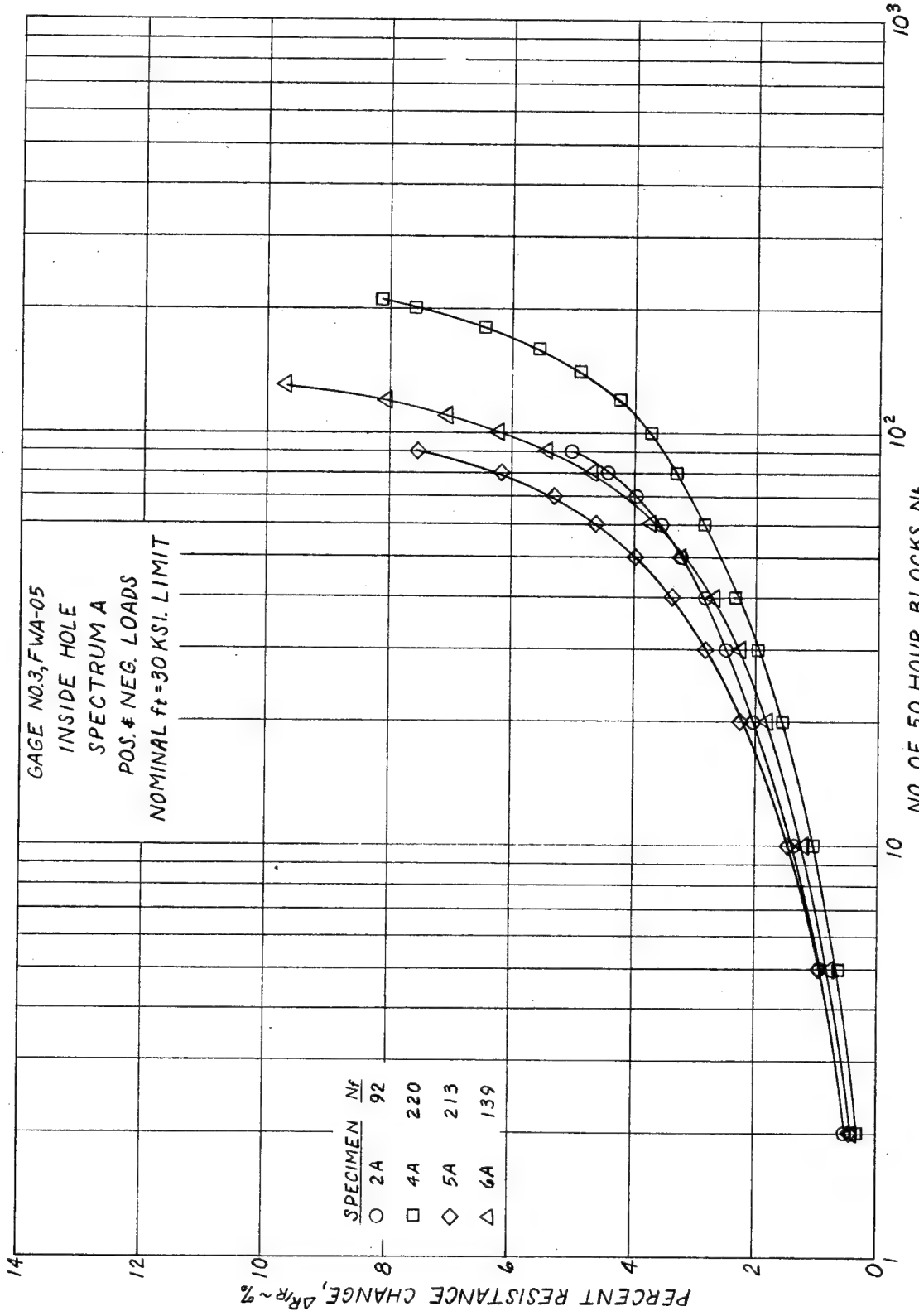

FIG. D-21 GAGE RESPONSE VS. NO. OF BLOCKS

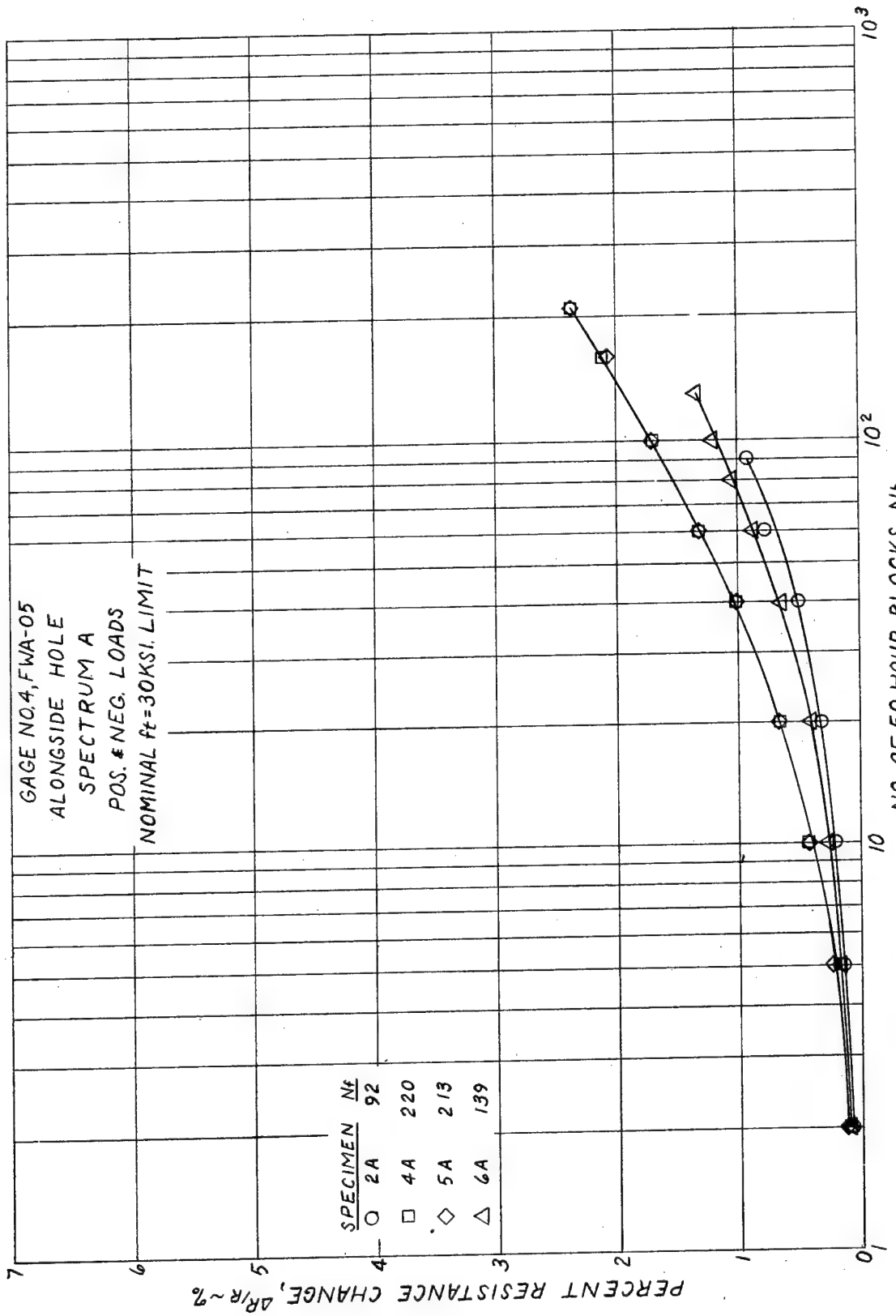

FIG. D-22 GAGE RESPONSE VS. NO. OF BLOCKS

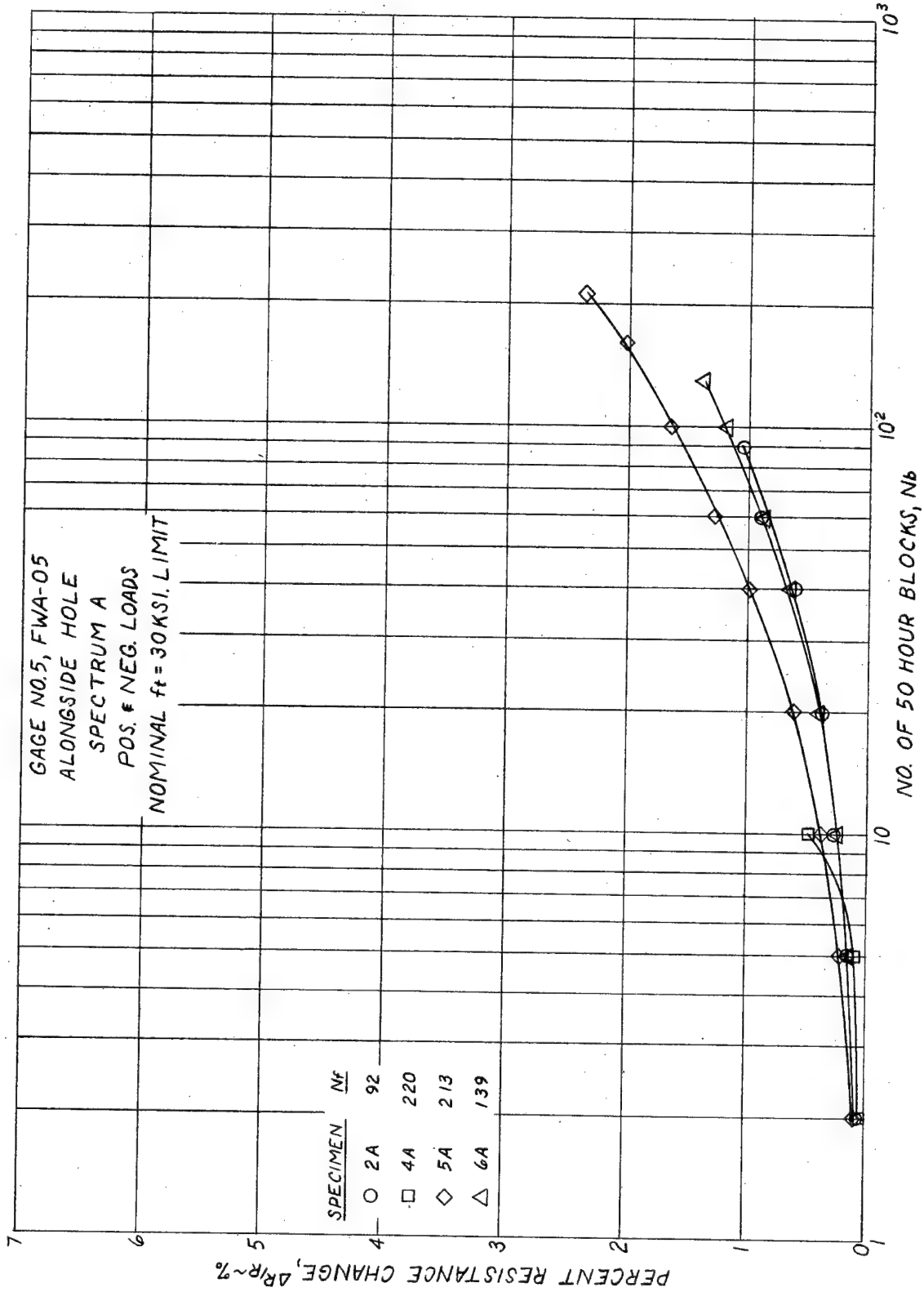

FIG. D-23 GAGE RESPONSE VS. NO. OF BLOCKS

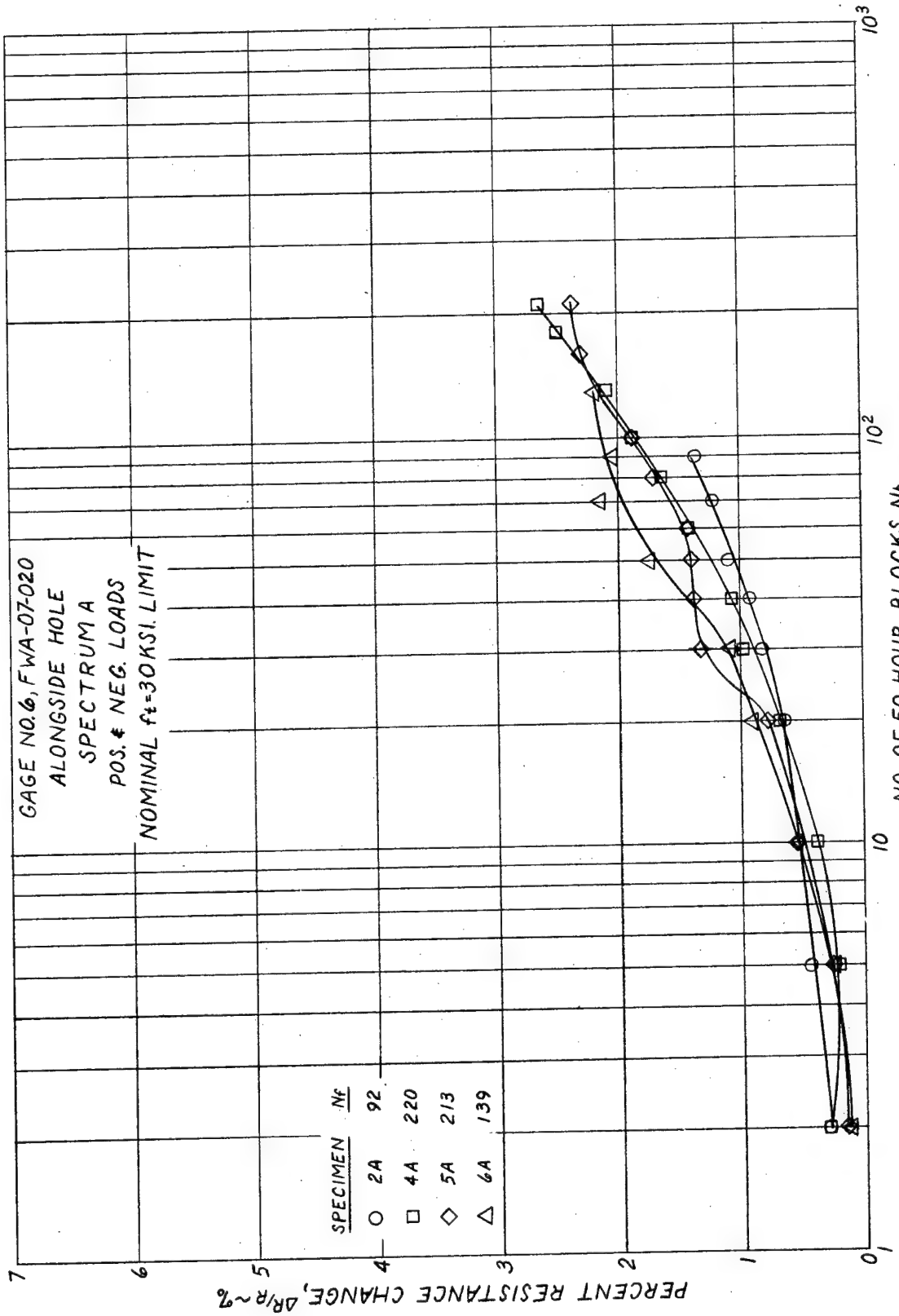

FIG. D-24 GAGE RESPONSE VS NO. OF BLOCKS

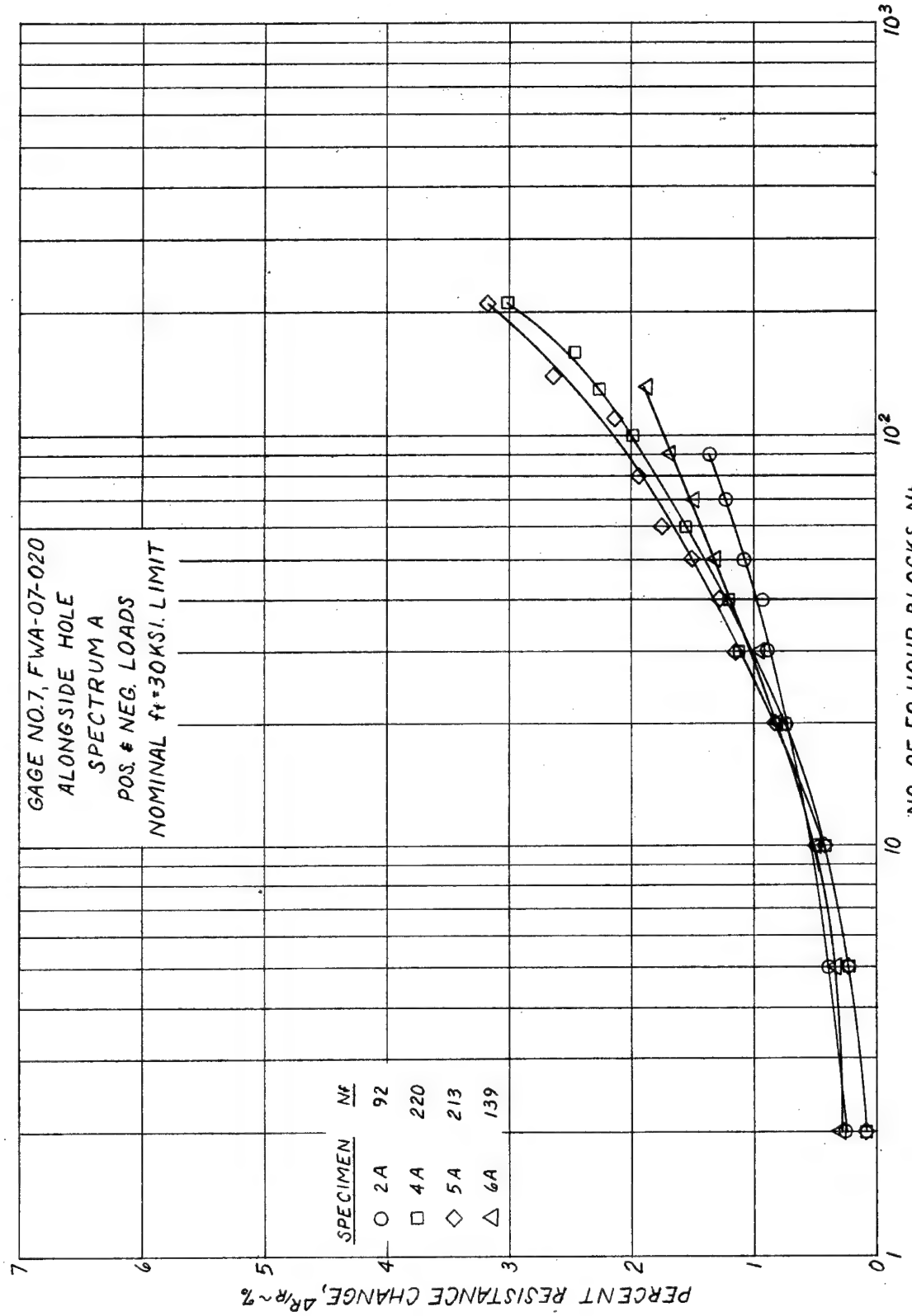

FIG. D-25 GAGE RESPONSE VS. NO. OF BLOCKS

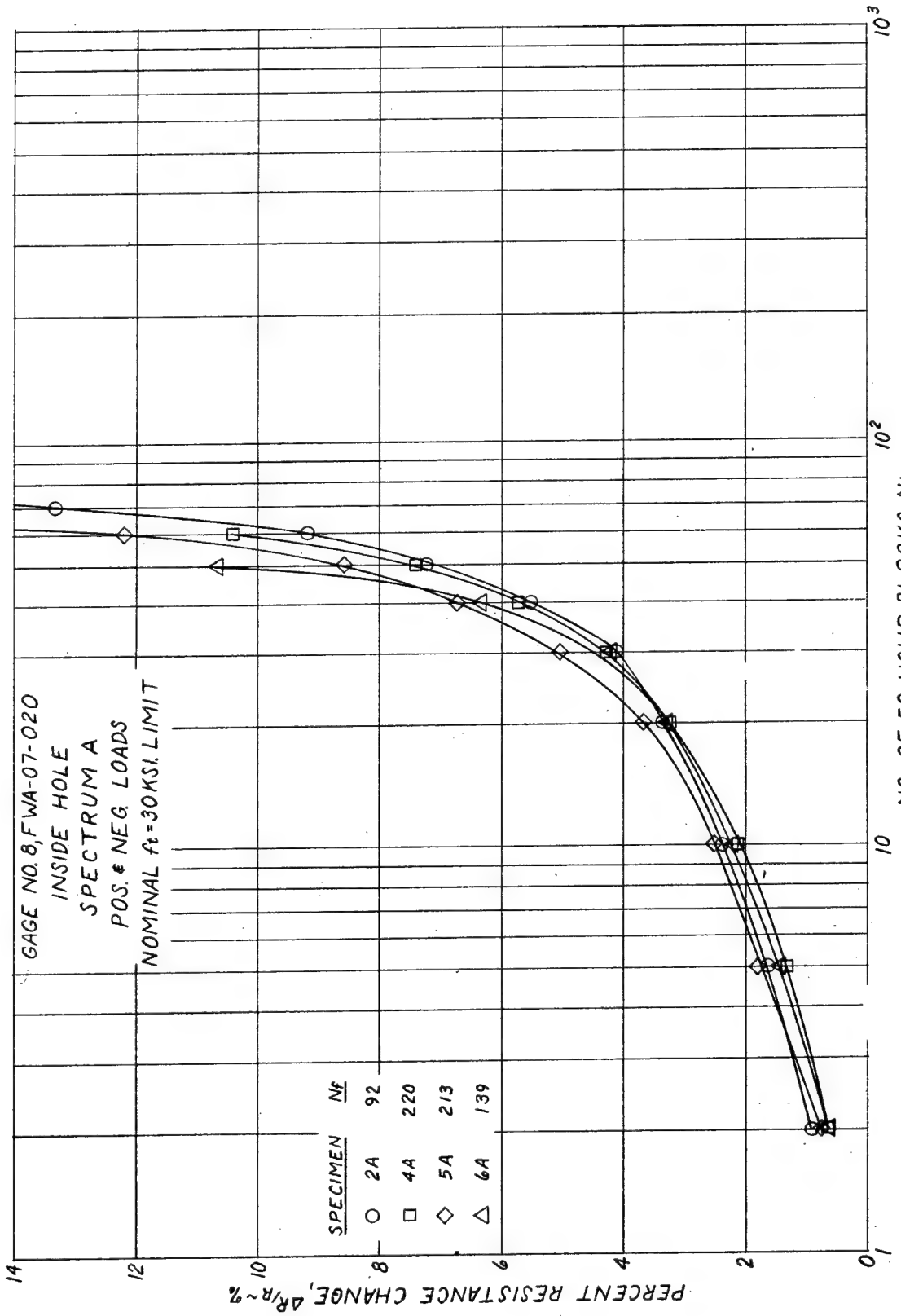

FIG. D-26 GAGE RESPONSE VS. NO. OF BLOCKS

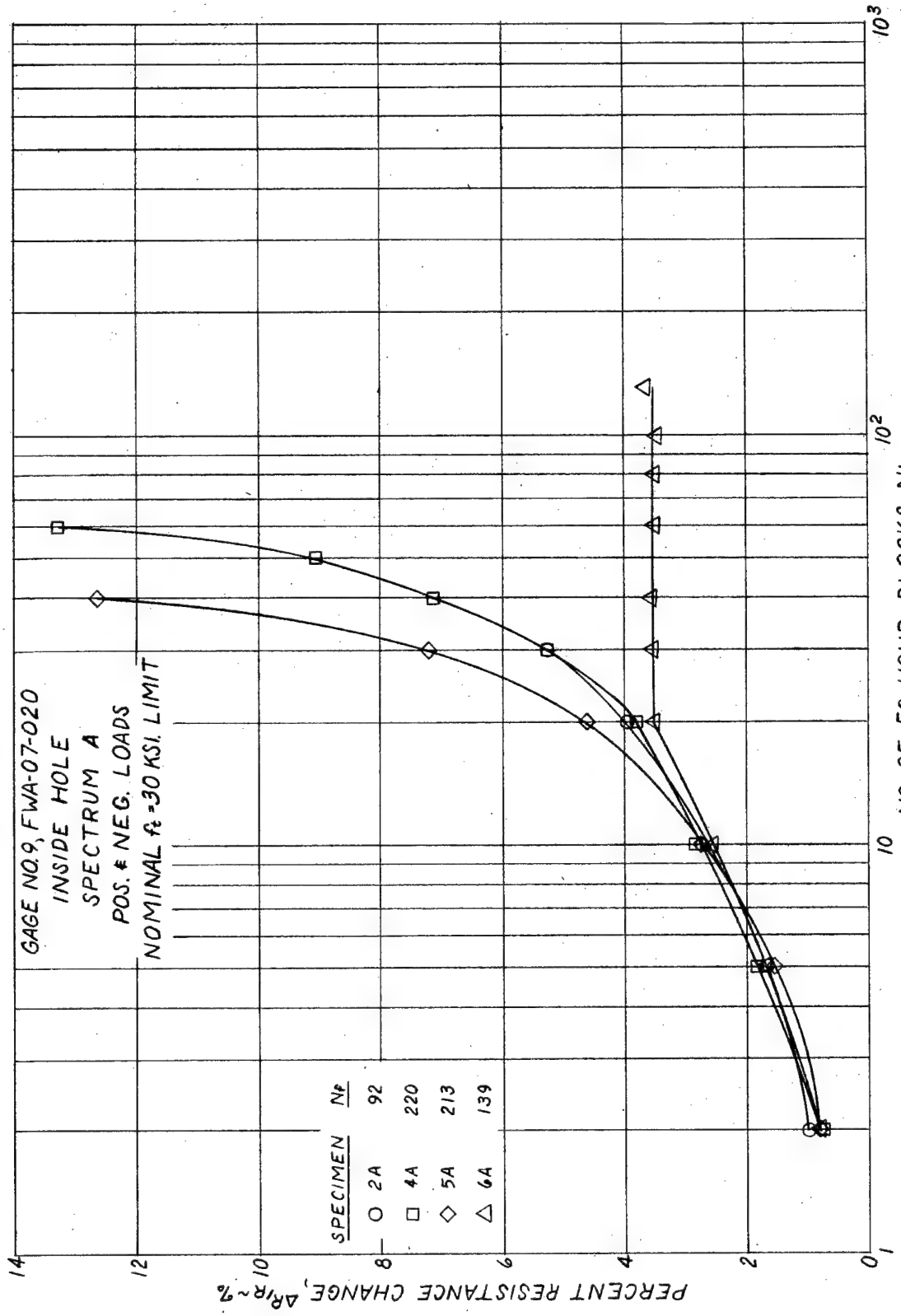

FIG. D-27 GAGE RESPONSE VS. NO. OF BLOCKS

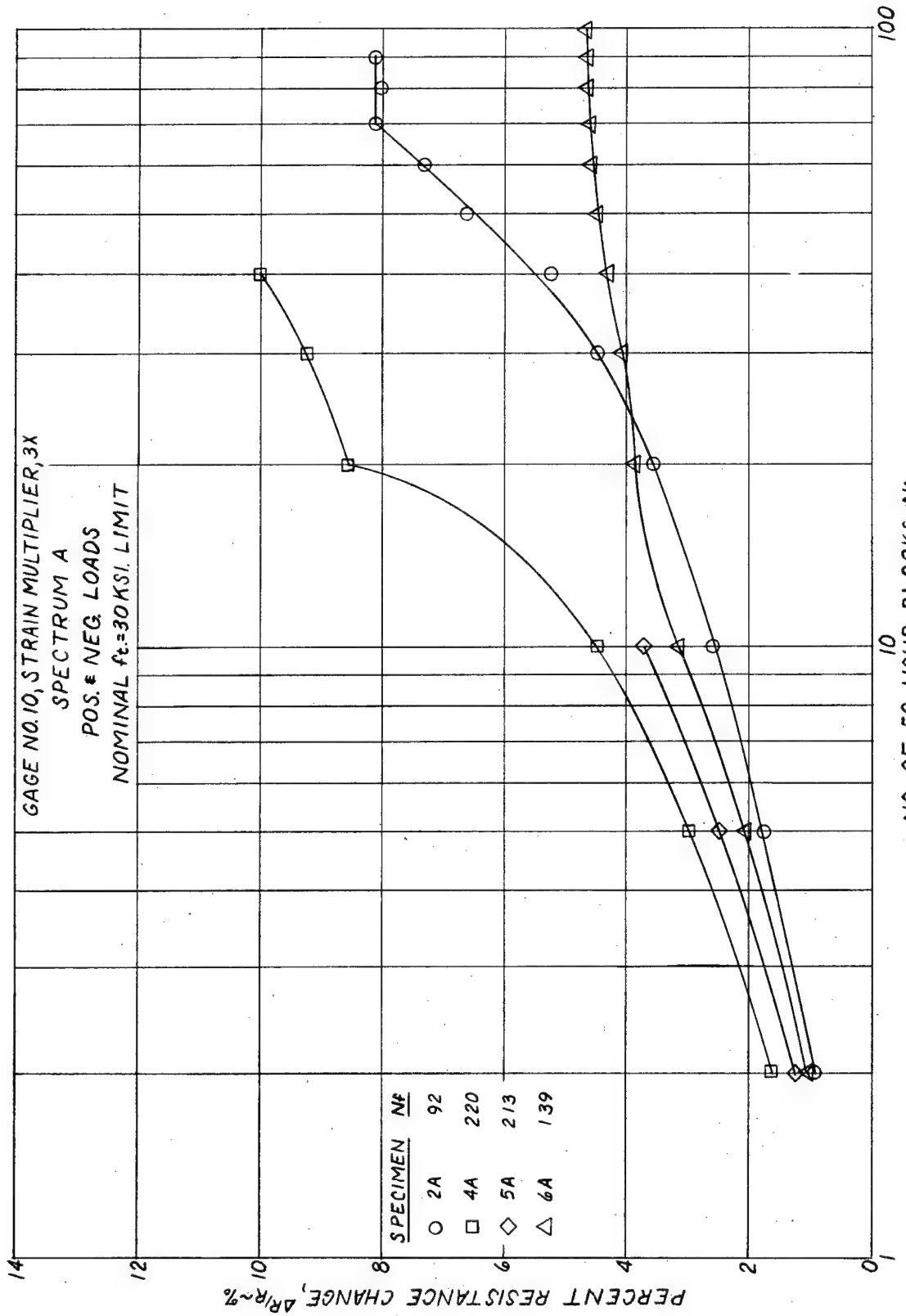

FIG. D-28 GAGE RESPONSE VS. NO. OF BLOCKS

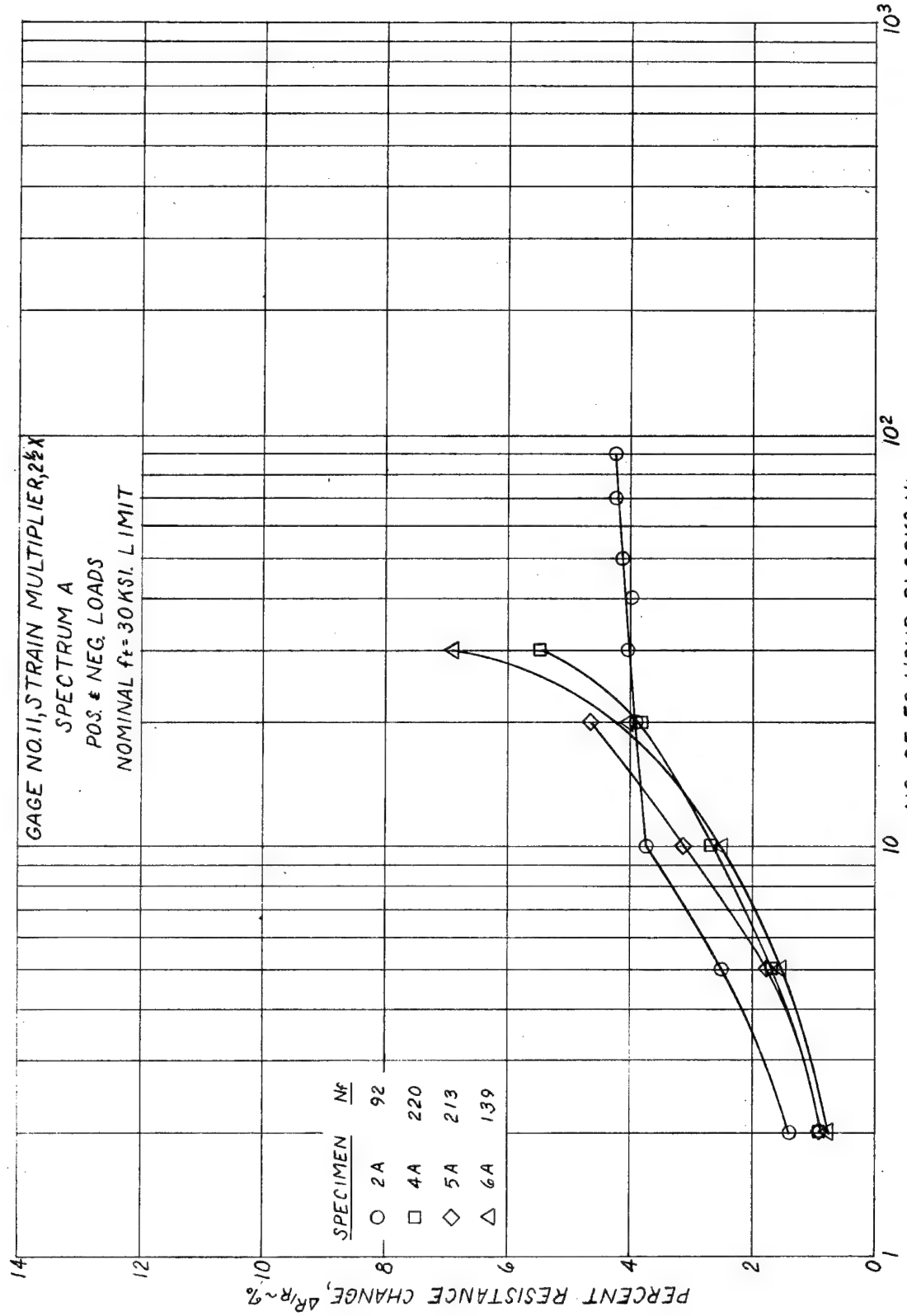

FIG. D-29 GAGE RESPONSE VS. NO. OF BLOCKS

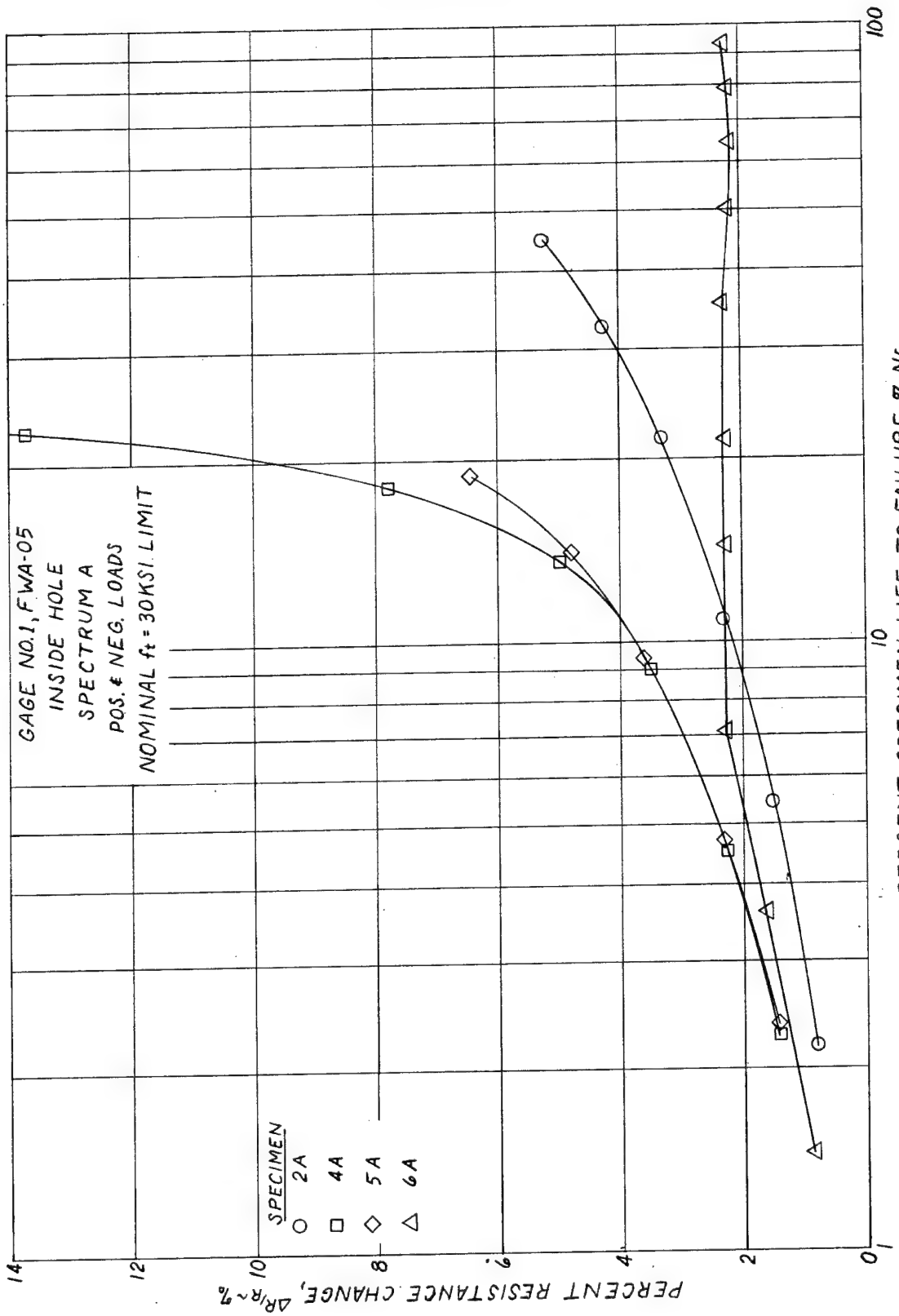

FIG. D-30 GAGE RESPONSE VS. SPECIMEN LIFE

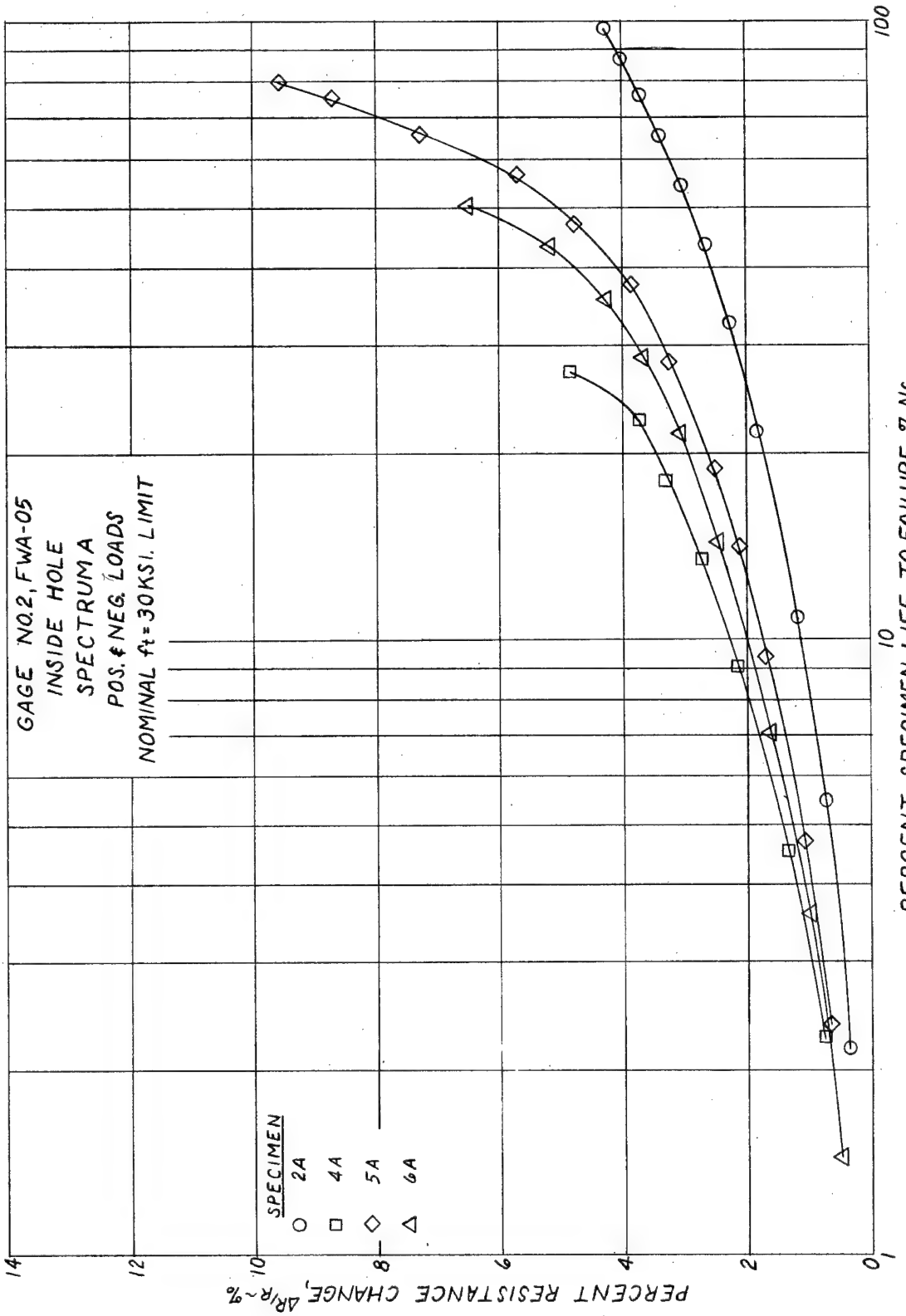

FIG. D-31 GAGE RESPONSE VS. SPECIMEN LIFE

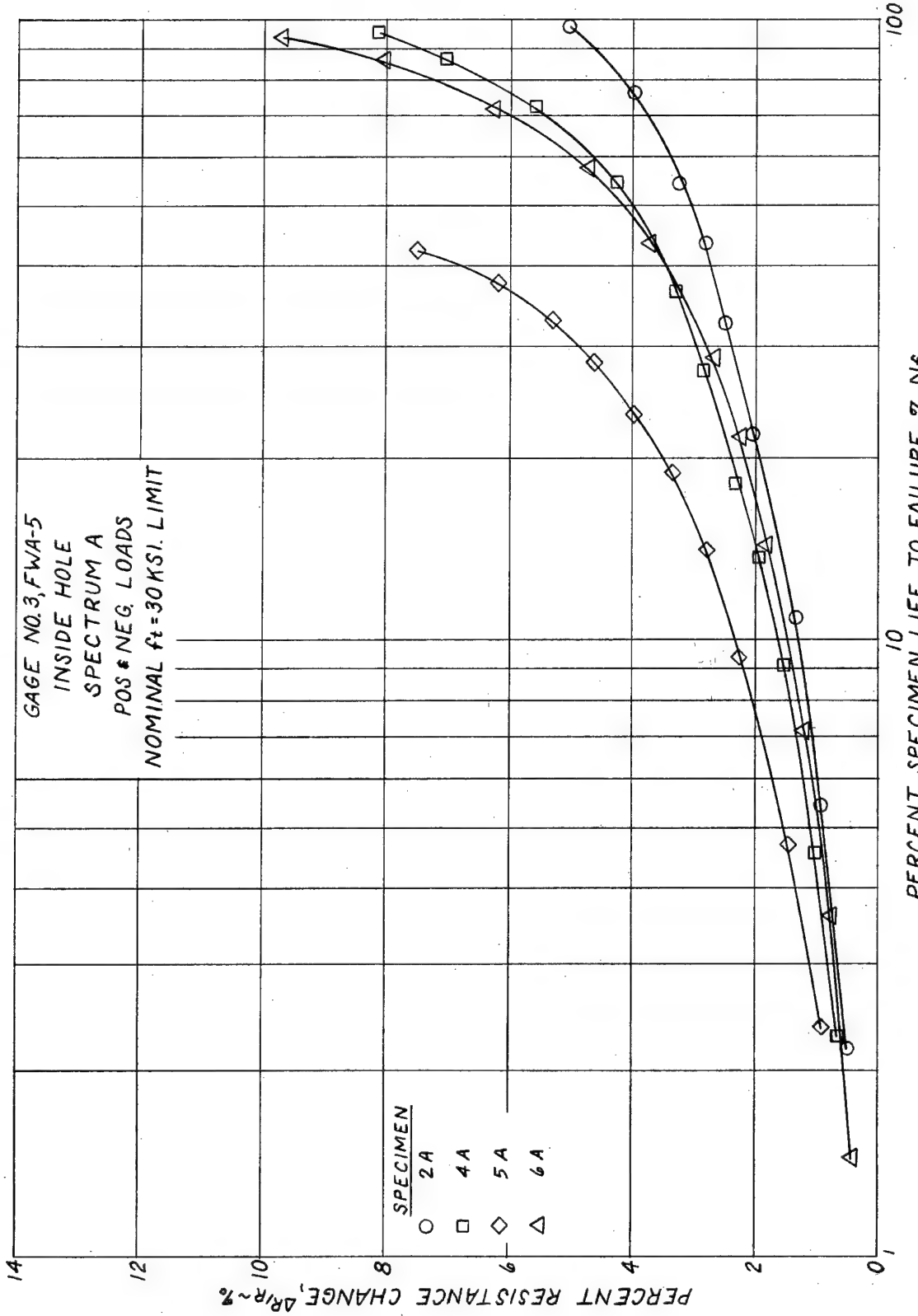

FIG. D-32 GAGE RESPONSE VS. SPECIMEN LIFE

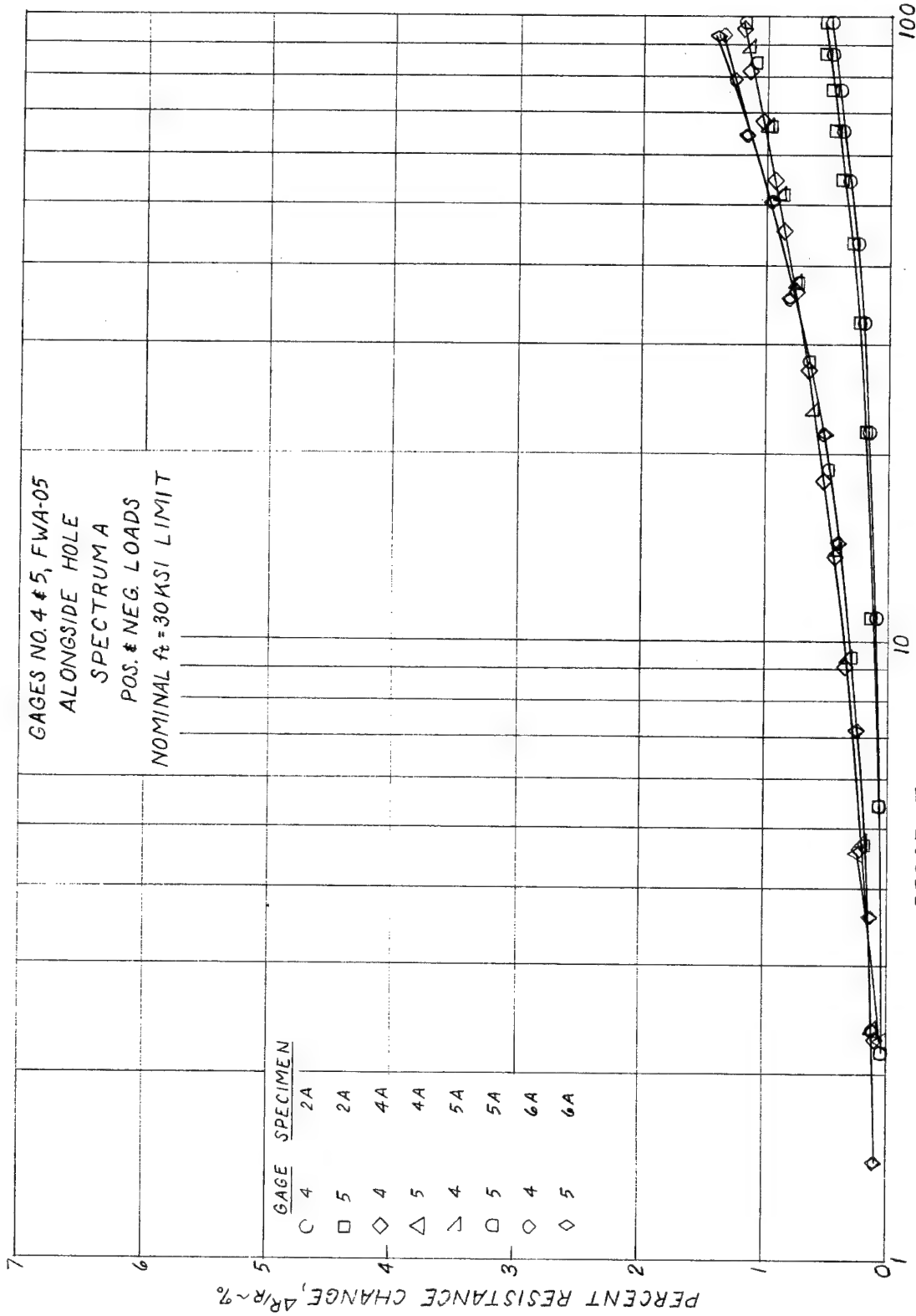

FIG. D-33 GAGE RESPONSE VS. SPECIMEN LIFE

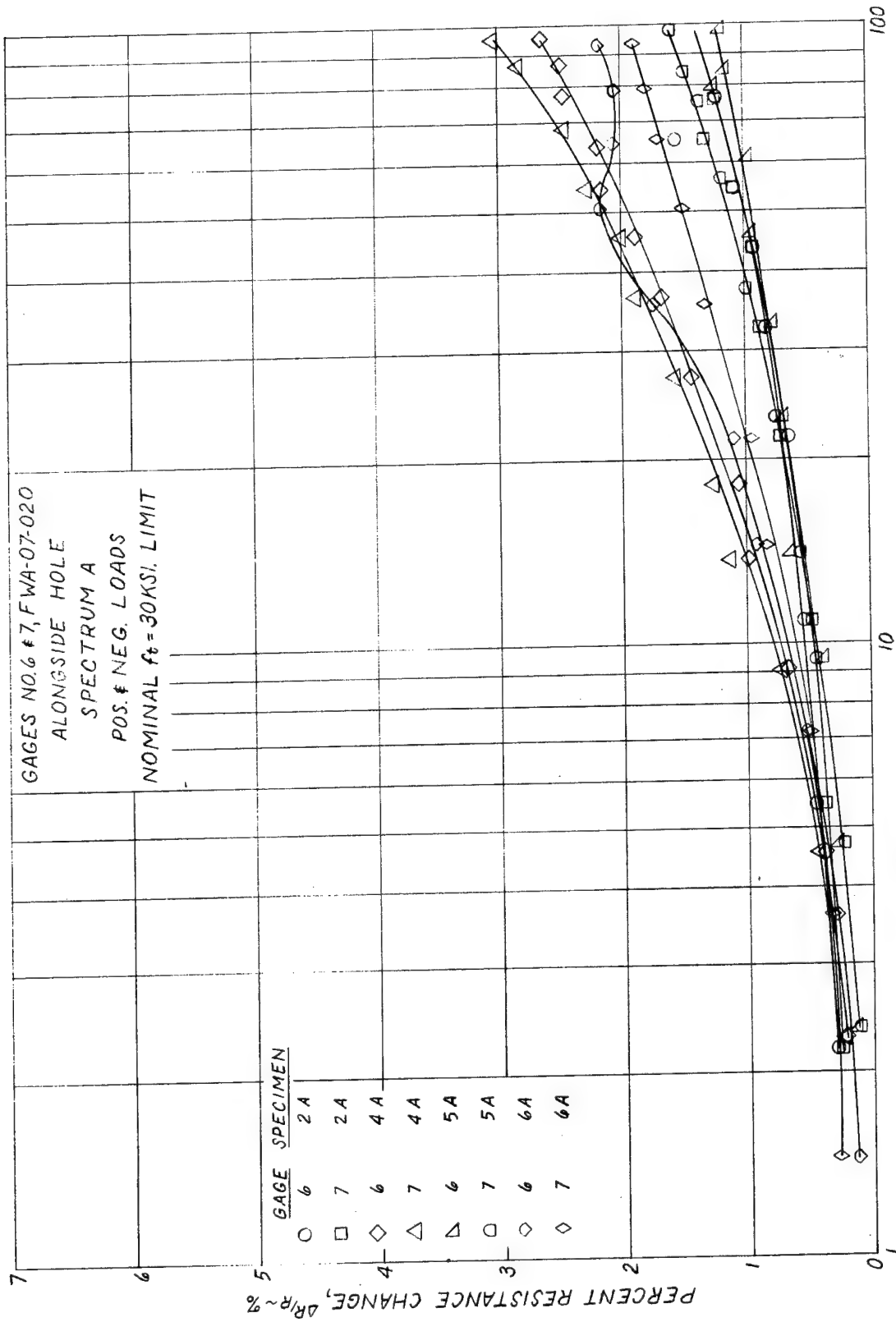

FIG. D-34 GAGE RESPONSE VS. SPECIMEN LIFE

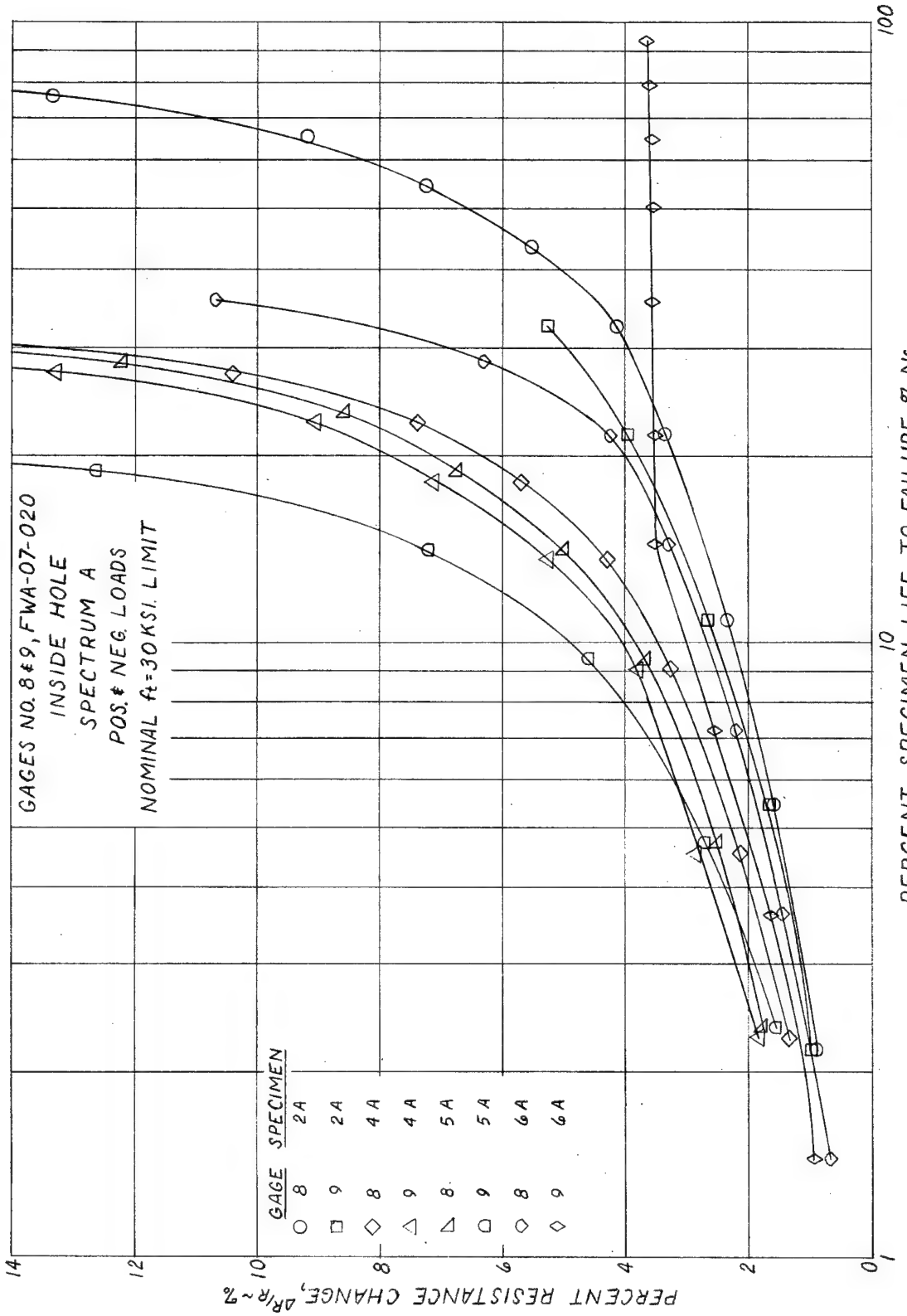

FIG. D-35 GAGE RESPONSE VS. SPECIMEN LIFE

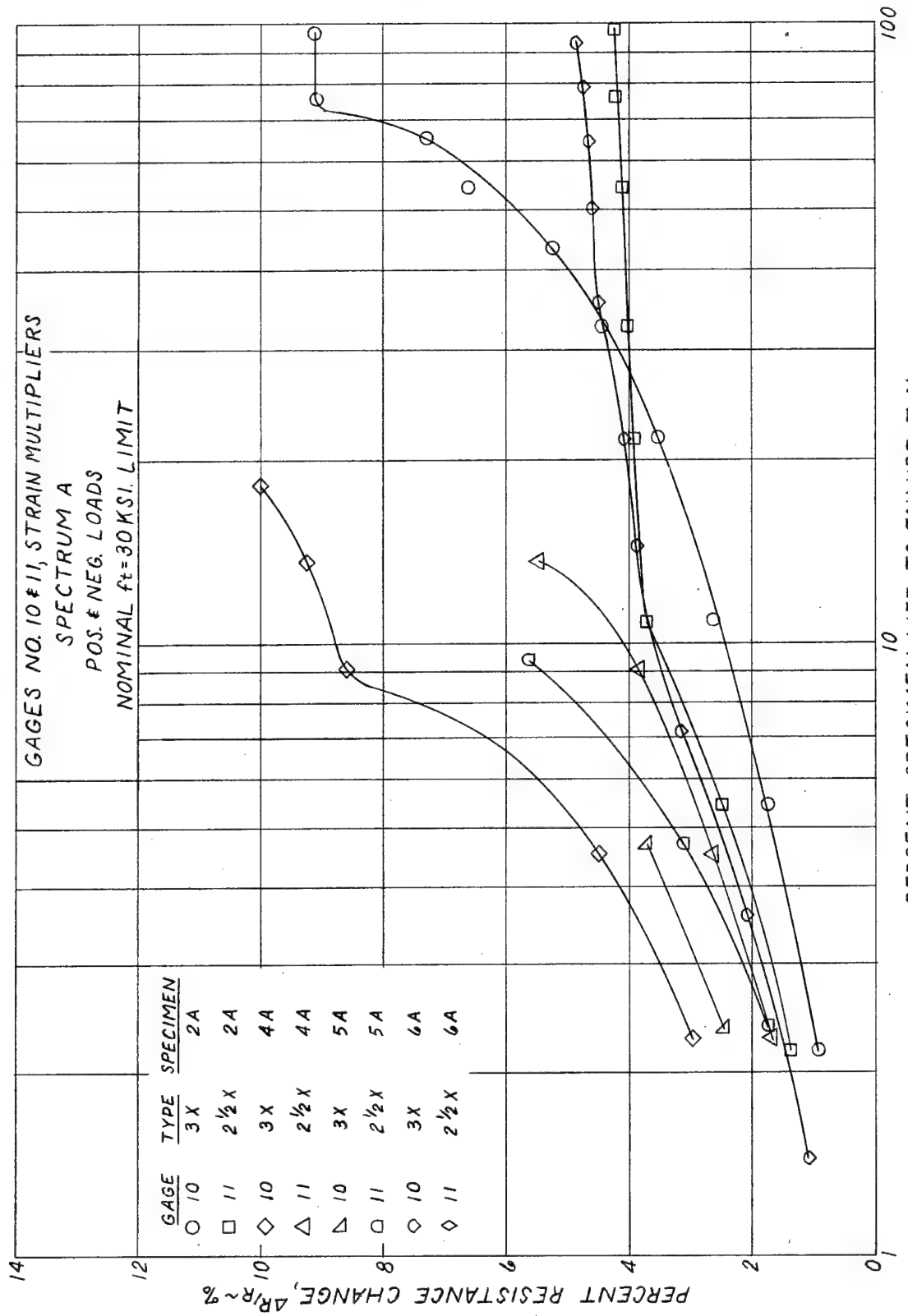

FIG. D-36 GAGE RESPONSE VS. SPECIMEN LIFE

UNCLASSIFIED
Security Classification

DOCUMENT CONTROL DATA - R & D

(Security classification of title, body of abstract and indexing annotation must be entered when the overall report is classified)

1. ORIGINATING ACTIVITY *(Corporate author)*
Air Vehicle Technology Department
Naval Air Development Center
Warminster, Pa. 18974

2a. REPORT SECURITY CLASSIFICATION
UNCLASSIFIED

2b. GROUP

3. REPORT TITLE
EVALUATION OF THE -S/N- FATIGUE LIFE GAGE UNDER CONSTANT AND VARIABLE AMPLITUDE LOADING

4. DESCRIPTIVE NOTES *(Type of report and inclusive dates)*
Final Report

5. AUTHOR(S) *(First name, middle initial, last name)*
Maurice S. Rosenfeld
Sidney Scheindlinger

6. REPORT DATE	7a. TOTAL NO. OF PAGES	7b. NO. OF REFS
5 Sept 1972	140	4

8a. CONTRACT OR GRANT NO.	9a. ORIGINATOR'S REPORT NUMBER(S)
b. PROJECT NO.	NADC-72071-VT
c AIRTASK NO. FXX.412.001 IED ST #3	9b. OTHER REPORT NO(S) *(Any other numbers that may be assigned this report)*
d.	None

10. DISTRIBUTION STATEMENT
Approved for public release; distribution unlimited.

11. SUPPLEMENTARY NOTES	12. SPONSORING MILITARY ACTIVITY
	Naval Air Systems Command Department of the Navy Washington, D. C. 20360

13. ABSTRACT

An experimental program was conducted to evaluate the -S/N- Fatigue Life Gage and a number of gage installations was evaluated for constant and variable amplitude loading.

The test results demonstrated that while there was a qualitative relation between gage resistance change and specimen life expended, a usable quantitative correlation was not attainable. Test results also proved that the fraction of specimen life to initial detectable crack was a better indicator of the time for retirement of a structure than was the fatigue life gage, although no estimate of the damage incurred can be obtained prior to crack detection.

DD FORM 1 NOV 65 1473 (PAGE 1)

02 014 6600

UNCLASSIFIED
Security Classification

14. KEY WORDS	LINK A		LINK B		LINK C	
	ROLE	WT	ROLE	WT	ROLE	WT
Fatigue (mechanics) Fatigue Life Monitoring Fatigue Life Gage						

DISTRIBUTION LIST (CONCLUDED)

REPORT NO. NADC-72071-VT

	No. of Copies
Micro-Measurements, Box 306, 38905 Chase Road, Romulus, Mich., 48174 (Attn: Mr. J. Dorsey)	3
NAVAIRDEVCEN, Warminster, Pa. 18974	48
(3 for ADT)	
(3 for VTA)	
(1 for AE)	
(1 for ASW)	
(1 for CS)	
(1 for VTM)	
(1 for SD)	
(1 for SDS)	
(1 for SDX)	
(10 for VTS)	
(25 for VTSR-3)	

(DISTRIBUTION LIST (CONTINUED FROM INSIDE BACK COVER)

REPORT NO. NADC-72071-VT

	No. of Copies
McDonnell Douglas-Astronautics Company, Department A2-260 Santa Monica, Calif. 90406	1
General Dynamics/Convair, San Diego, Calif. 92112	1
General Dynamics/Fort Worth, Texas 76101	1
Goodyear Aerospace Corp., Akron, Ohio 44305	1
Grumman Aerospace Engineering Corp., Bethpage, Long Island, N.Y. 11714	1
Aircraft-Missiles Div., Fairchild-Hiller Corp., Hagestown, Md. 21740	1
Kaman Aircraft Corp., Bloomfield, Conn. 06002	1
Lockheed Aircraft Corp., Lockheed-Calif. Co., Burbank, Calif. 91503	1
Lockheed-Georgia Co., Marietta, Ga. 30061	
(Attn: Mr. E. J. Bateh, Dept. 72-26)	1
(Attn: Technical Library)	1
LTV Aerospace Corp., Dallas, Texas 75222	1
Martin-Marietta Corp., Baltimore, Md. 21203	1
McDonnell Aircraft Corp., St. Louis, Missouri 63166	1
North American Rockwell Inc., Columbus Div., Columbus, Ohio 43216	1
North American Rockwell Corp., Los Angeles Div., Los Angeles, Calif. 90009	1
Northrop Corp., Norair Div., Hawthorne, Calif. 90250	1
Republic Aviation Div., Fairchild Hiller Corp., Farmingdale, Long Island, N.Y. 11735	1
Sikorsky Aircraft Co., Stratford, Conn. 06497	
(Attn: Dr. M. Salkind)	1
(Attn: Technical Library)	1
Laboratoriuns fiir Betriebsfestigkeit, 61 Darmstadt-Eberstadt Münitalstrasse 55-57, Germany (Attn: Mr. D. Schütz)	1
Ministry of Defence (P.E.) Royal Aircraft Establishment Structures Dept., Farnborough, Hants, England (Attn: Mr. R. D. J. Maxwell)	1
National Research Council, National Aeronautical Establishment Montreal Road., Ottawa K1A0R6, Ontario, Canada (Attn: Mr. J. A. Dunsby)	1
Department of Supply, Aeronautical Research Labs., Fishermen's Bend, Melbourne 3000, Australia (Attn: Dr. A. Payne)	1
U.S. Army Air Mobility R&D Lab Eustis Directorate - Structures Div., Fort Eustis, Va	1
National Aerospace Laboratory NLR, Voosterweg 31 Emmeloord, Netherlands (Attn: Dr. J. Schijve)	1
Vishay Intertechnology, 63 Lincoln Highway Malvern, Pa. 19355	3

DISTRIBUTION LIST (CONTINUED FROM BACK COVER)

REPORT NO. NADC-72071-VT

	No. of Copies
NASA Fatigue Section, Langley Field, Va. 23365	
(Attn: Mr. H. F. Hardrath)	1
(Attn: Technical Library)	1
National Bureau of Standards, Engineering Mechanics Section, Washington, D.C. 20234	1
Chief of Naval Research, Washington, D.C. 20360	
(Attn: Code 439)	1
(Attn: Technical Library)	1
Director, Naval Research Lab., Washington, D.C. 20390	1
George Washington University, Washington, D.C. 20360	
(Attn: Prof. A. M. Freudenthal)	1
Midwest Research Inst., Kansas City, Mo. 64110	1
University of Arizona, Department of Aerospace & Mechanical Engineering, Tucson, Arizona (Attn: Prof. E. B. Haugen)	1
University of Illinois, Urbana, Ill. 61803	
(Attn: Prof. T. J. Dolan)	1
(Attn: Prof. J. D. Morrow)	1
(A (Attn: Technical Library)	1
University of Knasas, Lawrence, Kansas 66044	
(Attn: Dr. R. R. Gatts)	1
University f Michigan, Ann Arbor, Mich. 48105	1
University of Minnesota, Minneapolis, Minn. 55455	
(Attn: Mr. A. Blatherwick)	1
Alcoa, Ne Kensington, Pa. 15068	1
Battelle Memorial Inst., Columbus, Ohio 43201	
(Attn Dr. H. J. Grover)	2
Belfour en, Inc., Traverse City, Mich. 49684	1
Cornell . Lab., Buffalo, N.Y. 14221	1
Dow Meta od., Co., Midland, Mich. 49201	1
Defense ls Info Center, Battelle Memorial Inst., Columbu , Ohio 43201	1
NASA, Lewis Research Center, Cleveland, Ohio 44135	
(Attn: Mr. S. S. Manson)	1
Naval Postg aduate School, Monterey, Calif. 93940	
(Attn: Technical Library)	1
Bell Aerosys tems Co., Buffalo, N.Y. 14205	1
Bell Helico ter Corp., Forth Worth, Texas 76101	1
Boeing Co., irplane Div., Wichita, Kansas 67210	1
Boeing Co., ommercial Airplane Division, Renton, ashington 98055	1
Boeing Co., Milita [illegible] Seattle, Washington 981	1
Boeing Co., Vertol Division, Morton, Pa. 19070	1
McDonnell Douglas, Douglas Aircraft Corp., Long Beach, Calif. 90808	
(Attn: Dr. H. Schelderup)	1
(Attn: Technical Library)	1

DISTRIBUTION LIST

REPORT NO. NADC-72071-VT
AIRTASK NO. FXX.412.001
IED ST #3

	No. of Copies
NAVAIR, AIR-604 (2 for retention, 4 for AIR-5302, 2 for AIR-530215, 1 for AIR-320N and 1 for AIR-4117B)	10
NAVAIRTESTCEN, Patuxent River, Md	1
NAVAVNSAFECEN, NASD, Norfolk, Va	1
CNAVANTRA, NAS, Corpus Christi, Texas	1
CNBATRA, NASD, Pensacola, Fla	1
CNARESTRA, NASD, Glenview, Ill	1
CNATRA, NAS, Pensacola, Fla	1
NAVAIRSYSCOMREPLANT	1
NAVAIRSYSCOMREPCENT	1
NAVAIRSYSCOMREPAC	1
NAVAIREWORKFAC, NASD, Alameda, Calif	1
NAVAIREWORKFAC, NAS, Jacksonville, Fla	1
NAVAIREWORKFAC, NAS, Norfolk, Va	1
NAVAIREWORKFAC, NAS, Quonset Point, R.I	1
NAVAIREWORKFAC, NAS, San Diego, Calif	1
NAVAIREWORKFAC, Cherry Point, N.C	1
CMNAVAIRLANT	1
CINSUSNAVEUR, Representative Germany, APO N.Y. 09757	6
USAF Systems Command, AFFDL (FDTS), WPAFB, Ohio	1
USAF Systems Command, AFFDL (FBT), WPAFB, Ohio 45433	1
USAF Systems Command, R&T Div., WPAFB, Ohio	
Attn: FDTR	2
Attn: ASNFS	1
Attn: MAMD	1
Attn: SEFS	1
Attn: FDDA/Mr. A. Kolb	1
Attn: MAAM/Mr. R. O. Hughes	1
Defense Res. & Dev. Staff, British Embassy Washington, D. C. via NAVAIR (AIR-5302)	2
Canadian Joint Staff, Navy Member Washington, D. C. via NAVAIR (AIR-5302)	1
Technical Advisor, AFLAS-B, Directorate of Aerospace Safety, Norton AFB, Calif	1
DDC	12
AFSC, Andrews Air Force Base, Washington, D. C. 20331 (Attn: SCAX)	1
FAA (FS-120) Washington, D. C. 20553 (Attn: Mr. J. Dougherty)	1
Scientific & Tech. Info Facility, College Park, Md. 20740 (Attn: NASA Rep.)	2
Administrator, NASA, Washington, D. C. 20546 (Attn: Secretary)	1

CONTINUED ON INSIDE OF COVER